REPORT NUMBER 157

MARCH 1965

Volume II
FINAL SYSTEMS ANALYSIS AND FLIGHT SIMULATION REPORT

XV-5A

LIFT FAN FLIGHT RESEARCH AIRCRAFT PROGRAM

CONTRACT NUMBER DA44-177-TC-715

GENERAL ELECTRIC

DDC AVAILABILITY NOTICES

1. Distribution of thid document is unlimited.

2. This document is subject to special report controls and each transmittal to foreign governments or foreign nationals may be made only with prior approval of US Army Aviation Materiel Laboratories, Fort Eustis, Virginia 23604.

3. In addition to security requirements which must be met, this document is subject to special export controls and each transmittal to foreign governments or foreign nationals may be made only with prior approval of USAAVLABS, Fort Eustis, Virginia 23604.

4. Each transmittal of this document outside the agencies of the US Government must have prior approval of US Army Aviation Materiel Laboratories, Fort Eustis, Virginia 23604.

5. In addition to security requirements which apply to this document and must be met, each transmittal outside the agencies of the US Government must have prior approval of US Army Aviation Materiel Laboratories, Fort Eustis, Virginia.

6. Each transmittal of this document outside the Department of Defense must have prior approval of US Army Aviation Materiel Laboratories, Fort Eustis, Va.

7. In addition to security requirements which apply to this document and must be met, each transmittal outisde the Department of Defense must have prior approval of US Army Aviation Materiel Laboratories, Fort Eustis, Virginia 23604.

8. This document may be further distributed by any holder only with specific prior approval of US Army Aviation Materiel Laboratories, Fort Eustis, Va. 23604.

9. In addition to security requirements which apply to this document and must be met, it may be further distributed by the holder only with specific prior approval of US Army Aviation Materiel Laboratories, Fort Eustis, Virginia 23604.

DISCLAIMER

10. The findings in this report are not to be construed as an official Department of the Army position unless so designated by other authorized documents.

11. When Government drawings, specifications, or other data are used for any purpose other than in connection with a definitely related Government procurement operation, the United States Government thereby incurs no responsibility nor any obligation whatsoever; and the fact that the Government may have formulated, furnished, or in any way supplied the said drawings, specifications, or other data is not to be regarded by implication or otherwise as in any manner licensing the holder or any other person or corporation, or conveying any rights or permission, to manufacture, use, or sell any patented invention that may in any way be related thereto.

12. Trade names cited in this report do not constitute an official endorsement or approval of the use of such commercial hardware of software.

DISPOSITION INSTRUCTIONS

13. Destroy this report when no longer needed. Do not return it to originator.

14. When this report is no longer needed, Department of the Army organizations will destroy it in accordance with the procedures given in AR 380-5. Navy and Air Force elements will destroy it in accordance with applicable directions. Department of Defense contractors will destroy the report according to the requirement of Section 14 of the Industrial Security Manual for Safeguarding Classified Information. All others will return the report to US Army Aviation Materiel Laboratories, Fort Eustis, Virginia 23604.

REPORT NUMBER 157

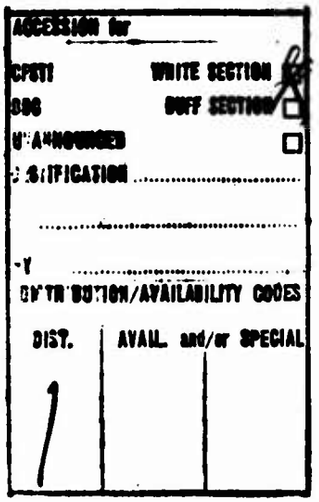

FINAL SYSTEMS ANALYSIS
AND
FLIGHT SIMULATION REPORT

VOLUME II

XV-5A Lift Fan
Flight Research Aircraft Program

March 1965

ADVANCED ENGINE AND TECHNOLOGY DEPARTMENT
GENERAL ELECTRIC COMPANY
CINCINNATI, OHIO 45215

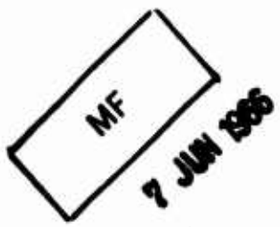

CONTENTS

CONTENTS (Cont.)

LIST OF FIGURES

LIST OF FIGURES (Continued)

LIST OF FIGURES (Continued)

SYMBOLS AND NOMENCLATURE

A_F	Main Fan Area, total for two fans, ft^2
A_{NF}	Nose fan area, ft^2
AVE	Subscript denoting average of right and left wing fans.
b	Wingspan, ft.
$\bar{c}$	Wing mean aerodynamic chord, ft.
$\bar{c}_e$	Elevator mean aerodynamic chord, ft.
c.g.	Center of gravity
C_D	Drag coefficient, $\frac{D}{qS_w}$
C_D^s	Slipstream drag coefficient, $\frac{D}{q^s A_F}$
C_{D_o}	Drag coefficient at zero lift
C_{D_t}	Tail drag coefficient, $\frac{D_t}{qS_t}$
C_L	Lift coefficient, $\frac{L}{qS_w}$
C_L^s	Slipstream lift coefficient, $\frac{L}{q^s A_F}$
C_{L_t}	Tail lift coefficient, $\frac{L_t}{qS_t}$
CM	Complete model
C_m	Pitching moment coefficient, $\frac{M}{qS_w\bar{c}}$.

C_m^s Slipstream pitching moment coefficient, $\frac{M}{q^s A_F D_F}$

C_N Normal force coefficient, $\frac{N}{qS_w}$

C_N^s Slipstream normal force coefficient, $\frac{N}{q^s A_F}$

C_{N_t} Tail normal force coefficient, $\frac{N_t}{qS_w}$

C_X Axial force coefficient, $\frac{X}{qS_w}$

C_X^s Slipstream axial force coefficient, $\frac{X}{q^s A_F}$

C_{X_t} Tail axial force coefficient, $\frac{X_t}{qS_w}$

C_Y Sideforce coefficient, $\frac{Y}{qS_w}$

C_Y^s Slipstream sideforce coefficient, $\frac{Y}{q^s S_w}$

C_{ℓ} — Rolling moment coefficient, $\frac{\ell}{qS_w b}$

C_{ℓ}^{s} — Slipstream rolling moment coefficient, $\frac{\ell}{q^s S_w b}$

C_n — Yawing moment coefficient, $\frac{N}{qS_w b}$

C_n^{s} — Slipstream yawing moment coefficient, $\frac{N}{q^s S_w b}$

$C_{N^s_\alpha}$ — $\frac{\partial C_N^{s}}{\partial \alpha}$

C_N^{s} — Slipstream normal force coefficient, $\frac{N}{q^s A_F}$

$C_{N_o}^{s}$ — Slipstream normal force coefficient at $\beta_v = \beta_v = \alpha = 0$

cps — Cycles Per Second

$$C_{L_q} \qquad \frac{\partial C_L}{\partial \left(\frac{q\bar{c}}{2V}\right)}$$

$$C_{L_{\dot{\alpha}}} \qquad \frac{\partial C_L}{\partial \left(\frac{\dot{\alpha}\bar{c}}{2V}\right)}$$

$$C_{m_q} \qquad \frac{\partial C_m}{\partial \left(\frac{q\bar{c}}{2V}\right)}$$

$$C_{m_{\dot{\alpha}}} \qquad \frac{\partial C_m}{\partial \left(\frac{\dot{\alpha}\bar{c}}{2V}\right)}$$

$$C_{Y_r} \qquad \frac{\partial C_Y}{\partial \left(\frac{rb}{2V}\right)}$$

$$C_{Y_p} \qquad \frac{\partial C_Y}{\partial \left(\frac{pb}{2V}\right)}$$

$$C_{n_r} \qquad \frac{\partial C_n}{\partial \left(\frac{rb}{2V}\right)}$$

C_{n_p} $\dfrac{\partial C_n}{\partial \left(\frac{pb}{2V}\right)}$

C_{ℓ_r} $\dfrac{\partial C_\ell}{\partial \left(\frac{rb}{2V}\right)}$

C_{ℓ_p} $\dfrac{\partial C_\ell}{\partial \left(\frac{pb}{2V}\right)}$

C_{h_e} Elevator hinge moment coefficient, $\dfrac{H_e}{qS_e\bar{c}_e}$

$C_{h_{\delta_e}}$ $\dfrac{\partial C_{h_e}}{\partial \delta_e}$

C_{h_α} $\dfrac{\partial C_{h_e}}{\partial \alpha}$

$\Delta C_{N_{\beta_v}}^{s}$ $\dfrac{\partial C_N^{s}}{\partial \beta_v}$, evaluated at $\beta_s = 0$

$\Delta C_{N_{\beta_s}}^{s}$ $\dfrac{\partial C_N^{s}}{\partial \beta_s}$, evaluated at β_v corresponding to proper T_c^{s} value.

$C_{N_T}^{s}$ $\dfrac{\partial C_{N_\alpha}^{s}}{\partial T} = \left(\dfrac{\partial C_{N_\alpha}^{s}}{\partial T}\bigg|_{\beta_v=0}\right)\alpha + \dfrac{\partial}{\partial \beta_v}\left(\dfrac{\partial C_{N_\alpha}^{s}}{\partial T}\right)\alpha\beta_v$,

variation of $C_{N_\alpha}^{s}$ with wing fan thrust and vector angle

$\left.\frac{\partial C_{N_T}^{s}}{\partial \alpha}\right|_{\beta_v=0}$ Slope of $C_{N_T}^{s}$. Change in slipstream normal force coefficient due to fan thrust with angle of attack at $\beta_v=0$.

$\frac{\partial}{\partial \beta_v}\left(\frac{\partial C_{N_\alpha}^{s}}{\partial T}\right)$ Variation of $\frac{\partial C_{N_\alpha}^{s}}{\partial T}$ with vector angle change.

ΔC_N^{s} (Sin α) Low speed variation of C_N^{s} with angle of attack over entire range of angles of attack.

$C_{X_\alpha}^{s}$ $\frac{\partial C_X^{s}}{\partial \alpha}$

$\Delta C_{X_{\beta_s}}^{s}$ $\frac{\partial C_X^{s}}{\partial \beta_s}$, evaluated at β_v corresponding to proper T_c^{s} value.

$\Delta C_{X_{\beta_v}}^{s}$ $\frac{\partial C_X^{s}}{\partial \beta_v}$, evaluated at $\beta_s = 0$

$C_{X_T}^{s}$ Same as $C_{N_T}^{s}$ term, with N replaced by X

$C_{L_{\delta_e}}$ $\frac{\partial C_L}{\partial \delta_e}$

$C_{N_{\delta_e}}$ $\frac{\partial C_N}{\partial \delta_e}$

$C_{m_o}^{s}$ Slipstream pitching moment coefficient at $\beta_v = \beta_s = \alpha = 0$

$C_{m_\alpha}{}^s$	$\frac{\partial C_m{}^s}{\partial \alpha}$
$\Delta C_{m_{\beta_s}}{}^s$	$\frac{\partial C_m{}^s}{\partial \beta_s}$, evaluated at β_v corresponding to proper $T_c{}^s$ value.
$\Delta C_{m_{\beta_v}}{}^s$	$\frac{\partial C_m{}^s}{\partial \beta_v}$, evaluated at $\beta_s = 0$.
$\frac{\partial C_m}{\partial \lvert\beta\rvert}$	Variation of pitching moment coefficient with sideslip angle.
$C_D S$	Fuselage side force coefficient multiplied by the fuselage projected side area, $\frac{Y_{fuse}}{q}$.
$\Delta C_m{}^s$ (Sin (α-50°))	Low speed variation of $C_m{}^s$ with angle of attack over entire range of angles of attack.
$C_{Y_\beta}{}^s$	$\frac{\partial C_Y{}^s}{\partial \beta}$
$C_{Y_{\delta_a}}$	$\frac{\partial C_Y}{\partial \delta_a}$
$C_{n_\beta}{}^s$	$\frac{\partial C_n{}^s}{\partial \beta}$
$C_{n_{\delta_a}}$	$\frac{\partial C_n{}^s}{\partial \delta_a}$

$C_{n_{\delta_r}}$ $\dfrac{\partial C_n}{\partial \delta_r}$

$C_{\ell_\beta}{}^s$ $\dfrac{\partial C_\ell{}^s}{\partial \beta}$

$C_{\ell_{\delta_a}}$ $\dfrac{\partial C_\ell}{\partial \delta_a}$

$C_{\ell_{\delta_r}}$ $\dfrac{\partial C_\ell}{\partial \delta_r}$

$C_{p_{NF}}{}^s$ Nose-fan power coefficient, $\dfrac{P_{NF}\rho^{1/2}}{\left(\dfrac{T_{o_{NF}}}{A_{NF}}\right)^{3/2}} A_{NF}$

$C_{p_{o_{NF}}}{}^s$ Nose-fan power coefficient at $T_{c_{NF}}{}^s = 1.0$

$C_p{}^s$ Main fan power coefficient, $\dfrac{P_F\rho^{1/2}}{\left(\dfrac{T_{ooo}}{A_F}\right)^{3/2}} A_F$

$C_{p_o}{}^s$ Main fan power coefficient at $T_c{}^s = 1$, $\beta_v = \beta_s = 0$

$C_{p_{\beta_s}}{}^s$ Main fan power coefficient increment due to β_s

$C_{L_{\alpha_t}}$ $\dfrac{\partial C_{L_t}}{\partial \alpha_t}$

$\Delta C_N^s(\alpha)$	Original low-speed data from which ΔC_N^s (Sin α) was derived.
$\Delta C_X^s(\alpha)$	Original low-speed data not used in this simulation. Its omission is explained in Section 2. 2. 2.
$\Delta C_m^s(\alpha)$	Original low-speed data from which ΔC_m^s (Sin (α- 50°)) was derived.
$C_{N_o}^{S}{}_{NF}$	Nose fan normal force coefficient. Not used in this simulation.
$C_{X_o}^{s}{}_{NF}$	Nose fan axial force coefficient. Not used in this simulation.
D	Drag, lbs. , damping, lb. /ft. /sec.
D_t	Drag of the horizontal tail, lbs.
D_F	Fan Diameter, feet.
E_{IN}	Input voltage.
E_O	Output voltage
F	Force, lbs. , Also Subscript Denoting Main Fan.
F_N	Net J-85 thrust in the turbojet mode.
f	frequency, cycles per second.
g	gravitational acceleration, ft. /sec.^{2}
g_x	gravity component along body x axis.
g_y	gravity component along body y axis.
g_z	gravity component along body z axis.

$G(jw)$	Frequency response of a system or component.
h	altitude, ft.
$\dot{h}$	rate of climb, $-(u\ell_z + vm_z + wn_z)$, ft./sec.
H_x	Angular momentum component along body x axis.
H_y	Angular momentum component along body y axis.
H_z	Angular momentum component along body z axis.
H_e	Elevator hinge moment, ft. lbs.
i_t	Tail incidence angle, degrees nose up from waterline.
$\hat{i}$	Unit vector along body x axis.
IN	Input
I_x	Body moment of inertia about x axis.
I_y	Body moment of inertia about y axis.
I_z	Body moment of inertia about z axis.
I_{xz}	Body product of inertia between x and y axes.
i	Complex operator, $\sqrt{-1}$
$\hat{j}$	Unit vector along body y axis.
$\hat{k}$	Unit vector along body z axis.
K_s	Elevator system spring constant referred to elevator hinge line.
K_i	Term used in calculating induced drag on horizontal tail.

$K_T \eta_T$	Horizontal tail efficiency factor.
K_{TS}	Thrust spoiler effectiveness.
$K_{N_{NF}}$	Function describing variation of nose fan thrust with thrust reverser door position.
$K_{X_{NF}}$	Not used in this simulation.
$\mathscr{L}$	Rolling moment, ft. lbs.
L	Lift, lbs.
LT	Refers to left wing fan.
ℓ_x	Cosine of angle between body x axis and inertial x axis.
ℓ_y	Cosine of angle between body x axis and inertial y axis.
ℓ_z	Cosine of angle between body x axis and inertial z axis.
ℓ_t	tail moment arm, feet.
ma	Milliamps
mv	Millivolts
$\mathscr{M}$	Pitching moment, ft. lbs.
m_x	Cosine of angle between body y axis and inertial x axis.
m_y	Cosine of angle between body y axis and inertial y axis.
m_z	Cosine of angle between body y axis and inertial z axis.
MF	Refers to main fans.
m	Mass, slugs.

$\dot{m}_{MF}$	Main fan mass flow rate, slugs/sec. (both fans).
$\dot{m}_{NF}$	Nose fan mass flow rate, slugs/sec.
MNF	"MODIFIED NEW FUNCTION", used in conjunction with ΔC_m^{δ} (Sin (α-50°)) in generating the low speed angle of attack caused variations in pitching moment.
N	Normal force, lbs. ; also 100 - N_g, percent
N	Yawing moment, ft. lbs.
n_x	Cosine of angle between body z axis and inertial x axis, also load factor in x direction, g's.
n_y	Cosine of angle between body z axis and inertial y axis, also load factor in y direction, g's.
n_z	Cosine of angle between body z axis and inertial z axis, also load factor in z direction, g's.
N_{RWF}	Right wing fan RPM, percent of maximum.
N_g	Percent gas generator RPM.
N_{LWF}	Left wing fan RPM, percent of maximum.
N_F	Wing fan RPM, percent of maximum.
N_{NF}	Nose fan RPM, percent of maximum.
OUT	Output
P_F	Wing fan power, a function of N_g, ft. lb./sec.
P_{NF}	Nose fan power, a function of N_g, ft. lb./sec.
POT	Potentiometer

PSF	Pounds per square foot.
POF #1	First phasing function used with low speed terms.
POF #2	Second phasing function used with low speed terms.
p	Body axis roll rate, rad./sec.
q^s	Slipstream dynamic pressure, $\frac{T_{ooo}}{A_F} + \rho \frac{V_T^2}{2}$, lbs/ft.^{2}
q^s_{AVE}	Average q^s for right and left wing fans.
q^s_{RT}	Right wing fan slipstream dynamic pressure.
q^s_{LT}	Left wing fan slipstream dynamic pressure.
q	Dynamic pressure, $\frac{\rho}{2} V_T^2$, lbs./ft.^{2}
q	Body axis pitch rate, rad./sec.
r	Body axis yaw rate, rad./sec.
R_q	Ratio of free stream to slipstream dynamic pressure, $\frac{q}{q^s}$. Also is equivalent to $1-T_c^s$.
RT	Refers to right wing fan.
RMS	Root mean square.
S_w	Wing area, ft.^{2}
$\dot{S}_x$	Velocity along inertial x axis, $ul_x + vm_x + wn_x$, ft./sec.
SA	Stability augmentation

$\dot{S}_y$	Velocity along inertial y axis, $u\ell_y + vm_y + wn_y$, ft./sec.
$\dot{S}_z$	Velocity along inertial z axis, $-\dot{h}$, $u\ell_z + vm_z + wn_z$, ft./sec.
S_x	$\int \dot{S}_x dt$, ground distance in inertial x direction.
S_y	$\int \dot{S}_y dt$, ground distance in inertial y direction.
S_z	$\int \dot{S}_z dt$, ground distance in inertial z direction.
S_t	Tail area, ft.^{2}
S_e	Elevator area, ft.^{2}
S	Laplace operator
t	time, seconds
T_j	Turbojet thrust. Equivalent to F_N.
$T_{ooo_{RT}}$	Right wing fan thrust if β_s, β_v and V_T were reduced to zero. A function of N_F and ρ only.
$T_{ooo_{LT}}$	Same as above for left wing fan.
T_{NF}	Nose fan thrust.
$T_{o_{NF}}$	Nose fan thrust if V_T were reduced to zero. A function of N_{NF} and ρ only.
TF	Short Notation for Transfer Function

T_c^s Thrust coefficient, $\dfrac{T_{ooo}/A_F}{\rho \frac{V_T^2}{2} + T_{ooo}/A_F}$

Also average T_c^s.

$T_{1/2}$ Time to one-half amplitude

T_2 Time to double amplitude

u Inertial velocity along body x axis.

u_w Component of wind velocity along body x axis.

u_a Aerodynamic velocity along body x axis. $u_a = u + u_w$.

V, V_T Total velocity, ft./sec., $\sqrt{u^2 + v^2 + w^2}$

v Volts

v Inertial velocity along body y axis.

v_w Component of wind velocity along body y axis.

v_a Aerodynamic velocity along body y axis. $v_a = v + v_w$.

W Weight, lbs.

w Inertial velocity along body z axis.

X Axial force, lbs.

x Distance along body x axis, ft., Positive fwd.

$\bar{x}$ Distance along body x axis from a point to c. g.

$\bar{x}_{NF}$	Distance from center of nose-fan to c. g., ft.
$\bar{x}_T$	Tail moment arm, ft. Equivalent to ℓ_t.
y	Distance along body y axis, ft., positive out rt. wing.
Y	Sideforce, lbs.
y_F	Wing fan moment arm ft.
$\bar{y}$	Distance along body y axis from a point to c. g.
z	Distance along body z axis, ft. Positive downward.
z_t	Tail moment arm in xz plane.
$\bar{z}$	Distance along body z axis from a point to c. g.
Z	Force along body Z axis, -N, pounds
α	Angle of attack, $\text{Sin}^{-1} \frac{w}{\sqrt{u^2 + w^2}}$, degrees.
α_{LIM}	Angle of attack, limited to some maximum value for purposes of this simulation, average.
β	Sideslip angle, $\text{Sin}^{-1} \frac{v}{V_T}$, degrees.
β_{LIM}	Sideslip angle, limited to some maximum value for purposes of this simulation.
$\beta_{s_{RT}}$	Right wing louver stagger angle, $\beta_{2_R} - \beta_{1_R}$, degrees.
$\beta_{s_{LT}}$	Left wing louver stagger angle, $\beta_{2_L} - \beta_{1_L}$, degrees.
β_v	Average louver vector angle, $\frac{\beta_{v_{RT}} + \beta_{v_{LT}}}{2}$, degrees.

$\beta_{v_{RT}}$ Right wing louver vector angle, $\frac{\beta_{1_R} + \beta_{2_R}}{2}$, degrees.

$\beta_{v_{LT}}$ Left wing louver vector angle, $\frac{\beta_{1_L} + \beta_{2_L}}{2}$, degrees.

$\beta_{2_{RT}}$ Forward right wing louver set angle, degrees, measured from the z axis direction, positive aft. The reference on the louver is a tangent to the rear louver surface, and the 7^{th} louver used as the reference.

$\beta_{1_{RT}}$ Aft right wing louver set angle, degrees, measured from the z axis direction, positive aft. The 8^{th} louver is used as the reference.

$\beta_{2_{LT}}$ Forward left wing louver angle.

$\beta_{1_{LT}}$ Aft left wing louver angle.

γ Flight path angle, equal to pitch angle minus angle of attack.

δ_{LAT} Percent lateral stick, positive right.

δ_e Elevator deflection, positive trailing edge down.

δ_a Total aileron angle, $\delta_{a_L} - \delta_{a_R}$.

δ_{a_R} Right aileron angle, positive trailing edge down.

δ_{a_L} Left aileron angle, positive trailing edge down.

δ_f Flap angle, positive trailing edge down.

δ_p	Nose fan thrust reverser position, positive in decreasing thrust direction, measured from maximum thrust position.
δ_d	Aileron droop angle, positive trailing edge down.
δ_r	Rudder position, positive trailing edge left.
ϵ	Downwash angle at tail.
ξ	Damping ratio.
η_T	Tail efficiency factor.
θ	Euler pitch angle.
θ_{RB}	Rigid body pitch angle.
θ_T	Tail total pitch angle.
θ_{BT}	Tail pitch angle due to bending at the tail.
ρ_o	Sea level standard day density, . 002378 slugs/ft.^{3}
ρ	Air density, slugs/ft.^{3}
σ	Density ratio, $\frac{\rho}{\rho_o}$, density at altitude compared to density at sea level.
σ	Standard Deviation of normal distribution.
$\sigma_j^{(i)}$	Normalized slope of i^{th} flexible body mode at point j.
τ	Time constant, seconds, or torque, foot-pounds.
Φ	Euler Roll Angle.
$\Phi(jw)$	Power Density spectrum.

Ψ	Euler yaw angle.
Ψ_w	Wind direction, measured from $\Psi = 0$.
ω	Angular frequency, rad./sec.
ω_N	Natural frequency of second order system, rad./sec.
Ω	Ohms
$\phi_j^{(i)}$	Normalized deflection of i^{th} flexible body mode at point j.

PREFACE

This is Volume II, of two volumes, published under Report No. 157. This volume presents the details of the studies made and also presents the results of these studies, as well as supporting analyses which may be found in the Appendix.

Volume I under separate cover details the mechanization and checkout/ verification of the Ryan Flight Simulator.

3.0 FLIGHT SIMULATOR AND SYSTEMS DYNAMICS STUDIES

The effect of the stability augmentation system on the aircraft in hover was analyzed by root locus techniques. The root locus studies of hover were performed by considering the roll-sideslip degrees of freedom separately from the pitch-forward translation degrees of freedom. Yaw was non-critical, and all development of this axis was done by piloted simulator evaluations. A summary of these studies is presented below:

3.1 ROOT LOCUS STUDY OF ROLL CONTROL SYSTEM

The forces and moments acting on the aircraft near hover come from ram drag aerodynamic effects or control effects on the fans. The equations showing the force and moment summations near hover that were used in this study are given below.

$$\Sigma \mathfrak{L} = q^{s}_{AVE} \frac{A_F}{2} y_F \Delta C_{N_{\beta_s}}^{s} \left(\beta_{s_{LT}} - \beta_{s_{RT}}\right) - 134v - 2\dot{m}_{MF} y_F^2 p \quad (1)$$

$$\Sigma Y = -31.8v \quad (2)$$

The equations of motion used are given as:

$$\dot{p} = \frac{I_{xz}}{I_x}\dot{r} + \frac{\Sigma \mathfrak{L}}{I_x} \quad (3)$$

$$\dot{v} = gm_z + \frac{\Sigma F_y}{m} \quad (4)$$

Substituting and transforming (Laplace) we obtain, if I_{XZ}/I_X is negligible;

$$I_x S^2 \varphi = q^{s}_{AVE} \frac{A_F}{2} y_F \Delta C_{N_{\beta_s}}^{s} (\Delta\beta_s) - 134v - 2\dot{m}_{MF} y_F^2 S\phi \quad (5)$$

$$mvS = W\varphi - 31.8\,v \quad (6)$$

Solving for the roll/sideslip transfer function, the result is:

$$I_x S^2 \varphi = q^s_{AVE} \frac{A_F}{2} y_F \Delta C_{N_{\beta_s}}^{s} (\Delta\beta_s) - 134v - 2\dot{m}_F y_F^2 S\varphi \qquad (7)$$

$$v = \frac{W\varphi}{mS + 31.8} \qquad (8)$$

The resulting final roll/sideslip transfer function is:

$$\frac{\varphi}{\Delta\beta_s} = \left(q^s_{AVE} \frac{A_F}{2} y_F \Delta C_{N_{\beta_s}}^{s} \right) \frac{(mS + 31.8)}{\left(I_x mS^3 + 31.8 I_x S^2 + 134W \right)} \qquad (9)$$

The roll control system is shown in Figure 140 of this section. The transfer functions of the individual components are shown below.

Rate Gyro

$$TF = \frac{K_R S \left(160^2\right)}{S^2 + 160S + 160^2}$$

where: K_R = 400 millivolts/deg./sec

Servos and Drive Network

$$TF = \frac{K_{SN} \left(22\right) \left(188^2\right)}{(S + 22)\left(S^2 + 2\,(188)\,S + 188^2\right)}$$

where:

$$K_{SN} = \frac{6.8°/\text{Wing}}{8ma} \times \frac{.666\ ma}{mv} \times .93,$$

and where the .93 factor accounts for reduced valve gain due to increased oil temperature over ambient.

Notch Filter

$$TF = K_N \left(\frac{1 + S^2/\omega_o^2}{1 + 4S/\omega_o + S^2/\omega_o^2} \right)$$

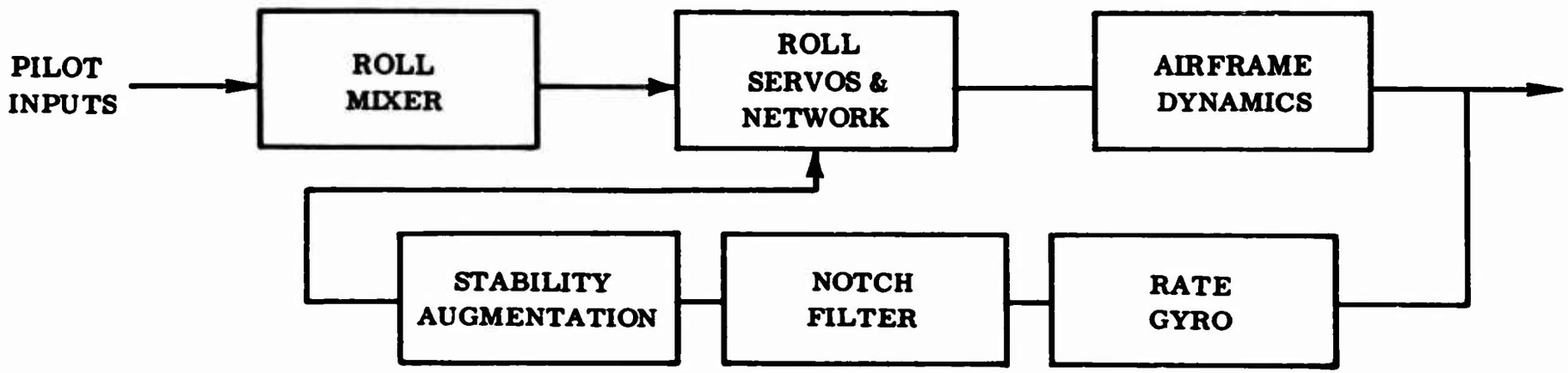

Figure 140 Roll Control System - Block Diagram

where: $\omega_o = 100$

$K_N = 0.58$

Stability Augmentation System Input Network

Holding Mode: $TF = \dfrac{K_H R (1/R\tau + S)}{(1/\tau + S)}$

Maneuvering Mode: $TF = K_M$

where: K_H Varies from 0 to 1.0

K_M Varies from 0 to .035

$R = .10; .05; .03; .02; .01; .0025$

$\tau = 10$ sec.

The over-all roll stabilization system gain is the product of the gains of the individual components.

Roll System Overall Gain:

Holding Mode: $\text{Gain} = \left(\dfrac{400 \text{ mv}}{\text{deg./sec}}\right)\left(\dfrac{6.8°/\text{Wing}}{8 \text{ ma}}\right)\left(\dfrac{.666 \text{ ma}}{\text{mv}}\right)$

$\times (.58)(.93)(K_H R) = \left(\dfrac{123 \text{ deg}}{\text{deg./sec}}\right) K_H R$

Maneuvering Mode: $\text{Gain} = \left(\dfrac{123 \text{ deg.}}{\text{deg./sec}}\right) \times .035 K_M$

The primary stabilization system leaves open to the pilot the capability of setting R, K_H and K_M.

R is set at any of the 6 possible settings from .10 to .0025 (positions 6 to 1 respectively), while K_H and K_M are set on pots which vary as shown in Figure 141.

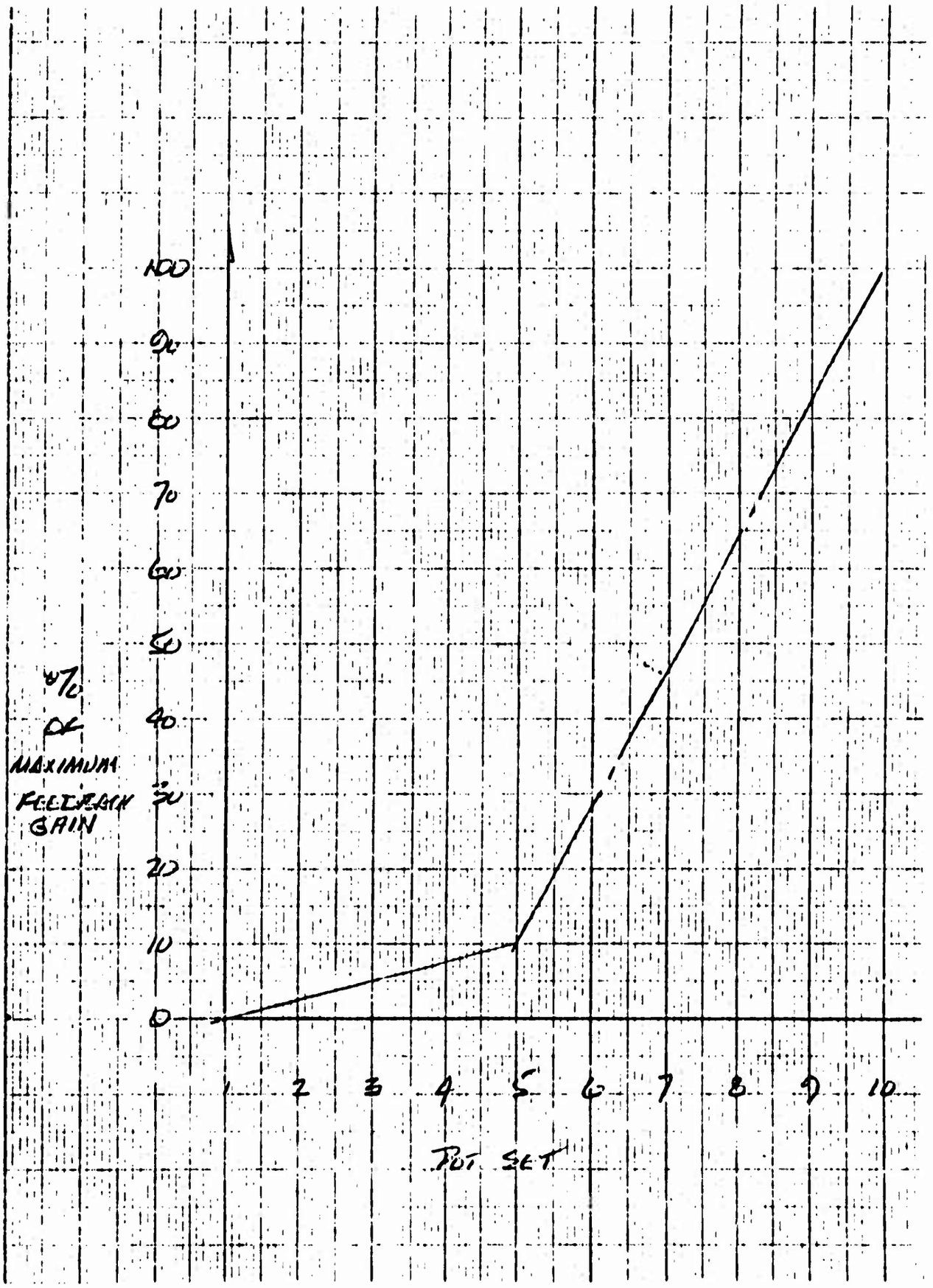

Figure 141 S A Pot Sets Versus Maximum Gain

The maximum gain in holding mode (pot set at position 10) is R × 123 deg/deg/sec.

The maximum gain in maneuvering mode (pot set at position 10) has been arbitrarily set at .035 × 123°/°/sec or 4.3 deg/deg/sec.

The two modes of the stability augmentation/aircraft system (maneuvering and holding) are studied separately below for the hovering conditions given in Table 1.

TABLE 1

NOMINAL CONDITIONS AT HOVER

$W = 9200$ Lbs.	$q^s = 202$ PSF
$I_{xz} = 919$ Slug-Ft.^{2}	$\dot{m}_{MF} = 12.56$ Slugs/sec/fan
$I_z = 17,418$ Slug-Ft.^{2}	$\dot{m}_{NF} = 4.38$ Slugs/sec
$I_x = 4252$ Slug-Ft.^{2}	$T_{NF} = 1500$ Lbs.
$I_y = 15,139$ Slug-Ft.^{2}	$\beta_s = 27°$

3.1.1 Holding Mode

In holding mode there are two variables open to the pilot; the over-all gain of the stability augmentation system, and R which is effectively the ratio of rate to position gain.

In the SA system, R can assume following values:

$$R = .10, .05, .03, .02, .01, .0025$$

For each of these values of R, a separate root locus has been drawn, showing the paths of travel of the roots as the system gain is varied from 0 toward infinity.

The numbered positions on the root locus plots are points at which specific gains were computed.

In the plots corresponding to an R of .0025, gains were not computed because a stable system is unattainable at this R.

In several cases, more than one plot was made for each R in order to compute gains on plots scaled for maximum accuracy.

Figures 142 through 149 show the root locus plots for roll/sideslip in hover and holding mode for each value of R.

In each case, the dominant mode of the system is the second order. Determination of which of the singularities on the S plane give rise to the second order can be determined by the reader.

The effect of the SA system on the dominant mode which the pilot sees and flies is summarized for various values of R in Figure 150.

Also shown on Figure 160 are the acceptable areas for location of the dominant second order mode according to References 3 and 10.

To determine whether or not the simulation agreed with the root locus results, the gains on the simulation at which the system goes unstable were determined for an R of .10 in both pitch and roll, and compared to the predicted gains for instability from the root locus. The gains from both sources agreed closely. (See Table 2.)

3.1.2 Maneuver Mode

In maneuvering mode only rate feedback is used to augment the stability of the aircraft. The root locus showing the effect of the stability augmentation system on the aircraft in maneuvering mode at hover is shown in Figure 151. As can be seen, large gains are required to first stabilize and then destabilize the aircraft.

3.1.3 Effect of Notch Network on Roll System

In order to evaluate the effect of the notch filter on the system in the holding mode, a root locus of the roll control system was constructed which did not contain the notch singularities.

The locus was constructed in two parts at a value of R of .10 and is presented in Figures 152 and 153.

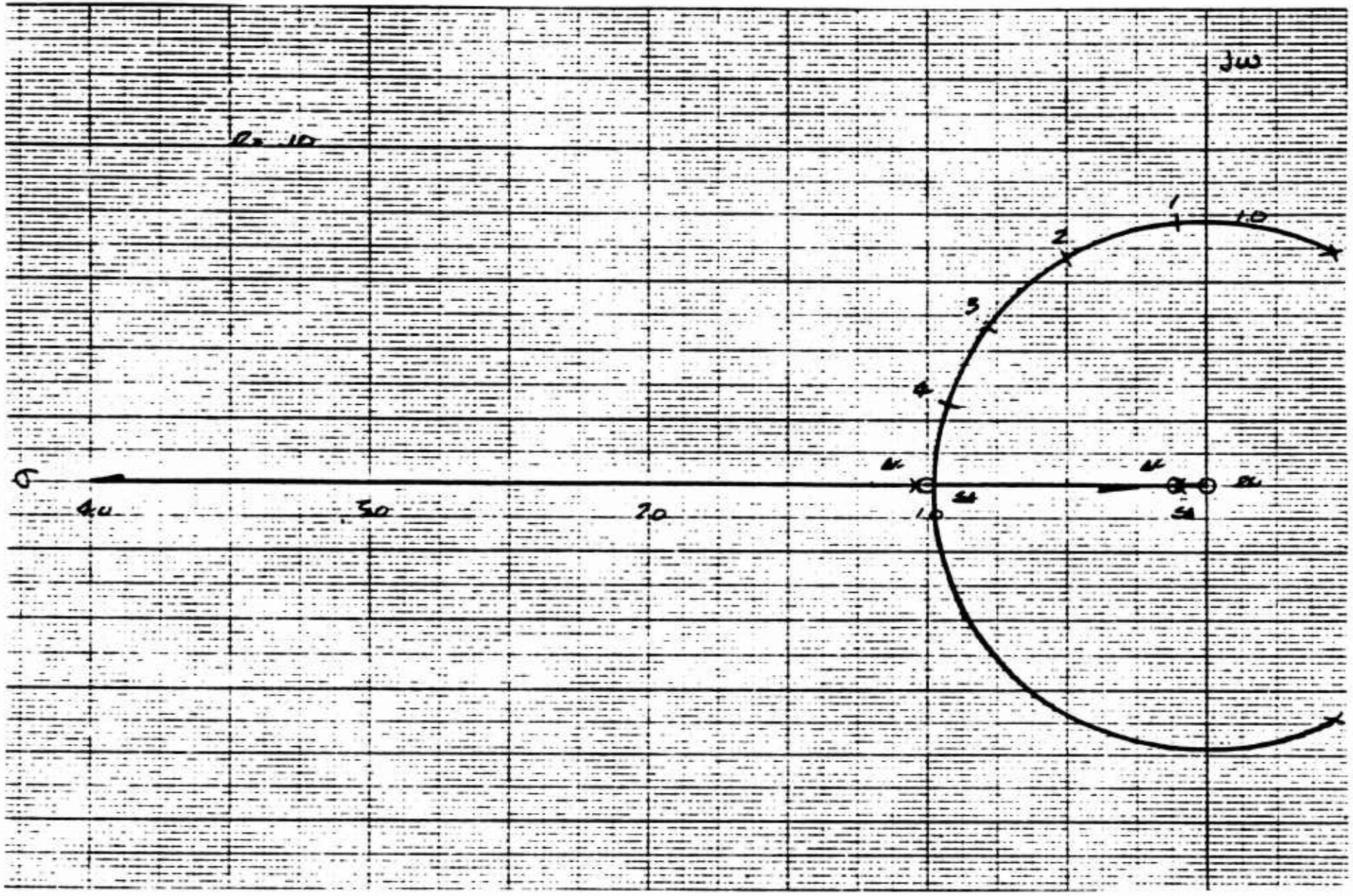

Figure 142 Roll System Hover Holding Root Locus, R = .1

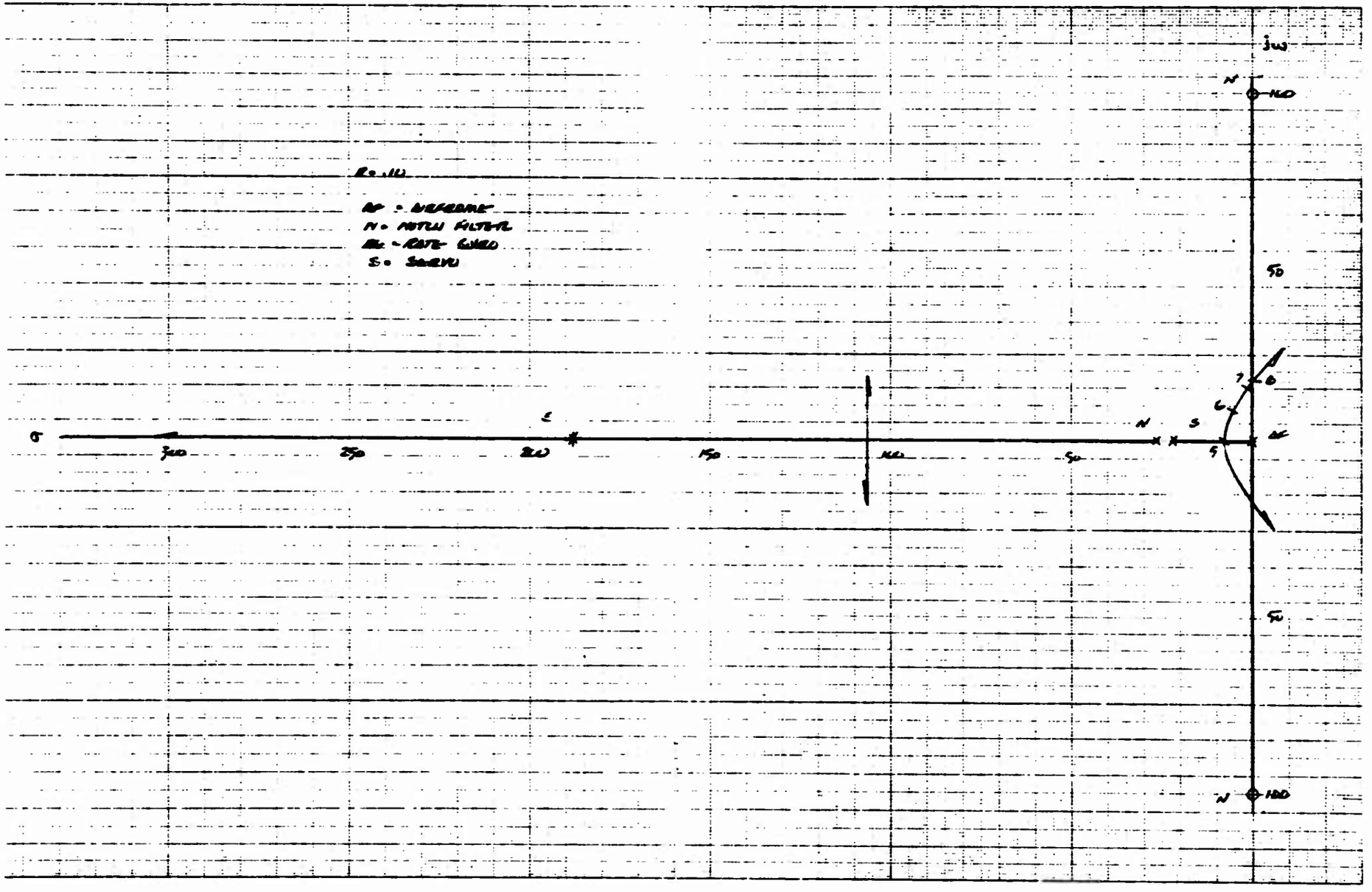

Figure 143 Roll System Hover Holding Root Locus, R = .1

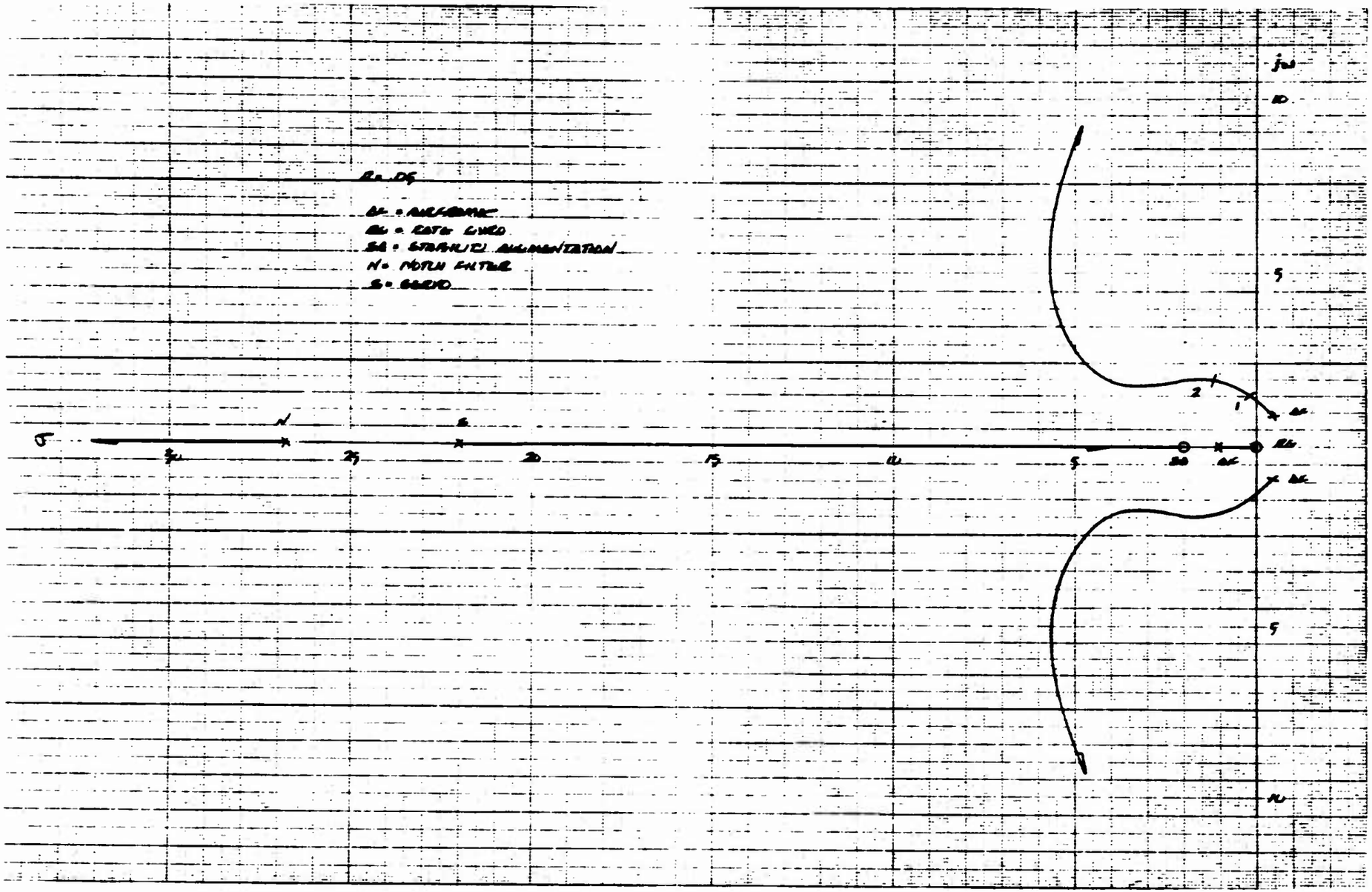

Figure 144 Roll System Hover Holding Root Locus, R = .05

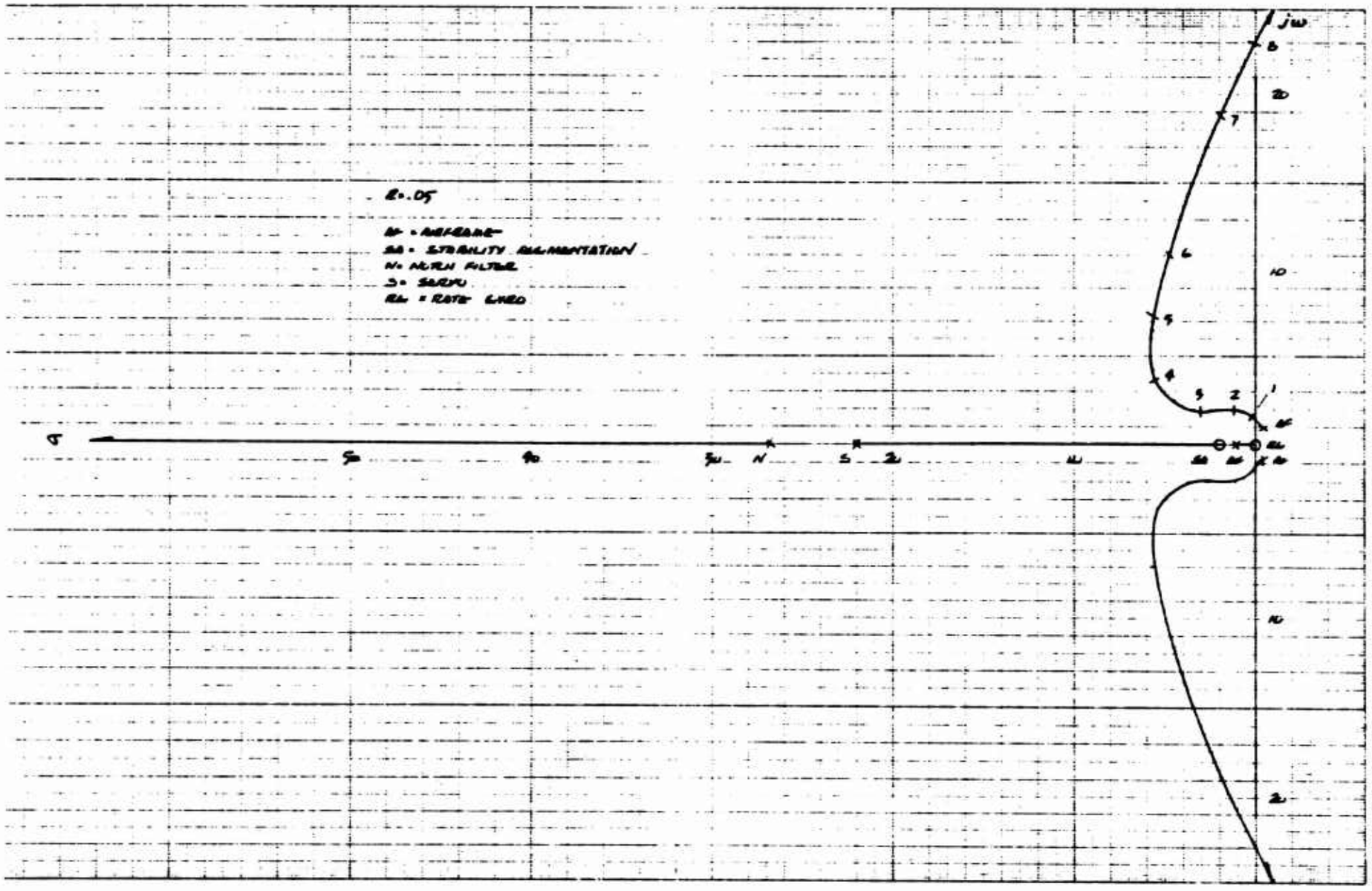

Figure 145 Roll System Hover Holding Root Locus, R = .05

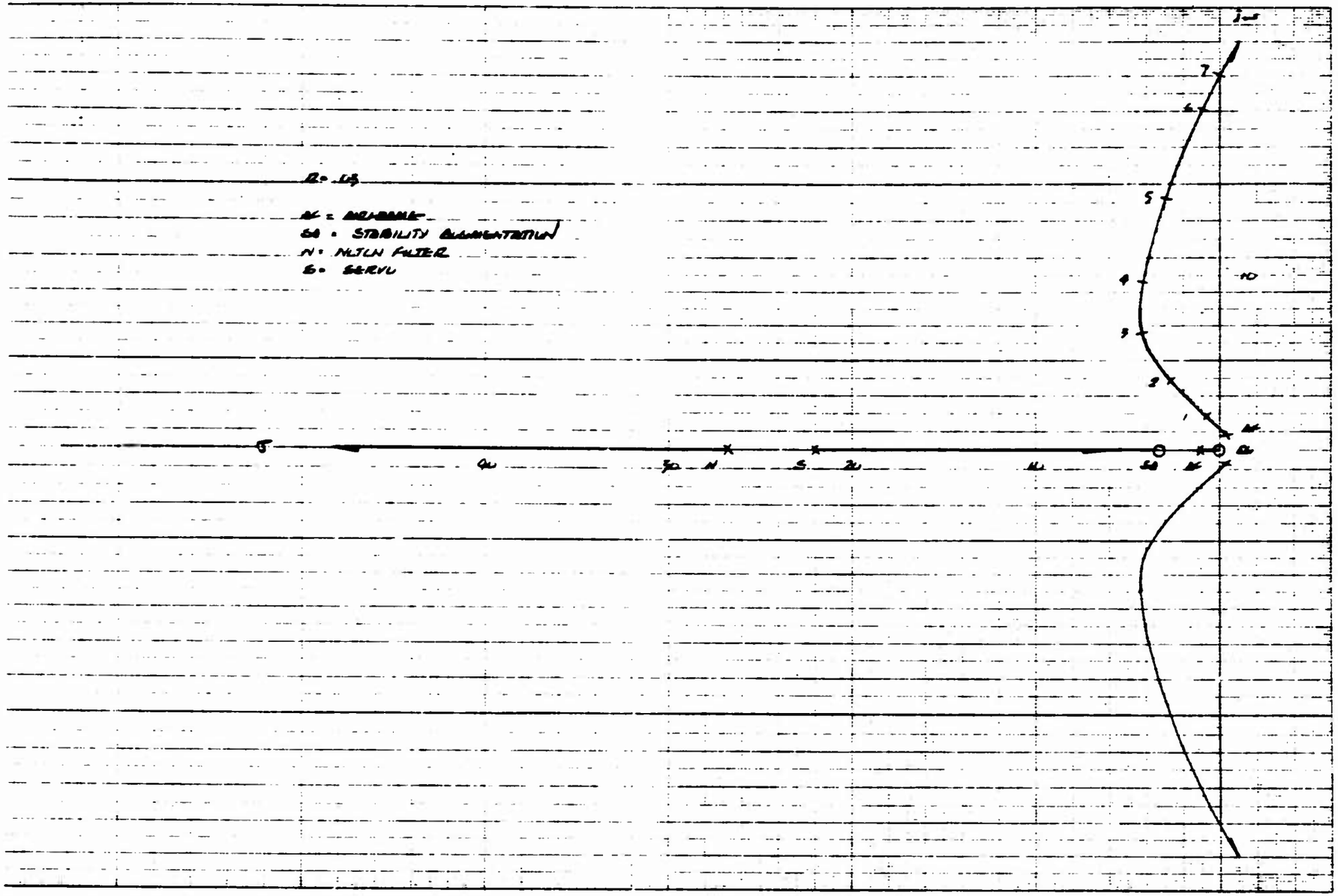

Figure 146 Roll System Hover Holding Toot Locus, R = .03

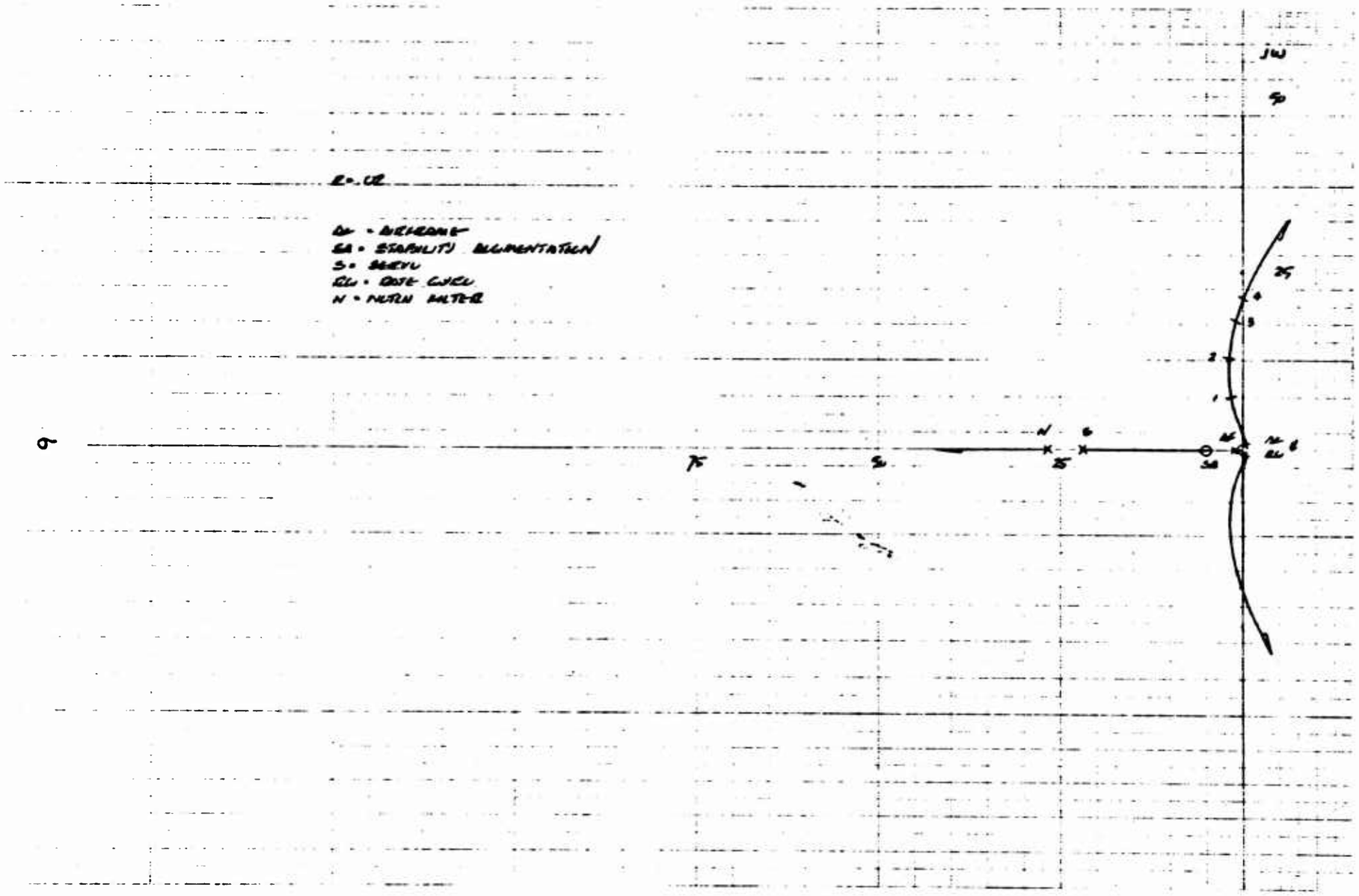

Figure 147 Roll System Hover Holding Root Locus, R = .02

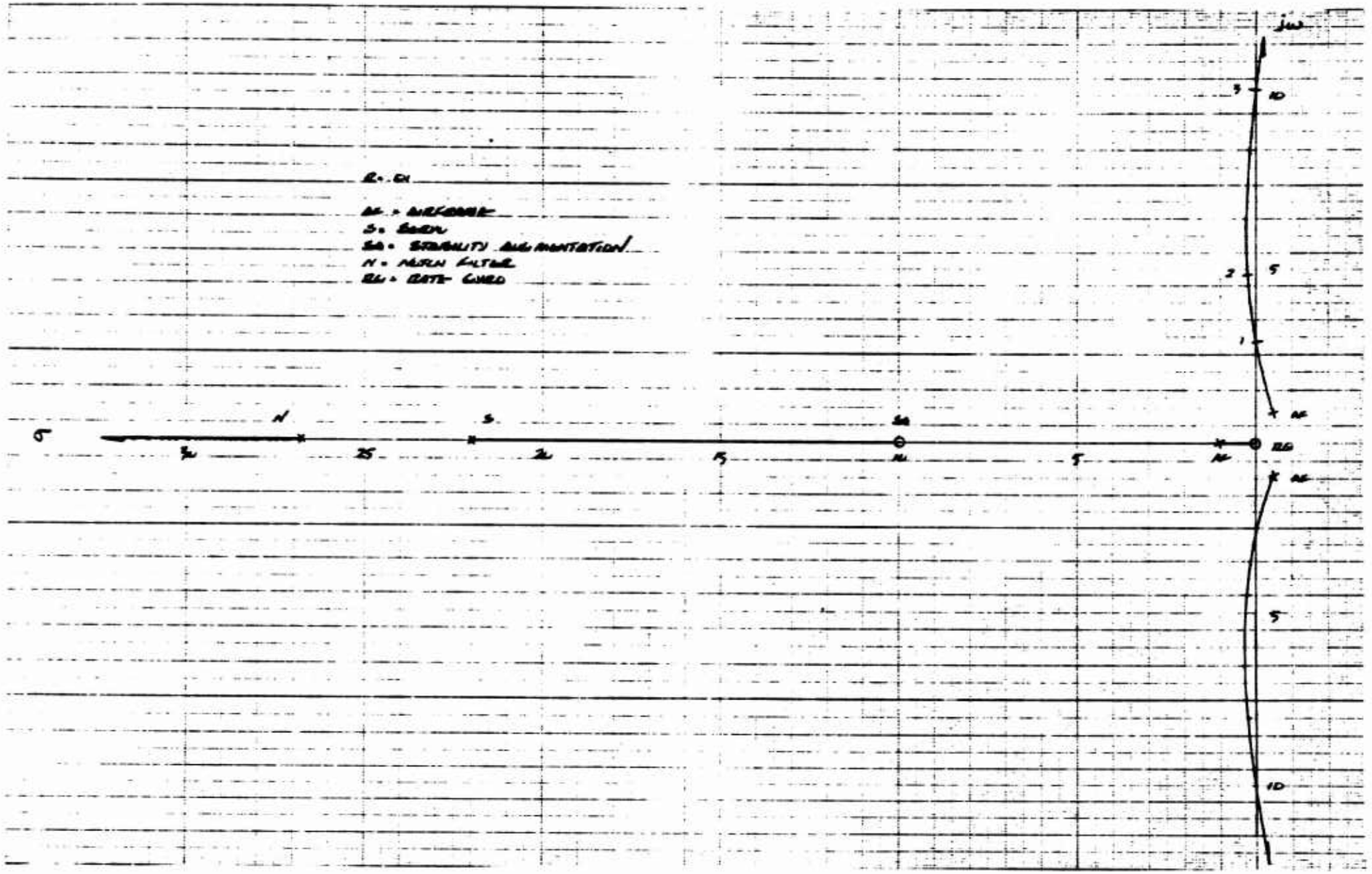

Figure 148 Roll System Hover Holding Root Locus, R = .01

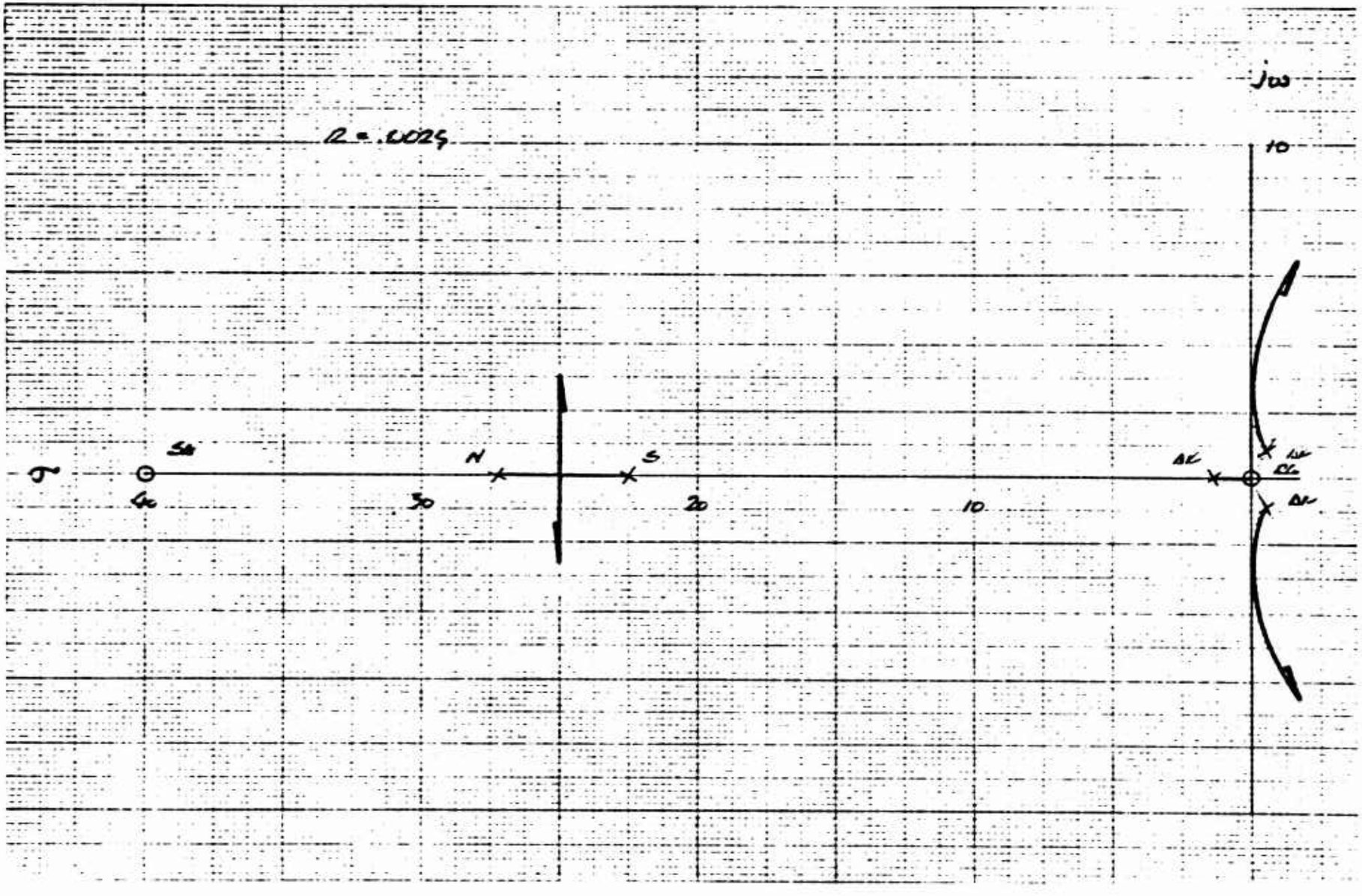

Figure 149 Roll System Hover Holding Root Locus, R = .0025

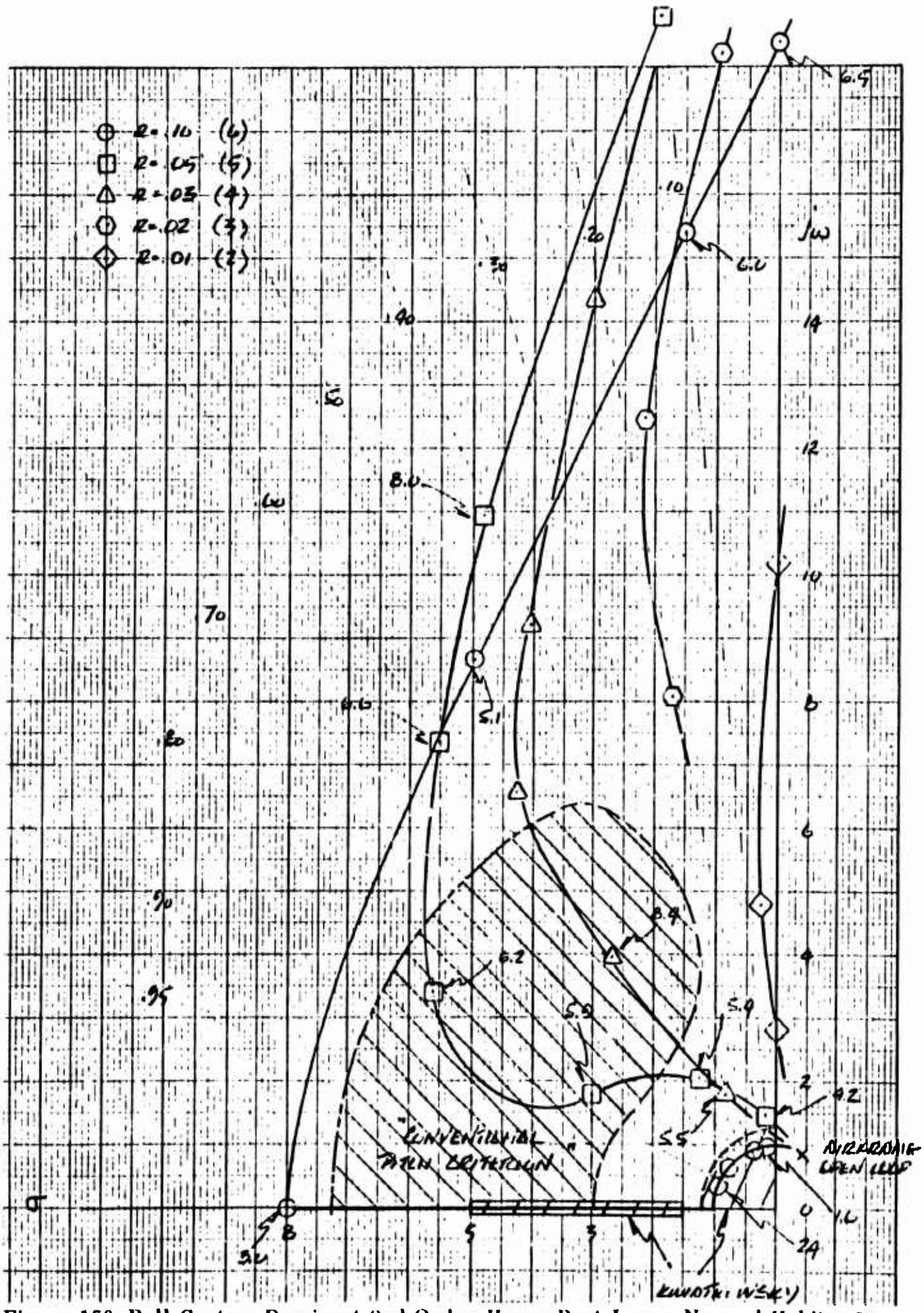

Figure 150 Roll System Dominant 2nd Order Hover Root Locus Normal Holding Mode

TABLE 2

EFFECT OF SAS (HOLDING MODE) ON DOMINANT 2ND ORDER

POINT	RATIO (R)	MAX. NET SA FEEDBACK (AT HIGH FREQUENCY)	DAMPING (ξ)	FREQ (ω_N)	GAIN** (K_H)	POT SET
1	.10	12.3° /° /sec	.10	.99	.026	1.9
2			.51	.99	.043	2.6
3			.80	.99	.052	3.1
4			.95	.99	.067	3.6
5			1.0	8.0	.076	4.0
6			.50	10.0	.162	5.4
7			.10	15.5	.415	6.7
8	.10	12.3	0	18.5	.575	7.6*
1	.05	6.15	.10	1.5	.122	5.1
2			.50	2.4	.244	5.8
3			.85	3.5	.384	6.6
4			.84	6.6	.472	7.1
5			.60	9.2	.595	7.6
6			.40	12.0	.960	9.8
7	.05	6.15	.10	18.8	2.460	---
1	.03	3.69	.40	2.0	.300	6.1
2			.56	4.8	1.085	---
3			.54	7.8	1.680	---
4			.40	10.4	2.304	---
5	.03	3.69	.20	14.7	4.080	---

*Stability Limit (Simulation yields 6^+)

**× 100 yields % of maximum capability

---Out of Range (Max. is 10 or 1.00 on Gain)
Airframe gain 3.84 rad/sec^2/rad

TABLE 2 (Cont)

EFFECT OF SAS (HOLDING MODE) ON DOMINANT 2ND ORDER

POINT	RATIO (R)	MAX. NET SA FEEDBACK (AT HIGH FREQUENCY)	DAMPING (ξ)	FREQ (ω_N)	GAIN** (K_H)	POT SET
6	.03	3.69	.05	19.2	6.500	---
1	.02	2.46	.20	8.25	3.950	---
2	|	|	.14	15.75	11.110	---
3	.02	2.46	.05	18.25	15.100	---
1	.01	1.23	0	2.85	2.210	---
2	.01	1.23	.05	4.85	4.950	---

**× 100 yields % of maximum capability

---Out of Range (Max. is 10 or 1.00 on Gain)
Airframe gain 3.84 rad/sec^2/rad

Reference to Figures 142 and 143, and comparison with Figures 152 and 153 show that the notch network causes the dominant second-order mode to become unstable at a lower frequency.

Table 3 shows the characteristics of the dominant second order and corresponding gains and pot settings for each of the points shown on Figures 152 and 153.

The over-all effect of the notch is a pronounced decrease in the amount of gain required to drive the dominant second order mode unstable.

The gain value presented in Tables 2 and 3 is the fraction of the maximum feedback gain available, and since the notch itself has a DC gain of 0.58, the maximum feedback gain available then is decreased by the notch.

In order to compare the true feedback gains required to destabilize the vehicle's dominant second order mode with and without the notch, the products of the percentage gain figures given and the maximum feedback capability will be compared.

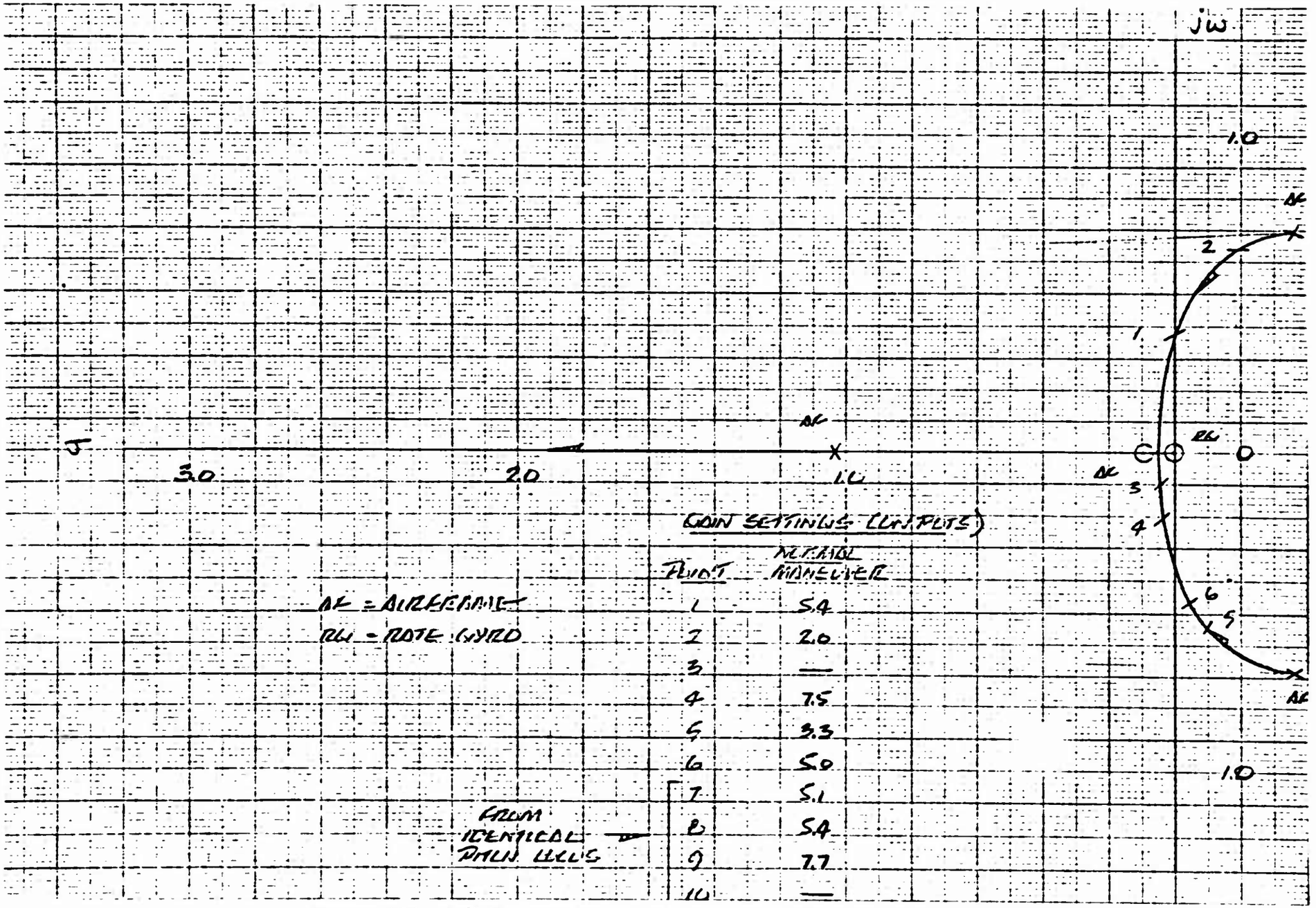

Figure 151 Roll System Hover Maneuvering Mode Root Locus

TABLE 3

EFFECT OF SAS (HOLDING MODE) ON DOMINANT 2ND ORDER WITH NO NOTCH NETWORK IN LOOP

POINT	RATIO (R)	MAX. NET SA FEEDBACK	DAMPING (ξ)	FREQ. (ω_N)	GAIN** (K_H)	POT SET
1	.10	21.2° /° /sec	.20	.99	.0178	1.6
2			.50	.99	.0236	2.0
3			.90	.99	.0305	2.2
4			1.0	5.0	.0546	3.1
5			1.0	10.6	.0630	3.4
6			.50	17.5	.1830	5.5
7			.10	30.0	.555	7.5
8	.10	21.2° /° /sec	0	35.2	.783	8.8

*Stability limit (with notch yields 7.6)

**× 100 yields % of maximum capability
Airframe gain 3.84 rad/sec^2/rad

Comparing the points on Figures 143 and 153 at which the locus crosses the $j\omega$ axis, and referring to Tables 2 and 3, we can calculate the maximum gain allowable for each case.

On Figure 143, point 8 is the point in question, and reference to Table 2 shows that this corresponds to a K_H of .575. The maximum net SA feedback gain for this case is 12.3 degrees stagger (per wing) per degree per second of roll rate. Since the net SA gain is the SA gain at high frequencies, and the high frequency gain of the network is equal to R times the static gain, the maximum static gain in this case is 123 degrees stagger per degree per second roll rate. This results in a maximum allowable gain of 71 deg/deg/sec, in the system with the notch.

On Figure 153, point 8, with reference to Table 3, has a gain of .783, and the maximum SA feedback gain available is 212 deg/deg/sec. The roll system without the notch, then, has a maximum allowable gain of 166 deg/deg/sec.

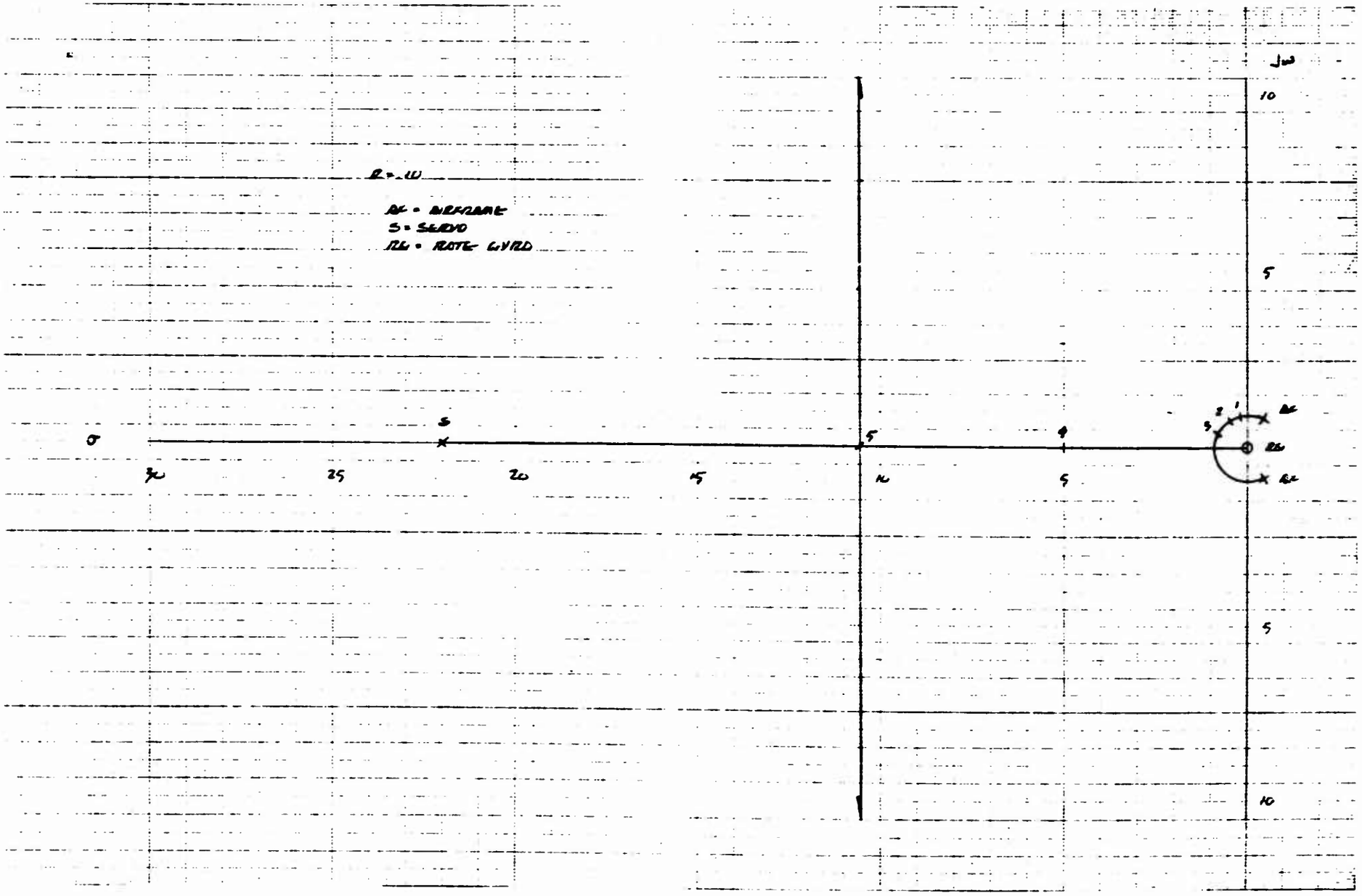

Figure 152 Roll System Hover Holding Root Locus (No Notch), R = .1

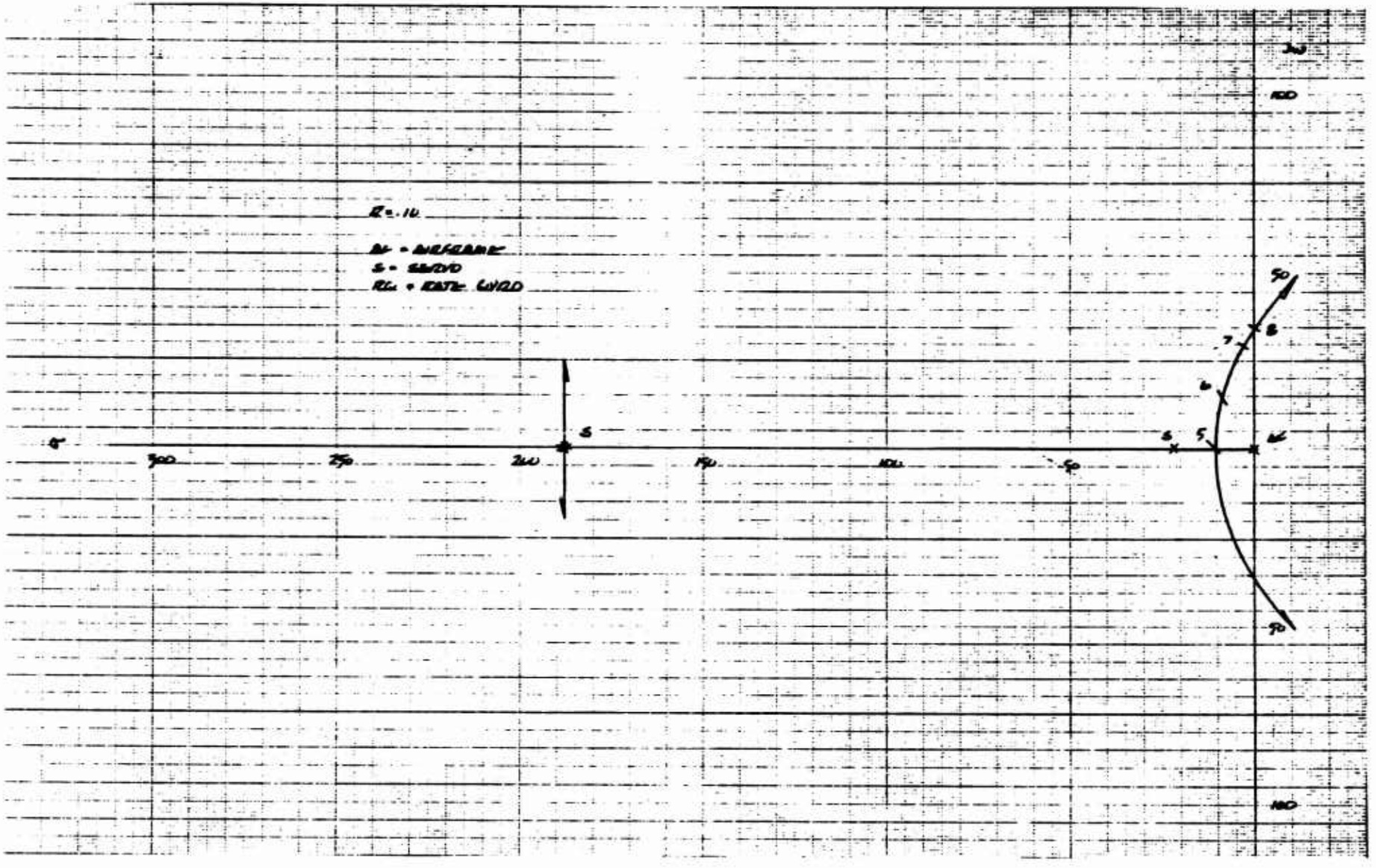

Figure 153 Roll System Hover Holding Root Locus (No Notch), R = .1

3.2 ROOT LOCUS STUDY OF PITCH CONTROL SYSTEM

The forces and moments acting on the aircraft near hover were derived from momentum or control effects on the fans. The equations showing the force and moment summations near hover used in this study are:

$$\Sigma \mathcal{M} = \frac{T_{NF}}{A_{NF}} A_{NF} \cdot K_{N_{NF}} \cdot \bar{x}_{NF} - 4.38\, q\, \bar{x}_{NF}^2 + 134u$$

$$\Sigma X = -31.8\, u - W\theta$$

The equations of motion used are given as:

$$\ddot{x} = \frac{\Sigma X}{m} - g\theta$$

$$\ddot{\theta} = \frac{\Sigma \mathcal{M}}{I_y}$$

Substituting and transforming (Laplace) we obtain:

$$mSu = -31.8u - W\theta$$

$$I_y \theta S^2 = \Sigma \mathcal{M}$$

Solving for the pitch / x transfer function, there results:

$$\frac{\theta}{K_{N_{NF}}} = \frac{T_{NF}(\bar{x}_{NF})\,(mS + 31.8)}{(mI_y)\,S^3 + \left(31.8I_y + 4.38\,\bar{x}_{NF}^{\,2} \cdot m\right)S^2 + \dfrac{T_{NF}(\bar{x}_{NF})(mS + 31.8)}{(4.38)(31.8)(\bar{x}_{NF}^2)S + 134W}}$$

Linearizing around the nominal hover nose fan door position, we obtain:

$$\frac{K_{N_{NF}}}{\delta_p} = .03/\text{Degree}$$

The resulting final pitch / x transfer function is:

$$\frac{\theta}{\delta_p} = \frac{(.03 \times 57.4)\,(T_{NF} \cdot \bar{x}_{NF})\,(mS + 31.8)}{(mI_y)\,S^3 + \left(31.8\,I_y + 4.38\,\bar{x}^2_{NF} \cdot m\right)S^2}$$

$$+ (4.38)\,(31.8)\,(\bar{x}^2_{NF})S + 134W$$

The pitch control system is shown in Figure 154. The transfer functions of the individual components are:

Rate Gyro

$$TF = \frac{K_R S(160^2)}{S^2 + 160S + 160^2}$$

where: $K_R = \frac{400\ mv}{Deg/Sec}$

Servos and Drive Network

$$TF = \frac{K_{SN}\,(22)(188^2)}{(S + 22)\,(S^2 + 2\xi\,S(188) + 188^2)}$$

where: $K_{SN} = \frac{8.75\ deg}{8\ ma} \times \frac{.666\ ma}{mv} \times .93$

Notch Filter

$$TF = K_N \frac{(1 + S^2/\omega o^2)}{(1 + 4S/\omega o + S^2/\omega o^2)}$$

where: $\omega o = 100$ Rad

$K_N = 0.58$

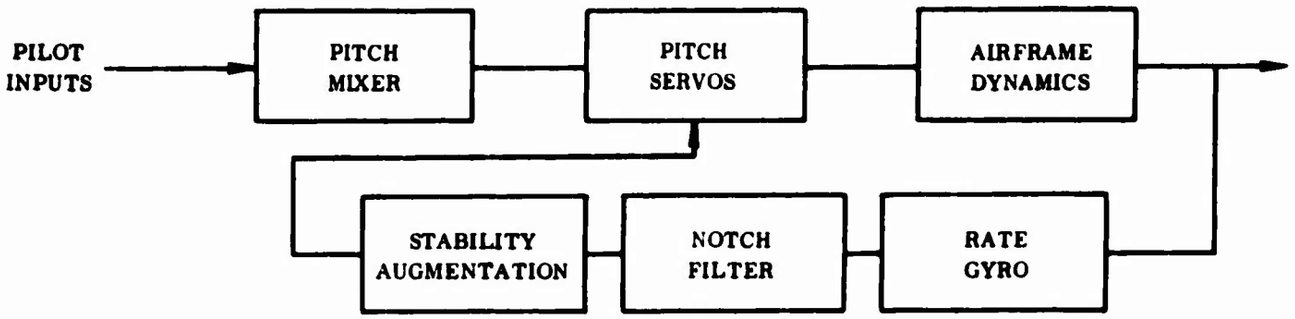

Figure 154 Pitch Control System - Block Diagram

Stability Augmentation System Input Network

$$\text{Holding Mode: } TF = \frac{K_H R \left(S + \frac{1}{R\tau}\right)}{S + \frac{1}{\tau}}$$

Maneuvering mode: $TF = K_M$

where: K_H Varies from 0 to 1.0

K_M Varies from 0 to .035

$R = .10; .05; .03; .02; .01; .0025$

$\tau = 10$ Sec.

The over-all pitch stabilization system gain is the product of the gains of the individual components.

Pitch System Over-all Gain

$$\text{Holding Mode: Gain} = \left(\frac{400 \text{ mv}}{\text{deg./Sec}}\right)\left(\frac{8.75 \text{ deg}}{8 \text{ ma}}\right)\left(\frac{.666 \text{ ma}}{\text{mv}}\right)$$

$$\times (.93)\,(.58)\,K_H R = \left(\frac{158°}{\text{deg/Sec}}\right) K_H R$$

Maneuvering Mode: Gain $= \left(\frac{158 \text{ deg}}{\text{deg/Sec}}\right) K_M$

The primary stabilization system leaves open to the pilot the capability of setting R, K_H and K_M.

R is set at any of the six possible settings from .10 to .0025 (positions 6 to 1 respectively), while K_H and K_M vary as shown in the figure of the previous section.

The maximum gain in holding mode (pot set at position 10) is R x 158 deg/deg/sec.

The maximum gain in maneuvering mode (pot set at position 10) has been arbitrarily set at .035 x 158 deg/deg/sec. or 5.52 deg/deg/sec.

The two modes of the auto pilot/aircraft system (maneuvering and holding) are studied separately below for the hovering conditions shown in Table 1.

3.2.1 Holding Mode

In holding mode, there are two variables open to the pilot; the over-all gain of the stability augmentation system and R, which is effectively the ratio of rate to position gain.

For each of the possible values of R, separate root locus plots must be drawn showing the path of travel of the roots as the gain varies from zero toward infinity.

Since the characteristic equations of the airframe in pitch and roll exhibit similar form however, the root locus plots in pitch and roll are also of similar form.

At high gains the plots are in fact identical. Therefore, the root locus study of the pitch system at high gains made use of the same root locus plots drawn for roll, and new plots were only drawn for the pitch system at values of R of .10 and .05, the plots in which the low gain region is of interest.

Figures 155 and 156 then show root locus plots of the system in pitch at values of R of .10 and .05 respectively.

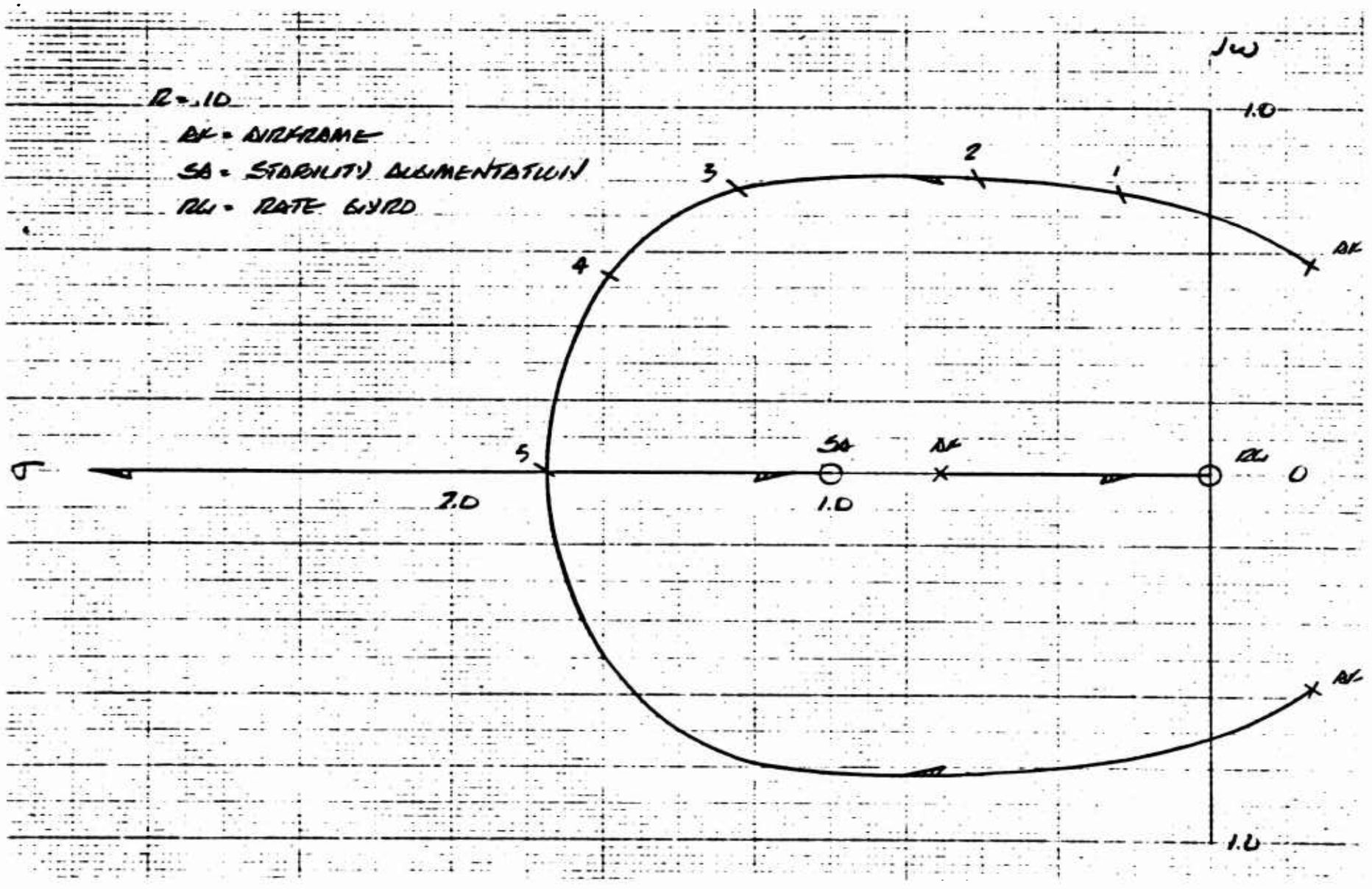

Figure 155 Pitch System Hover Holding Root Locus, R = .1

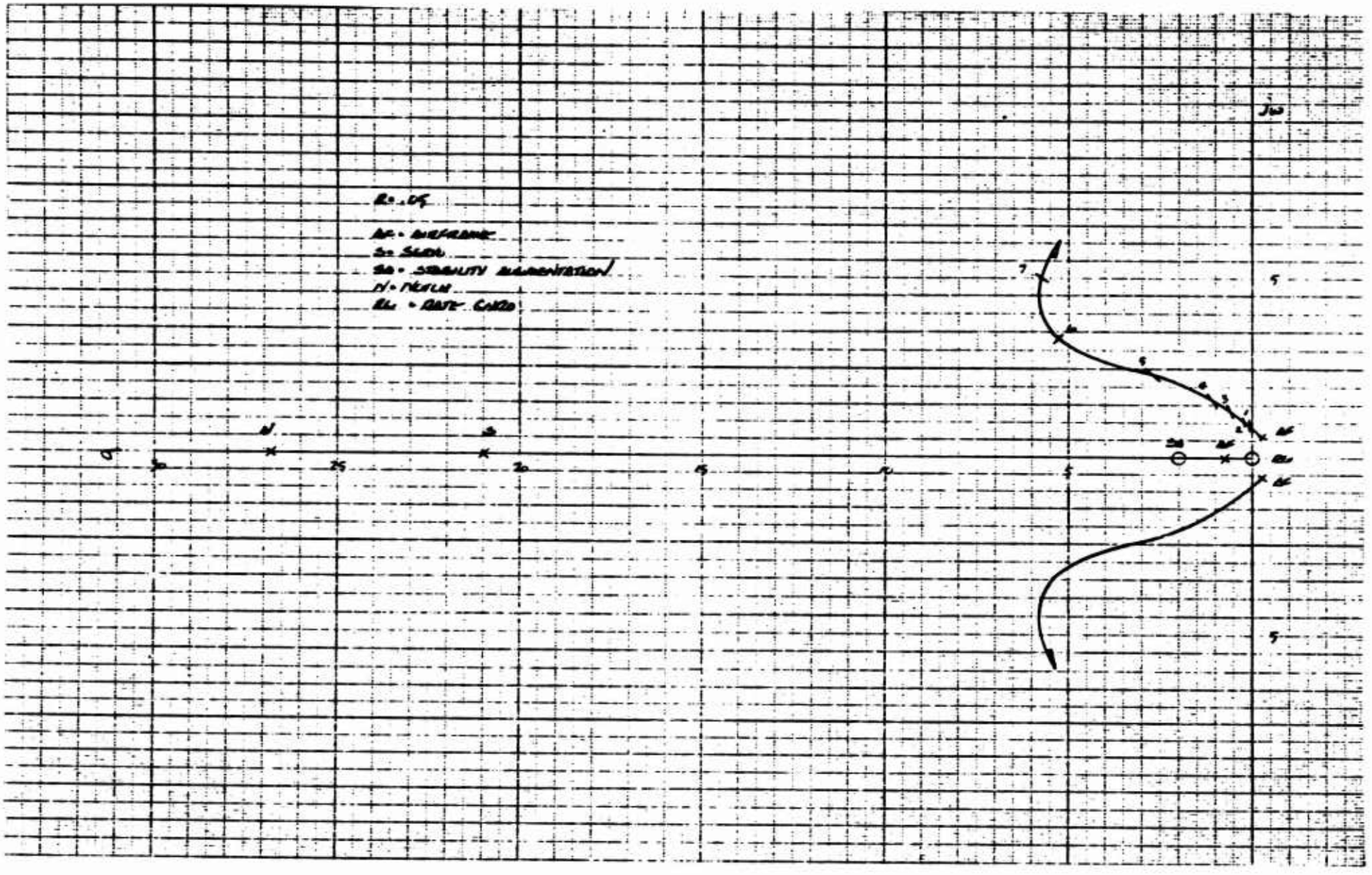

Figure 156 Pitch System Hover Holding Root Locus, R = .05

The numbered positions on these plots are points at which specific gains were computed.

For values of R below .05, gains were computed for the pitch system corresponding to the numbered positions on the corresponding root locus plot shown in the roll root locus study.

As in the roll study, since the airframe cannot be stabilized in pitch at an R of .0025, gains were not computed for this value of R.

The dominant mode in pitch is the second order. The effect of the stability augmentation system on this mode is summarized in the figures and Table 4.

Figure 157 shows also the acceptable regions for location of the dominant 2nd order according to References 3 and 10.

To determine whether or not the simulation agreed with the root locus results, the gain at which the system becomes unstable for a value of R of .10 was determined from both simulation and the corresponding root locus. Reference to Table 4 will show that the results from both sources agreed closely.

3.2.2 Maneuver Mode

In maneuvering mode, rate feedback alone is used to augment the stability of the aircraft. The root locus plots showing the effect of the stability augmentation system on the aircraft in maneuvering mode at hover is shown in Figure 158 for low gain values. At high gain values, the maneuvering mode root locus is identical to the locus drawn for the roll study, (Figure 159).

Subsequent simulator work showed a definite pilot preference for rate damping alone in the pitch axis. The system was modified by permanently shorting the pitch holding capacitor, which then resulted in the pitch system being in the maneuvering mode at all times. The pitch stick switches remained operative, which allowed a different damping value to be selected for the stick-centered and stick-displaced conditions. Figure 159 thus is representative of the pitch "holding" mode with shorted capacitors.

3.2.3 Nose Fan Thrust Reverser Door Resonance

The effect of door resonance on the pitch system with and without the notch filter was also investigated by root locus means.

TABLE 4

EFFECT OF SAS (HOLDING MODE) ON DOMINANT 2ND ORDER

	POINT	RATIO (R)	MAX. NET SA FEEDBACK	DAMPING (ξ)	FREQ. (ω_N)	GAIN** (K_H)	POT SET
PITCH LOCUS	1	.10	15.8 °/°/sec	.30	.80	.017	1.6
	2			.60	1.02	.024	1.9
	3			.85	1.48	.049	2.8
	4			.95	1.68	.061	3.5
	5			1.00	1.75	.068	3.7
ROLL LOCUS	5			1.00	8.0	.073	3.8
	6			.50	10.0	.143	5.3
	7			.10	15.5	.368	6.5
	8	.10	15.8	0	18.5	.509	7.2*
PITCH LOCUS	1	.05	7.9	.05	.90	.029	2.1
	2			.20	1.02	.048	2.9
	3			.40	1.42	.107	5.1
	4			.55	1.95	.270	5.9
	5			.75	3.55	.316	6.2
	6			.85	6.25	.396	6.7
	7	.05	7.9	.75	7.60	.451	6.9
ROLL LOCUS	1	.03	4.74	.40	2.0	.264	5.9
	2			.56	4.8	.955	9.7
	3			.54	7.8	1.48	---
	4			.40	10.4	2.02	---
	5	.03	4.74	.20	14.7	3.59	---

*Stability limit (simulation yields 7)

**× 100 yields % of maximum capability

---Out of range (Max is 10.0 or 1.00 on gain.
Airframe Gain = 3.2 rad/sec^2/rad)

TABLE 4 (Cont)

EFFECT OF SAS (HOLDING MODE) ON DOMINANT 2ND ORDER

	POINT	RATIO (R)	MAX. NET SA FEEDBACK	DAMPING (ξ)	FREQ. (ω_N)	GAIN** (K_H)	POTSET
ROLL LOCUS	6	.03	4.74	.05	19.2	5.70	---
	1	.02	3.16	.20	8.25	.226	5.7
	2	|	|	.14	15.75	.630	7.9
	3	.02	3.16	.05	18.25	.865	9.2
	1	.01	1.58	0	2.85	.25	5.8
	2	.01	1.58	.05	4.85	.56	7.5

**× 100 yields % of maximum capability

---Out of range (Max is 10.0 or 1.00 on gain).
Airframe gain = 3.2 rad/sec^2/rad.

The first estimate was that the second order portion of the servo (including the door linkages, door masses and spring constants) response would be a critically damped mode at 30 cycles/second. This estimate assumed that the door linkage was fairly rigid.

As tested later on the simulator hardware, however, the door/linkage/servo response had a second order mode at 10 cps and a damping ratio of .05.

The change in characteristic of this second order effect was due to the flexibility of the door linkage. This effect was labeled door resonance.

Figures 160 and 161 are plots of the system with and without the notch and with door resonance at a nominal value of 10 cps and .05 damping.

The value of gain at which the system's dominant second order mode becomes unstable is computed for each door resonance case below.

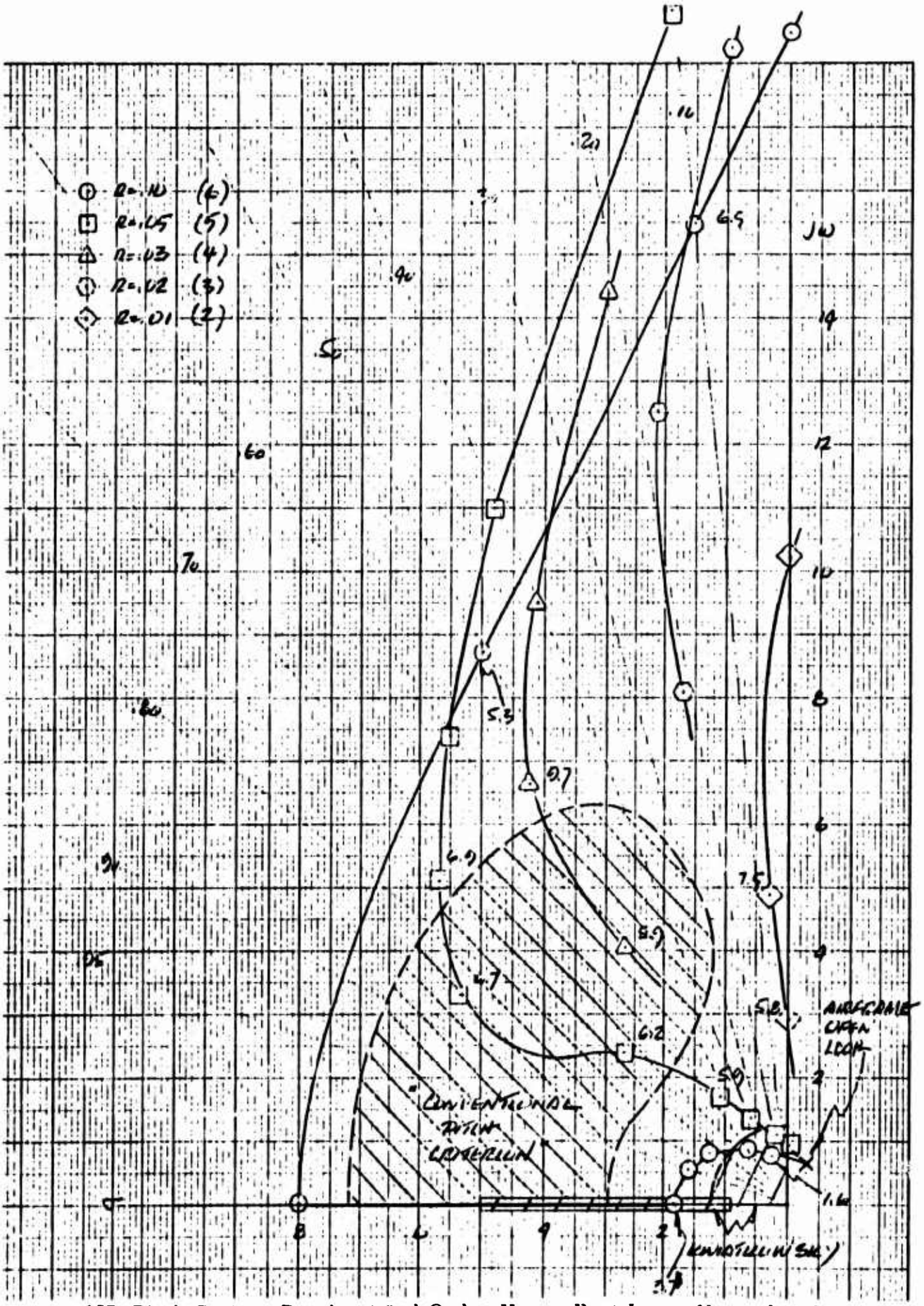

Figure 157 Pitch System Dominant 2nd Order Hover Root Locus Normal Holding Mode

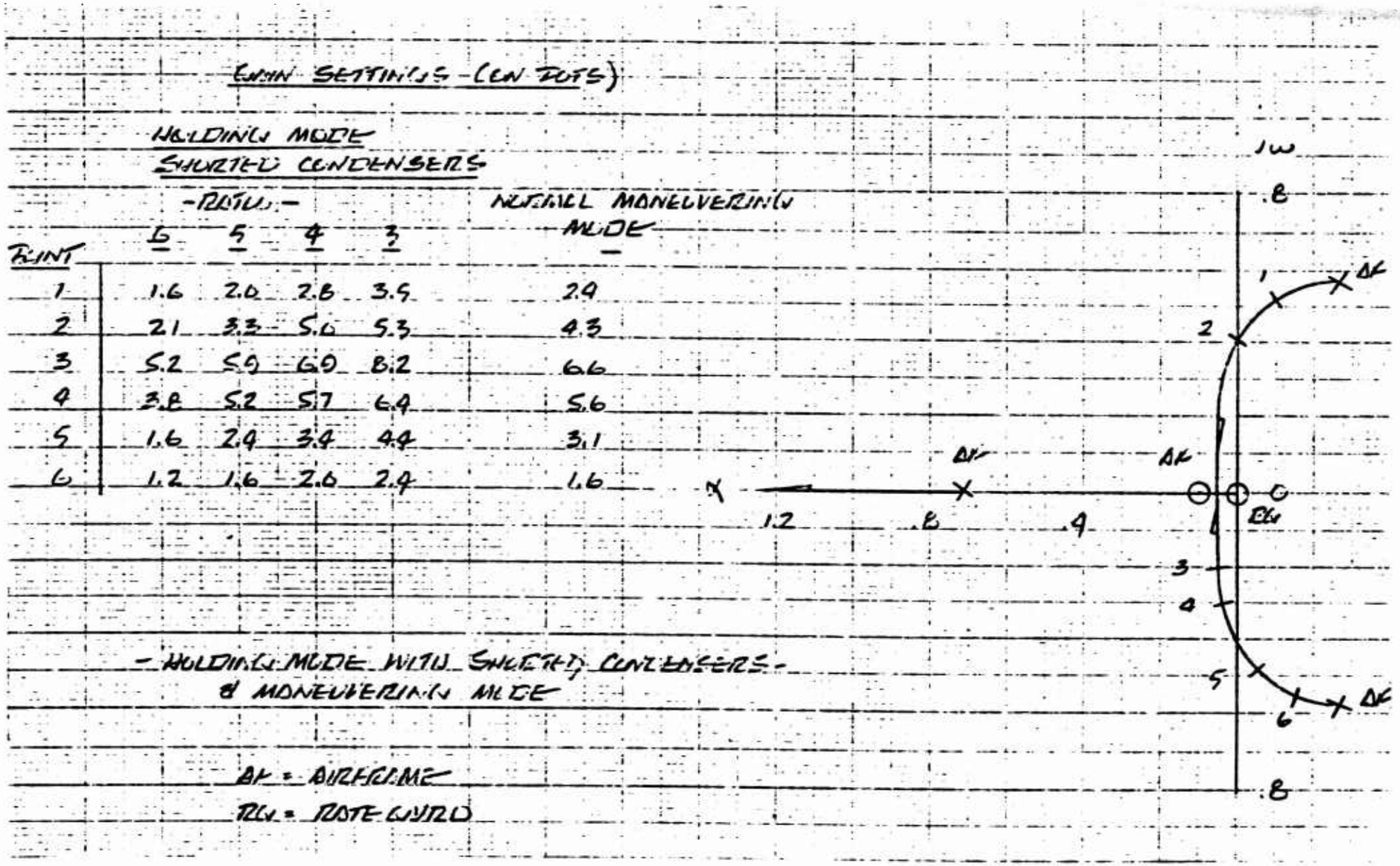

Figure 158 Final Pitch System Hover Root Locus

GAIN SETTINGS (LON. FDTS)

PITCH SET / PLANT	HOVERING MODE SHIELDED CONDENSERS 6	5	4	3	NORMAL MANEUVERING MODE —
7	3.4	5.1	5.6	6.1	5.4
8	4.3	5.4	6.0	6.8	5.6
9	6.1	7.8	10.0	—	9.2
10	—	—	—	—	—

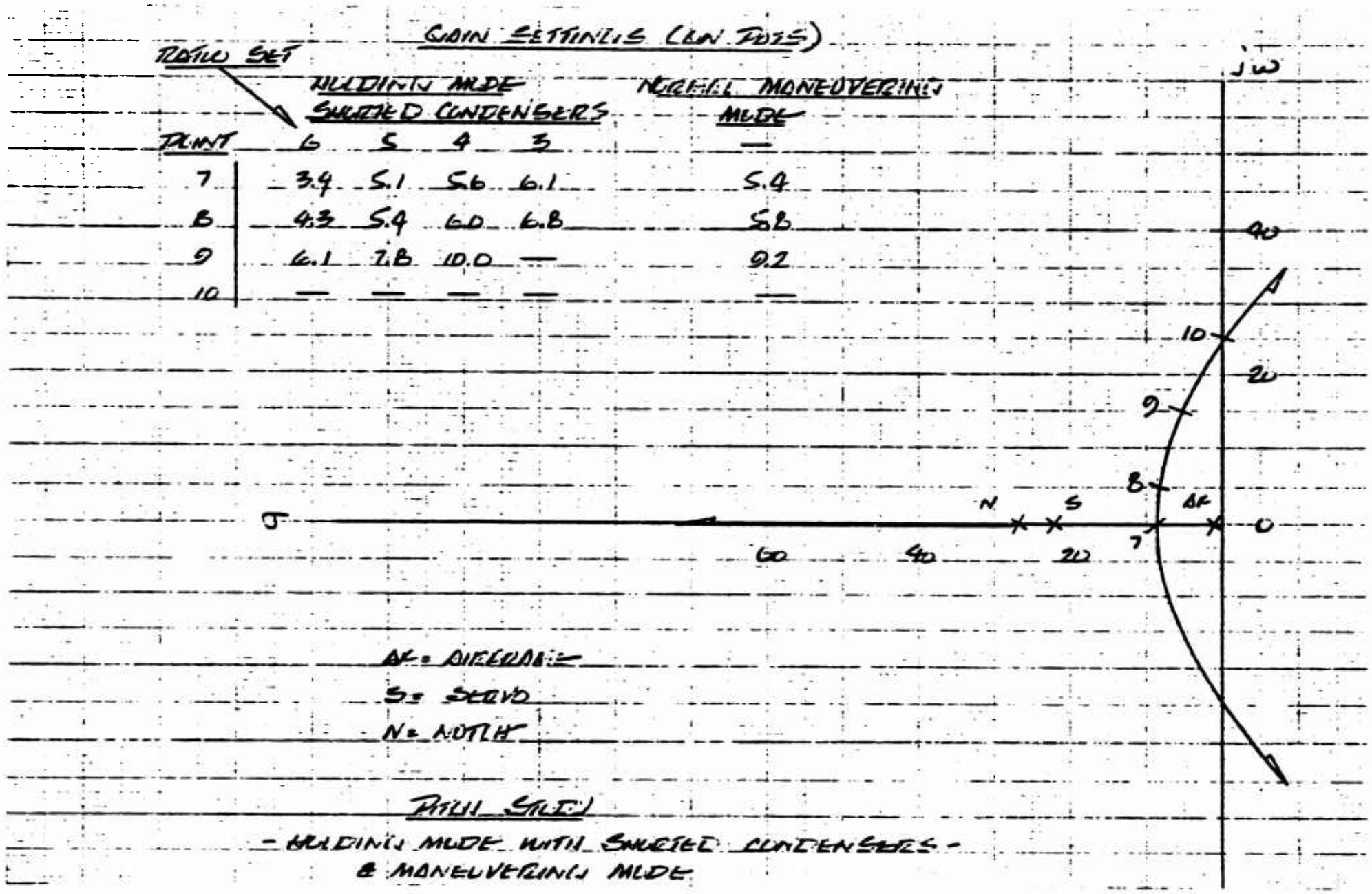

Figure 159 Final Pitch System Hover Root Locus

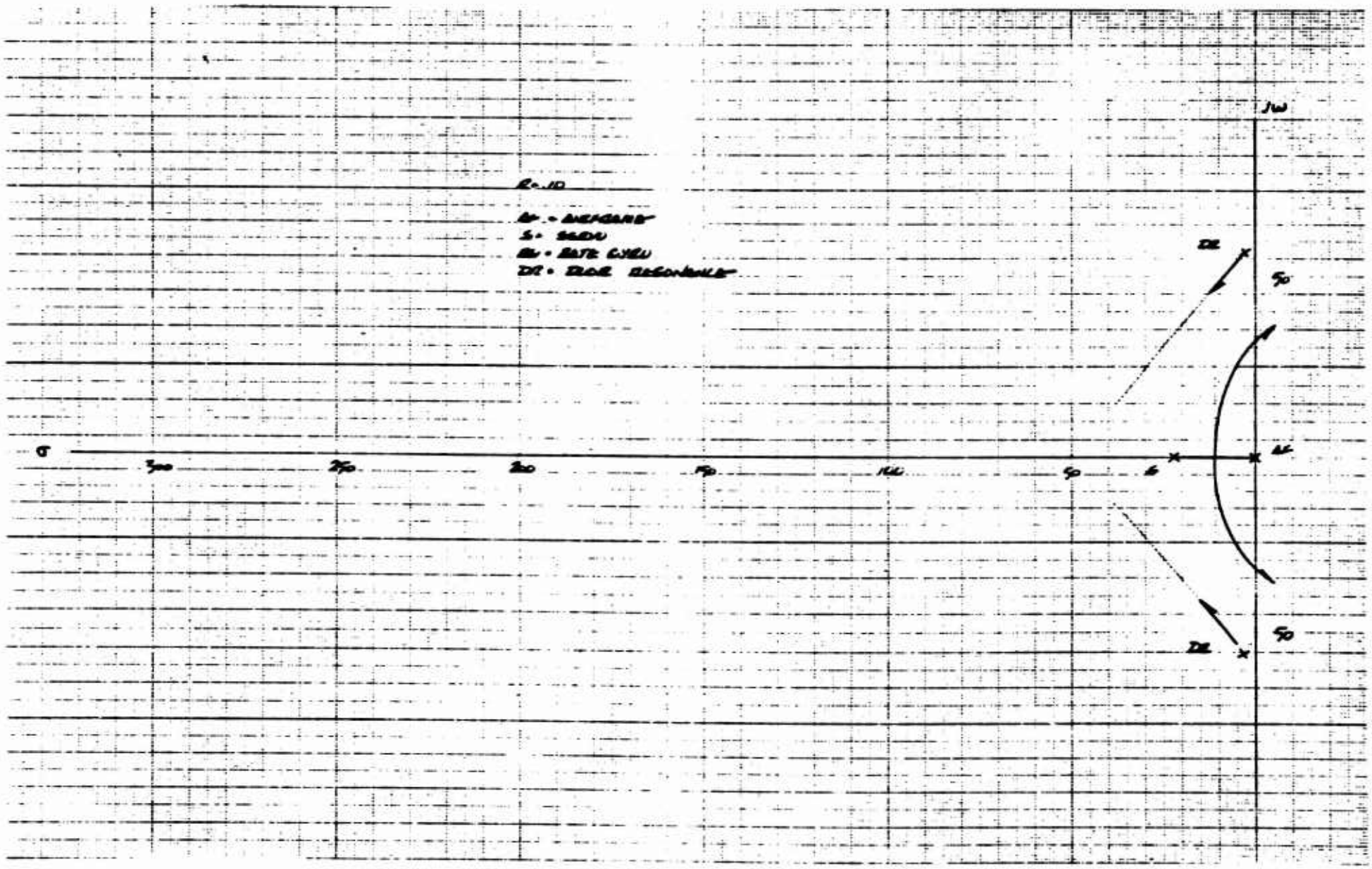

Figure 160 Pitch System Hover Root Locus Including Door Resonance and No Notch

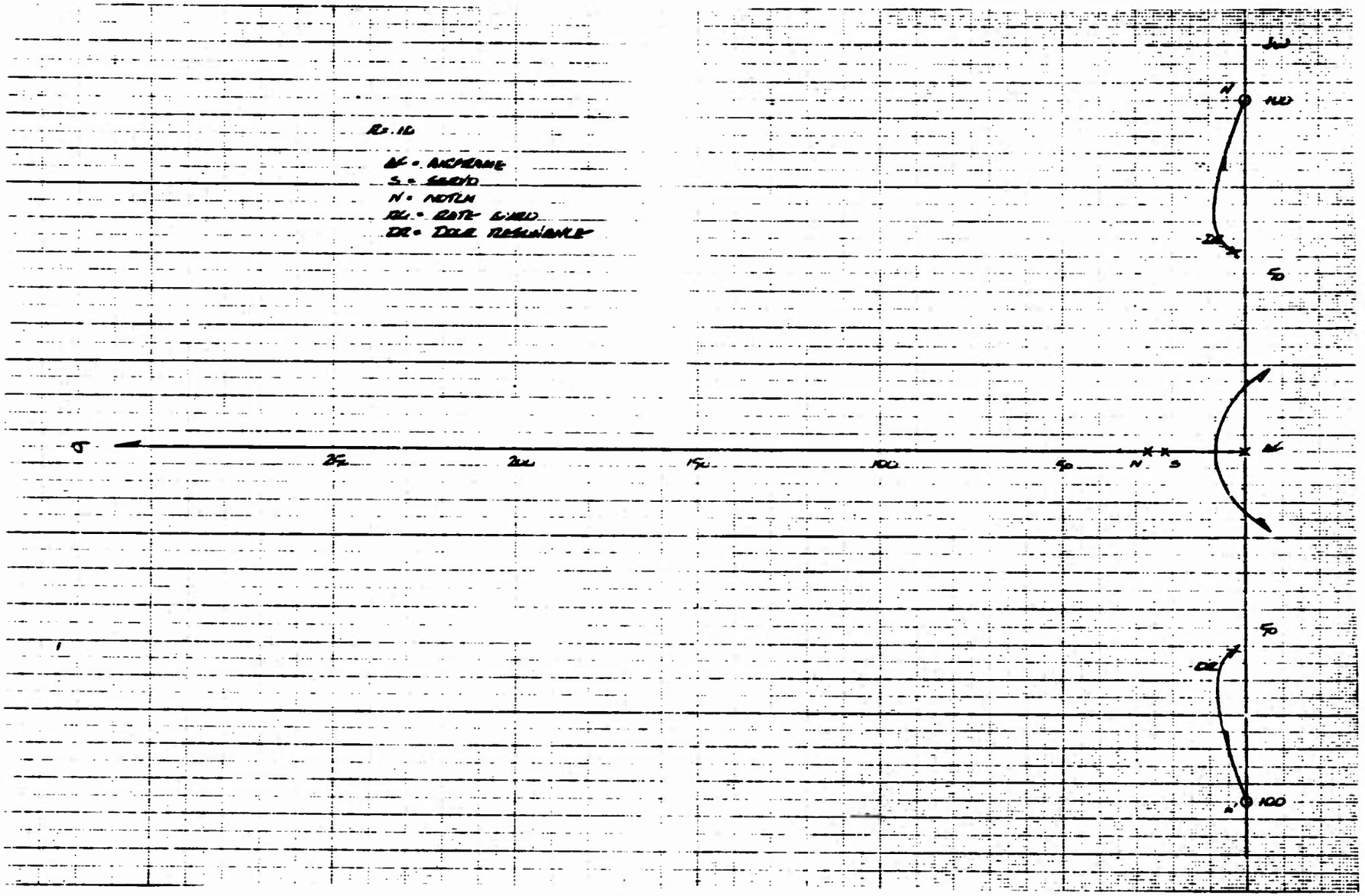

Figure 161 Pitch System Hover Root Locus Including Door Resonance and Notch

CASE	MAX SA FEEDBACK CAPABILITY	ω_N	ξ	GAIN**	POT SET
No Notch and Resonance	27.2 deg/deg/sec	32.0	0	0.437	6.8
Notch and Resonance	15.8 deg/deg/sec	18.5	0	0.505	7.3

NOTES: 1. Nose fan thrust reverser door control effectiveness = 48,000 Ft. Lbs./Rad.
2. **× 100 Yields % of max. feedback capability
3. R = .10, holding mode

Comparison of the product of percentage gain and maximum gain capability in each case with the same product from Table 4 of this section shows that with the notch, door resonance has little effect on the system rigid body modes, while without the notch, door resonance considerably lowers the gain at which the first rigid body mode (the dominant second order) goes unstable.

CASE	REQUIRED FEEDBACK FOR INSTABILITY OF DOMINANT SECOND ORDER
Notch and No Resonance	8.1 deg/deg/sec
Resonance and No Notch	11.9 deg/deg/sec
Resonance and Notch	7.9 deg/deg/sec
No Resonance and No Notch	19.9 deg/deg/sec

3.2.4 Addition of Nose Fan Reverser Door Dampers

During the ground tests of the engines and fans, the reverser doors on the nose fan exhibited large vibrations at or near the door resonance frequency due to excitation resulting from nose fan slipstream turbulence.

The decision was made to add a damper to the nose fan doors to damp the door resonance mode.

Frequency response tests of the nose fan doors after the damper was installed showed a door resonance second order mode of approximately 11.5 cps and a damping ratio of 0.2.

This frequency and damping for the door second order response was not sufficiently changed to justify a new study of resonance effects. Conclusions drawn from the study without the damper are valid.

3.3 FLIGHT SIMULATOR HOVER STUDIES

A study of the handling qualities of the XV-5A in hover was conducted on the simulator.

The purpose of the study was to expose the test pilots to the entire range of handling qualities that the aircraft could exhibit with various settings of the stability augmentation system.

Each "configuration" of the aircraft (a selected set of gains for the autopilot), presented to the pilot, was flown through a given task and then rated by the pilot.

The entire spectrum of possible hover configurations from zero stability augmentation gain to maximum allowable stability augmentation gain was studied and "best" stability augmentation system settings were chosen. A summary of this study is presented below.

3.3.1 Test Method

A comprehensive study of the system required variation of all nine settings of the SA system: holding gain, maneuvering gain and ratio, in yaw, pitch and roll; variation in moments of inertia about all three axes, variation in c.g. position, and variations in steady state and gusty wind conditions.

In order to make the study more practical, the following assumptions were made:

1. Within the range of variations of acceptable yaw axis dynamics, changes in yaw stability augmentation settings would have little or no effect on the pilot rating of the pitch and roll axes.

2. Variations in the moments of inertia are small enough so that a set of gains optimized for a midrange set of moment of inertia values will be negligibly displaced from the optimum set for any other set of moment of inertia values.

3. So long as longitudinal trim is used to trim the stick in pitch before each test, c.g. changes will make no difference in pilot ratings.

4. An RMS wind variation equal in magnitude to 1/2 the steady state wind chosen for any test would represent a realistic wind variation scaling no matter what steady state wind were chosen.

5. A set of gains optimized for the worst wind condition expected during test operation of the vehicle would be acceptable at all other wind conditions.

With these assumptions in mind, the number of variables can be reduced to six, i.e., the stability augmentation settings in pitch and roll.

The aircraft configuration used for the tests is summarized in Table 5.

TABLE 5

W	9200 Lbs.	Yaw Holding	3.5
c.g.	243	Yaw Maneuver	3.5
I_x	4252 Slug/Ft^2	Yaw Ratio	5
I_y	15139 Slug/Ft^2	Wind Steady State	20 Feet/Sec
I_z	17418 Slug/Ft^2	RMS Gust	10 Feet/Sec

3.3.2 Rating System

The Cooper rating scale was employed by the simulator pilots to give a quantitative measure of the acceptability of the aircraft in each gain configuration.

The only problem encountered in the use of the system was a tendency for the pilots to "squeeze the scale", using only numbers from 3 to 6, on the one hand seeming to feel that no configuration was good enough to rate a rating of 1 or 2, and on the other hand, that no configuration was impossible to fly.

Shown in Table 6 is a copy of the Cooper Rating System as used in the test.

TABLE 6

	Adjective Rating	Numerical Rating	Description	Primary Mission Accomplished	Can Be Landed
NORMAL OPERATION	Satisfactory	1.	Excellent, includes optimum	Yes	Yes
		2.	Good, pleasant to fly	Yes	Yes
		3.	Satisfactory, but with mildly unpleasant characteristics	Yes	Yes
EMERGENCY OPERATION	Unsatis-factory	4.	Acceptable but with unpleasant characteristics	Yes	Yes
		5.	Unacceptable for normal operation	Doubt	Yes
		6.	Acceptable for emergency operation only	Doubt	Yes
NO OPERATION	Unaccept-able	7.	Unacceptable even for emergency condition	No	Doubt
		8.	Unacceptable - dangerous	No	No
		9.	Unacceptable - uncontrollable	No	No
	Unprint-able	10.	Scratch aircraft	No	No

COOPER RATING SCALE

3.3.3 Assigned Pilot Mission

Each flight was flown through the same assigned mission which was:

1. Lift off a landing pad and climb to an altitude of approximately 80 feet.

2. Translate to a second landing pad approximately 420 feet away.

3. Hover over this second pad for approximately 1 minute.

4. Land on this second pad.

The entire maneuver was carried out in a gusty wind of 20 feet/second steady state and 10 feet/second RMS variation, with a spectrum defined in Appendix 3.

The direction of the wind relative to the aircraft was as shown below. The pilot was instructed to keep the aircraft pointed toward the second landing pad throughout the flight.

Upon completion of the mission, the pilot was asked to evaluate the ease or difficulty of handling the aircraft in roll and pitch (by the Cooper rating system) and then give an overall rating to the system.

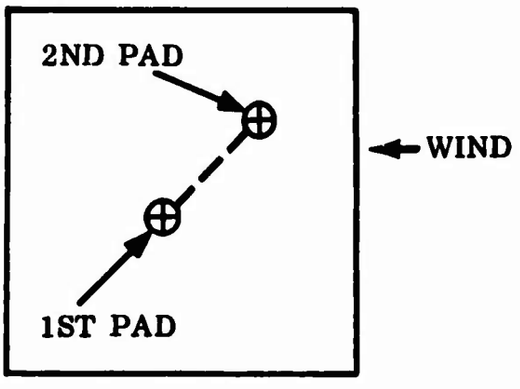

The entire process of aircraft configuration setup, flight of the aircraft through the assigned mission, and evaluation of the aircraft, took about 3.5 minutes/cycle.

3.3.4 Testing Scheme

The method by which the effects of test variable change on the aircraft were evaluated is known as the Greco-Latin Squares testing method.

Traditional methods of testing a system dependent on several variables are built around the idea of changing one variable at a time while holding all the others constant. The Greco-Latin Square testing method, REF. 7, (referred to as the GLS testing method) holds only one variable constant between successive tests while changing all the others. This scheme

affords considerable economy in the number of tests required to evaluate a complex system.

As an output, the GLS testing method provides a second order curve fit in the input variables to the output variable.

Use of the GLS testing methods requires that a series of tests be set up in which the input variables vary as shown in the square of Table 7.

Squares of different sizes can be used; the size determining the maximum number of input variables and, of course, the minimum number of tests required.

Each input variable is required to assume "g" levels, where "g" is the size of the square.

3.3.5 Test Set-Up

The six input variables for the hover study were the roll and pitch, holding gains, maneuvering gains, and ratios.

The possible range of variation of each was divided into 4 equal segments, giving 5 test levels for each test variable as set up on the cockpit panel gain controls of the stability augmentation system.

The test levels chosen for the study are given in Table 8.

Arranging these levels as called out in Table 7 results in Table 9, which denotes the SA settings for each of the 25 test conditions.

In order to make certain the pilot did not develop any prejudice toward particular SA settings during the test, all settings were made by simulator personnel and concealed from the pilot.

3.3.6 Test Results

Shown in Table 10 are the Cooper ratings assigned by the pilot to the aircraft for each of the 25 conditions flown. In addition to the Cooper ratings, complete flight records including ground track were taken for each flight.

TABLE 7

5 X 5 SYMMETRIC SQUARE

b ⟶

a ↓

-2	-2	-1	-2	0	-2	1	-2	2	-2
1	0	2	1	-2	2	-1	-2	0	-1
-1	2	0	-2	1	-1	2	0	-2	1
-2	-1	-1	-1	0	-1	1	-1	2	-1
2	-1	-2	0	-1	1	0	2	1	-2
1	0	2	1	-2	2	-1	-2	0	-1
-2	0	-1	0	0	0	1	0	2	0
-2	-2	-1	-1	0	0	1	1	2	2
-2	-2	-1	-1	0	0	1	1	2	2
-2	1	-1	1	0	1	1	1	2	1
-1	2	0	-2	1	-1	2	0	-2	1
0	1	1	2	2	-2	-2	-1	-1	0
-2	2	-1	2	0	2	1	2	2	2
0	1	1	2	2	-2	-2	-1	-1	0
2	-1	-2	0	-1	1	0	2	1	-2

X_O	X_R
X_1	X_4
X_2	X_3

CODE

$X_R = a$

$X_O = b$

TEST LEVELS OF INPUT VARIABLES
-2, -1, 0, 1, 2

3.3.7 Reduction of Test Results

Two significant results can be derived from the tests. These are:

A. A "most acceptable" aircraft/SA system can be determined.

B. Correlations between pilot rating and chosen performance indices such as x and y deviations from the landing pad during hover over a spot can be determined.

TABLE 8

TEST LEVELS OF INPUT VARIABLES

LEVEL	-2	-1	0	1	2
VARIABLE					
R_R	2	3	4	5	6
H_R	2	3	4	5	6
M_R	2	3	4	5	6
R_P	2	3	4	5	6
H_P	2	3	4	5	6
M_P	1	3	5	7	9

3.3.8 Method of Reduction

The results of the tests were reduced by a digital computer program which provides the coefficients (F) of the following equation. The input variables for this test have been substituted into the equation:

$$Q = F + F_R M_R + F_O M_P + F_1 H_P + F_2 R_P + F_3 R_R \qquad (1)$$

$$+ F_4 H_R + F_{11} H_P^2 + F_{22} R_P^2 + F_{33} R_R^2 + F_{44} H_R^2$$

$$+ F_{12} H_P R_P + F_{13} H_P R_R + F_{14} H_P H_R + F_{23} R_P R_R$$

$$+ F_{24} R_P H_R + F_{34} R_R H_R$$

TABLE 9

PITCH ——————— ROLL

TEST NO.	M_P	H_P	R_P	M_R	H_R	R_R
1	1	5	3	2	4	6
2	3	6	4	2	5	2
3	5	2	5	2	6	3
4	7	3	6	2	2	4
5	9	4	2	2	3	5
6	1	6	5	3	3	4
7	3	2	6	3	4	5
8	5	3	2	3	5	6
9	7	4	3	3	6	2
10	9	5	4	3	2	3
11	1	2	2	4	2	2
12	3	3	3	4	3	3
13	5	4	4	4	4	4
14	7	5	5	4	5	5
15	9	6	6	4	6	6
16	1	3	4	5	6	5
17	3	4	5	5	2	6
18	5	5	6	5	3	2
19	7	6	2	5	4	3
20	9	2	3	5	5	4
21	1	4	6	6	5	3
22	3	5	2	6	6	4
23	5	6	3	6	2	5
24	7	2	4	6	3	6
25	9	3	5	6	4	2
	②	③	①	②	③	①

GRECO-LATIN SQUARES TECHNIQUE
DETERMINATION OF "BEST" SA SETTINGS
PITCH/ROLL SYSTEM IN HOVER

YAW NOMINAL SETS $R_Y = 5.0$, $M_Y = 3.5$, $H_Y = 3.5$

$$\begin{matrix} M_P & M_R \\ H_P & H_R \\ R_P & R_R \end{matrix} \equiv \begin{matrix} X_0 & X_R \\ X_1 & X_4 \\ X_2 & X_3 \end{matrix}$$

TABLE 10

OUTPUT - TEST FOR BEST SA GAINS

COOPER RATING			
TEST NO.	OVER-ALL	ROLL AXIS	PITCH AXIS
1	4	4.5	2.5
2	4	5	3
3	4.5	5	4
4	5	6	4
5	4.5	5	3.5
6	4	4	3
7	4	4	4
8	4	3	4
9	4	5	4
10	4	4	4
11	5	5	5
12	4	5	4
13	4	3	4
14	3	3	3
15	4	4	3
16	3	3	3.5
17	3	3	3
18	4	4	3
19	3	3	3
20	3	3	3
21	2	2	2
22	3	3	3
23	3	3	3
24	2.5	2	3
25	2.5	2.5	2

where:

M_R = Roll Maneuver Gain Setting

M_P = Pitch Maneuver Gain Setting

H_R = Roll Holding Gain Setting

H_P = Pitch Holding Gain Setting

R_R = Roll Ratio Setting

R_P = Pitch Ratio Setting

Q = The desired output variable, in this case, Cooper rating.

As can be seen, the equation shown above does not provide a second order fit in terms of all six variables. The two variables which are assumed to have nearest to a linear effect on the output variable are fit to the first degree only. In our case, the maneuvering gains in the pitch and roll axes were chosen for the first degree fits.

3.3.9 Determination of Best Stability Augmentation System Settings

The test results as reduced by the computer program are shown in Table 10. This Table gives the coefficients fitting the pilot rating of the aircraft (see equation (1) above).

To minimize the pilot rating ("best" performance corresponding to a minimum PR) the derivatives of equation (1) with respect to each of the SA gains was taken. Since the curve fit is linear in M_R and M_P, there are no cross coupling terms involving these variables and minimization of the equation with respect to these two variables can be done indendently of the minimization with respect to the holding made variables, H_R, H_P, R_R and R_P.

The equations resulting from the above differentiations are:

$$\frac{\partial Q}{\partial H_P} = F_1 + 2F_{11}H_P + F_{12}R_P + F_{13}R_R + F_{14}H_R \qquad (2)$$

$$\frac{\partial Q}{\partial R_P} = F_2 + F_{12}H_P + 2F_{22}R_P + F_{23}R_R + F_{24}H_R \qquad (3)$$

$$\frac{\partial Q}{\partial R_R} = F_3 + F_{13}H_P + F_{23}R_P + 2F_{33}R_R + F_{34}H_R \qquad (4)$$

$$\frac{\partial Q}{\partial H_R} = F_4 + F_{14}H_P + F_{24}R_P + F_{34}R_R + 2F_{44}H_R \qquad (5)$$

Setting these equations to zero and substituting the values of the coefficients called out in Table 10, we obtain the following matrix, the solution of which yields the values of the holding variables H_R, H_P, R_R and R_P, which correspond to a minimum pilot rating (since the second order coefficients are all positive).

$$\begin{vmatrix} (H_P) & (R_P) & (R_R) & (H_R) \\ .088 & .033 & .0431 & .0076 \\ .033 & .178 & .0076 & -.047 \\ .043 & .0076 & .0070 & .063 \\ .0076 & -.047 & .0031 & .148 \end{vmatrix} = \begin{vmatrix} .734 \\ .524 \\ .564 \\ .804 \end{vmatrix} \quad (6)$$

The solution of the matrix yields:

$$H_R = 5.04$$

$$R_R = 3.84$$

$$R_P = 4.61$$

$$H_P = 4.30$$

The nearest realizable values for the ratios are positions 4 and 5, respectively.

Reference to Figure 143 of the roll root locus study and Figure 166 of the pitch root locus study in hover shows that the pilots preferred roll and pitch dynamic characteristics which placed the dominant second order mode midway between the acceptable regions for location of this mode as defined in References 3 and 10.

Since the signs of the coefficients of the maneuvering gains are both negative, the optimum setting for both these gains is the highest possible (within the investigated gain range). These gains then should be set at $M_P = 9$ and $M_R = 6$.

The pilot rating corresponding to these best gains then is determined by inserting the following gain values into equation (1):

BEST SA SYSTEM GAINS

$R_R = 4$ $\quad$ $R_P = 5$

$H_R = 5$ $\quad$ $H_P = 4.3$

$M_R = 6$ $\quad$ $M_P = 9$

The pilot rating corresponding to these gain values is 2.32.

3.3.10 Correlations Between Pilot Ratings and Other Performance Indices

Since rather extensive flight records were kept, comparisons between pilot rating and other indices of performance could be made. Several comparisons were attempted and are shown below. Each involved generating a least squares linear fit to the data.

3.3.11 Comparison of Pilot Rating and Maximum Straight Line Deviation

One possible index of performance was the accuracy with which the pilot was able to fly the assigned flight path from his initial to his final hover positions. This path was a straight line, and deviations from it were measured from the ground track record of each flight. These deviations are given in inches in Column 2 of Table 11. The scale factor was 1 inch = 150 feet.

Solving the following equations

$$n K_o + K_1 \Sigma x = \Sigma y \tag{7}$$

$$K_o \Sigma x + K_1 \Sigma x^2 = \Sigma xy \tag{8}$$

where:

n is the number of tests

x is the pilot rating

y is the deviation

will yield the K_o and K_1 required in the following equation,

$$y = K_o + K_1 x, \tag{9}$$

which is the least squares straight line fit to the given data.

This fit is plotted in Figure 162 as well as the data points determined from the test.

3.3.12 Comparison of Pilot Rating and Maximum Hover Deviation

Another possible index of performance was the accuracy with which the pilot could hover over a spot. The maximum deviation from the final hover position was measured from the recorded ground track for each flight. These deviations are given in inches (where 1 inch equals 150 feet) in Table 11, Column 3. The least squares linear fit to this data is plotted in Figure 162 as well as the individual data points for each test.

As can be seen, the correlation between pilot rating and maximum hover deviation is not the strongest.

3.3.13 General Comments on the Hover Study

The study of the aircraft in hover as outlined above accomplished its main tasks, which were to provide the pilot with a look at the entire range of hover handling qualities open to him through adjustment of the stability augmentation system gains. It measured his opinion of the aircraft at each of the gain combinations studied and through the process summarized above, provided a "best", or most likeable, set of gains.

The study did not however exhaust all its possibilities. The data taken is open to a much more complete analysis.

Data taken can be the source of possible correlations between pilot rating and dominant second order root positions, rotational rates and accelerations, linear rates and accelerations, stick displacements and many other possible substitute indices of pilot hovering performance.

Furthermore, more tests might be made which would investigate more thoroughly the effects of winds, weight changes and moment of inertia changes or possible equivalent effects.

General improvements in the study could also be made, such as separating the modes of the stability augmentation system so that the aircraft could be studied while strictly in one mode or the other. A better set of general results would require that the opinions of more than three pilots be averaged.

TABLE 11

HOVER R/P 5

RUN	ST. LINE DEVIATION	HOVERING DEVIATION	PR
1	.99	.29	4
2	1.04	.75	4
3	1.06	.49	4.5
4	.7	.65	5
5	1.1	.51	4.5
6	.95	.62	4
7	1.05	.24	4
8	1.11	.40	4
9	.9	.62	4
10	1.1	.2	4
11	.83	.94	5
12	.85	.36	4
13	.58	1.09	4
14	.625	.49	3
15	.56	.71	4
16	1.05	.36	3
17	.78	.50	3
18	.54	.36	4
19	.51	.71	3
20	.42	.78	3
21	.34	.30	2
22	.38	.50	3
23	.19	.56	3
24	.29	.53	2.5
25	.36	.37	2.5

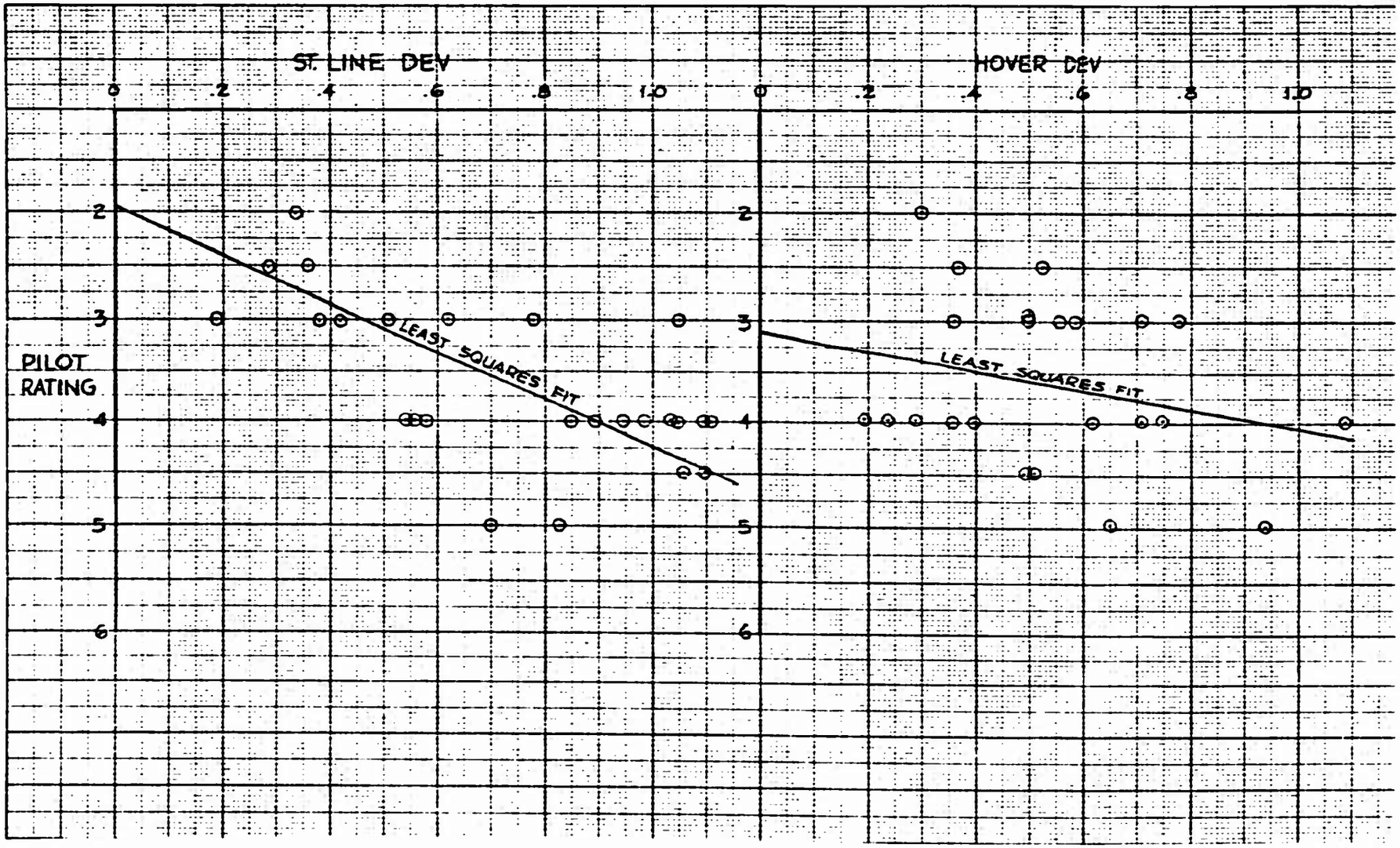

Figure 162 Pilot Rating Versus Straight Line Deviation and Hover Deviation

3.4 FLIGHT SIMULATOR TRANSITION STUDIES

3.4.1 Purpose of Studies

The purpose of the transition study was to answer the following specific questions raised during the predesign and design phases of the program and to specifically determine:

1. Whether or not the aircraft had sufficient pitch control power to accomplish transition at c.g.'s compatible with the requirements of conventional flight.

2. Whether or not the horizontal stabilizer fan mode automatic trim scheme was utilitarian.

3. Whether or not roll-yaw coupling would significantly compromise aircraft handling with increasing vector angles.

4. Whether or not stability augmentation would be required during transition.

5. If stability augmentation was required, whether or not the stability augmentation, as set up for low-speed fan-powered flight, would be acceptable for transition.

6. Whether or not the hardware systems were compatible with the requirements of transition regime flight.

The investigations of these and other problem areas that arose during the transition studies are discussed below.

3.4.2 Initial Transition Flights

Prior to initiation of studies to answer the questions reviewed above, familiarization flights were made by the pilots to determine whether there were any gross errors in the aircraft as simulated, or in the computer and hardware components and simulation schemes themselves.

In particular, the consequences if any of using two sets of data in the simulation of aerodynamic effects as well as somewhat artificial means for switching from one set of data to the other had been questioned. These first flights showed that the transition from low speed to high speed data was smooth, continuous and undetectable by either the pilot or

examination of the recorder outputs. At this point, attention was turned to the specific problem areas called out.

3.4.3 Pitch Control Power

The most significant aerodynamic characteristic of the XV-5A at low speeds is the tendency to pitch up with increasing forward velocity, and to roll out of a sideslip maneuver.

This tendency is due to an apparent fan center of pressure shift in the direction of the relative wind with increasing velocity.

The maximum sideslip velocity is limited by this characteristic to be the velocity at which the fan induced moment becomes equal to the roll control power available.

In forward flight however, pitch control power is provided by the horizontal tail and elevator, as well as the nose fan.

For this reason, the pitch control power provided by the nose fan should not limit forward velocity. The nose fan need only be large enough to provide pitch control power until the tail becomes effective.

To achieve forward velocity, however, the pilot must increase his louver vector angle (or nose the aircraft down). Since $C_{m_{\beta_V}}{}^{s}$ becomes more positive with increasing vector angle (for vector angles below 35°, and the lower velocities of the transition flight regime), vectoring aggravates the pitch control power situation.

Reviewing these facts, it is seen that on the plus side of the control power problem, the following pitch control power sources are effective:

1. A nose fan delivering an amount of pitch control power that remains almost constant with increasing forward velocity.

2. A tail and elevator delivering an amount of pitch control power that increases with the square of the forward velocity.

On the minus side of the pitch control problem, the following factors aggravate the situation:

3. The fan induced moment which is proportional to forward velocity.

4. The decreasing beneficial negative main fan moment which results when the pilot vectors to increase forward velocity, and in doing so rotates the fan lift vector out of the z body axis (accounted for in $\Delta C_{m_{\beta_v}}{}^{s}$ as mentioned above).

Factors 1 thru 3 create the chief pitch control characteristic of the XV-5A in transition.

The surplus of pitch control power available over pitch control power required varies with velocity:

1. Decreasing as the aircraft first comes out of hover, the pitch control power required rises rapidly due to the strong but linear variation in fan induced pitching moment.

2. Reaching a minimum when the rate of increase of tail effectiveness becomes equal to the rate of increase of pitching moment required due to the fan induced moment and,

3. Increasing as the velocity rises above this minimum surplus point due to the rate of increase in tail effectiveness being more rapid than the rate of increase of the required pitch control moment due to the increasing fan induced pitching moment.

For every value of forward velocity, there is a trimmed vector angle and a pitch control power surplus.

A certain portion of this surplus must be retained for the purpose of stabilizing the aircraft against outside disturbances such as gusts.

The remaining surplus is available for countering the adverse pitching moment effect of increasing louver vector angle above the trim value to accelerate the aircraft (ref. to item 4 above) to higher forward velocities.

Shown in Figure 163 is the trim vector angle versus velocity.

Shown in Figure 164 is the maximum vector angle which can be trimmed out in pitch versus velocity.

The difference between these two vector angles represents the amount the pilot can allow the vector angle to "lead" the trim vector angle at any velocity in order to develop the axial force required to accelerate the aircraft to a higher velocity.

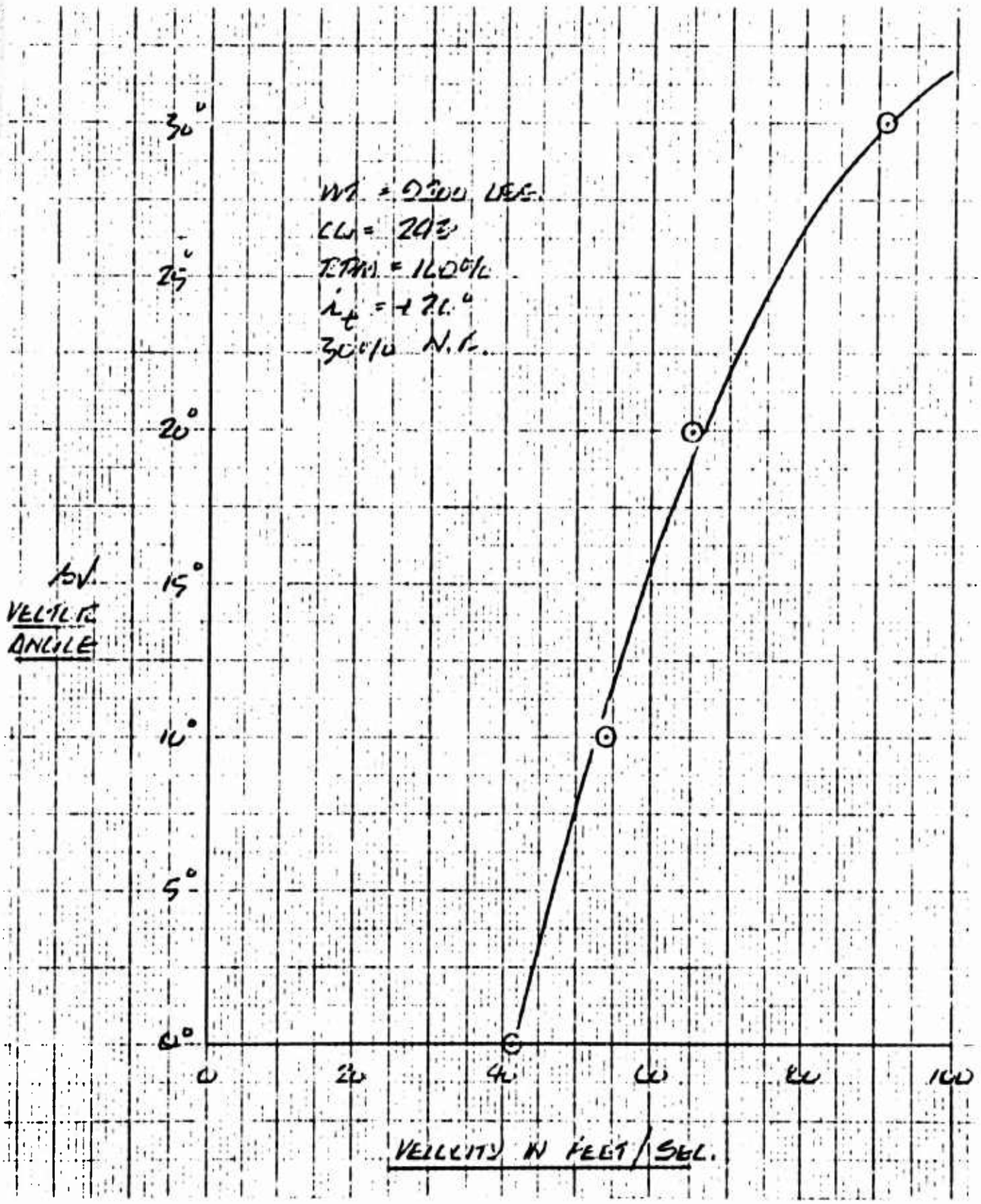

Figure 163 Maximum Trimmed Velocity Versus Vector Angle

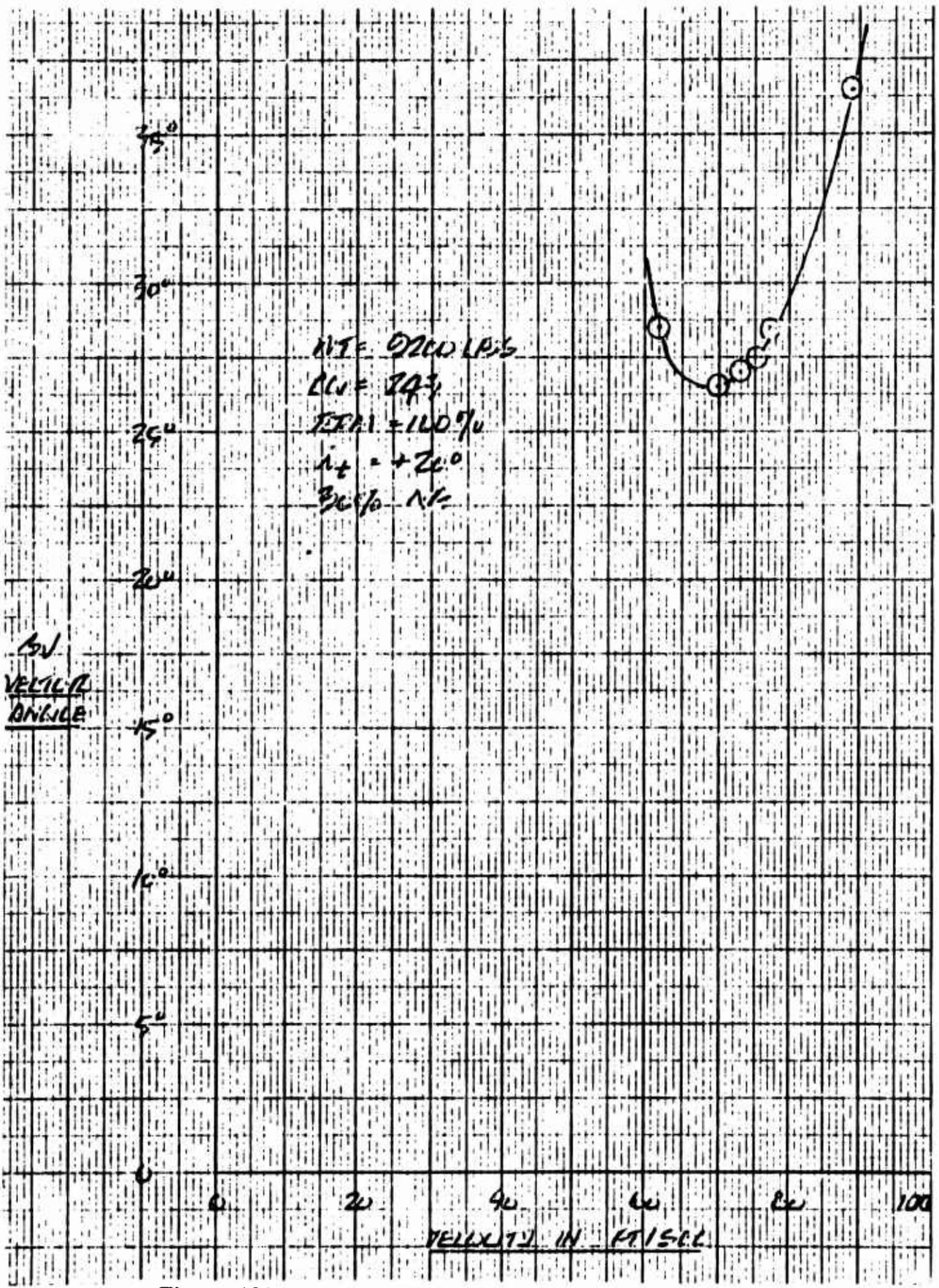

Figure 164 Maximum (Trimmed Pitching Moment) Vector Angle Versus Velocity

This "vector lead" is shown plotted versus velocity in Figure 165.

Figures 163, 164 and 165 are for the nose fan with 30% thrust reversed capability (refer to Section 2.10) and allow no surplus control power for purposes of stabilizing the aircraft against disturbances.

In order to accomplish a constant altitude transition safety, the pilot must limit his vector lead to values somewhat less than those shown in Figure 165.

This vector lead limitation determines the maximum axial acceleration the aircraft can achieve at each velocity for a constant altitude transition. This maximum acceleration, as a function of velocity, determines the minimum time in which a constant altitude transition can be accomplished.

If the pilot wishes to accomplish transition in less than this minimum time, altitude must be sacrificed to achieve the acceleration required to keep the velocity above the minimum needed to accomplish trim at the concurrent vector angle. The vector lead still cannot be exceeded, but with the added acceleration the velocity, and hence trim vector angle, builds up more rapidly, and actual vector can therefore be increased more rapidly.

Shown in Figure 166 are two transition vector angle-velocity plots, the one requiring the most time being the constant altitude transition.

All figures shown are for a 30% thrust reversal nose fan configuration. With the 20% thrust reversal nose fan configuration originally simulated, constant altitude transitions could not be accomplished over the entire range of c.g. positions required for conventional flight.

For a summary of the vectoring method for flight through transition, refer to Section 3.6.

3.4.4 Tail Trim

At the outset of the transition studies, the aircraft had an automatic pitch trim provision. When the stick was displaced longitudinally outside a set of switches located on either side of the longitudinal stick center position, the horizontal stabilizer actuator was activated to drive the stabilizer in such a direction as to move the longitudinal stick trim position back toward center stick.

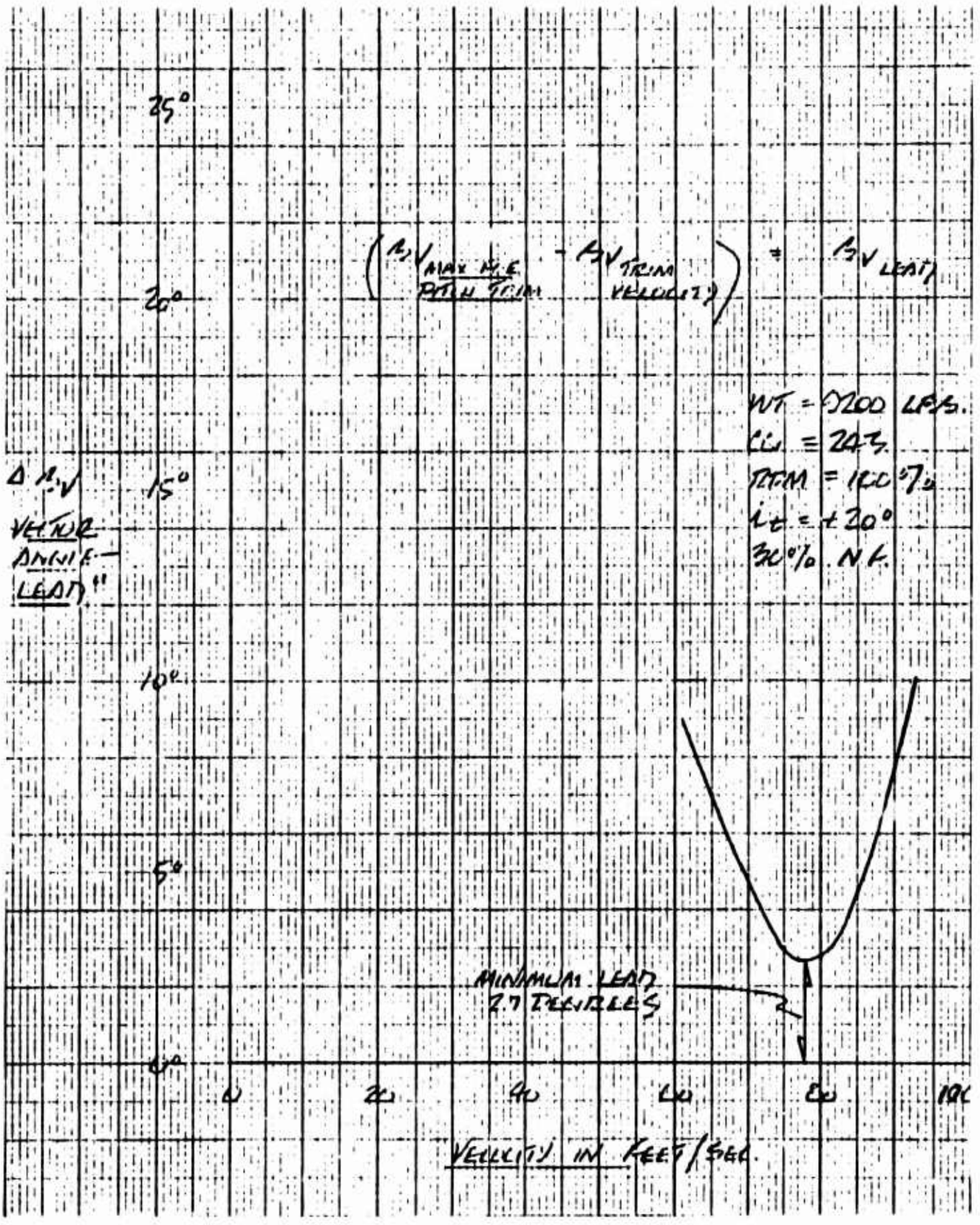

Figure 165 Maximum Vector Lead Versus Velocity

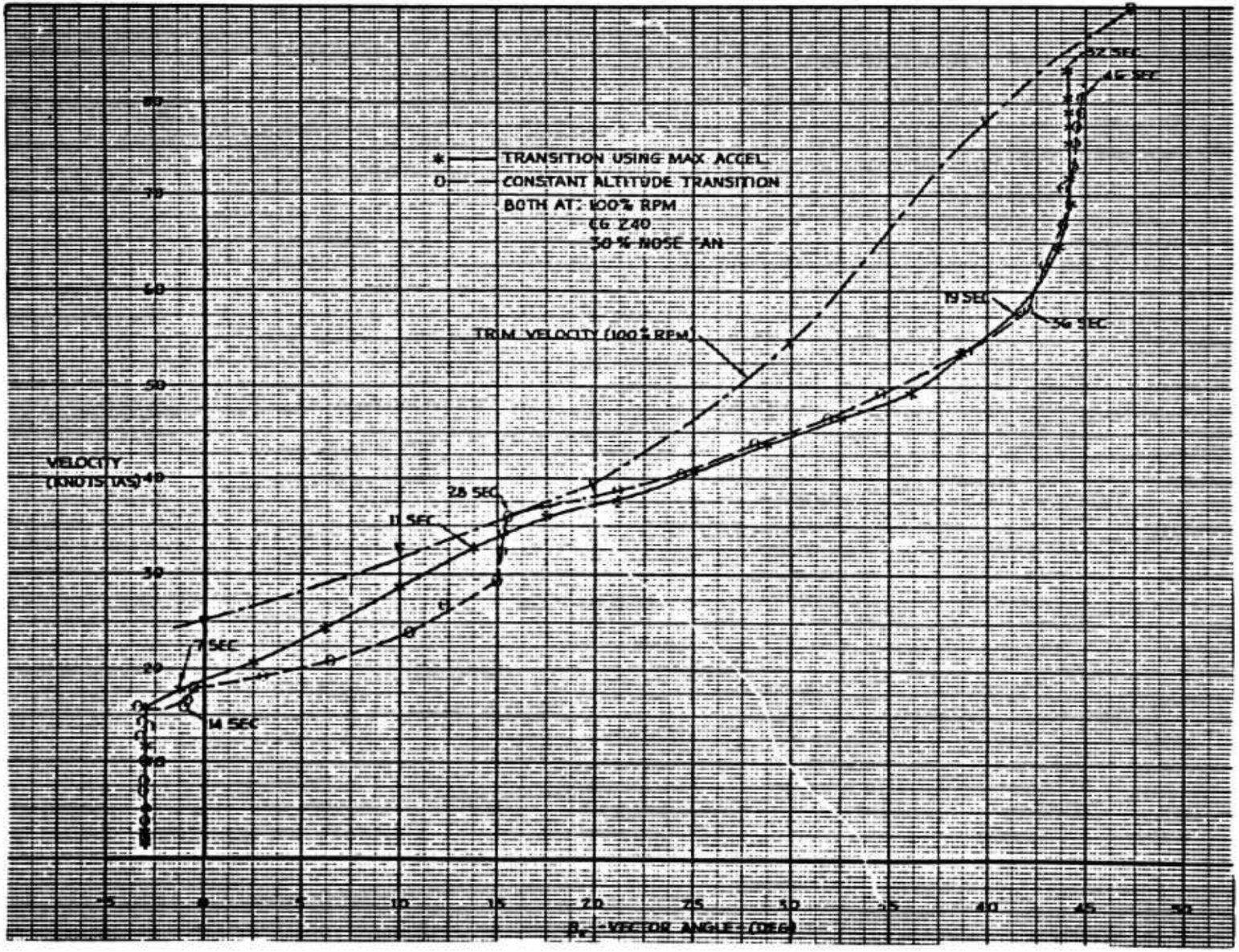

Figure 166 Vector Angle and Velocity Relationships During Transitions

The pilots found this system rather difficult to fly at the velocities associated with vector angles above 20 degrees. At these velocities, the stabilizer encounters sufficient dynamic pressure to become effective, and operating at a rate of 4 degrees per second, it is too powerful and too slow to be useful as a short term control device, and too fast to function as a long period control.

Due to the immense amount of pitch control available from the horizontal stabilizer and its mismatched response rate, the pilots found themselves continuously fighting the system.

To alleviate this problem the system was modified to program the tail to full-up below 40° vector angle, stabilizer trim being accomplished above this point only by pilot actuation of the stick grip trim switch provided. Furthermore, the stabilizer actuation rate was reduced to 2.8 degrees/second. This system was flown by the pilots and found to be very satisfactory.

3.4.5 Hardware

All hardware functioned as expected. In particular, the higher louver vector actuator rate of 50°/15 seconds required by the actuator vendor proved satisfactory.

3.4.6 Stick Forces

In hover the XV-5A uses mechanical springs to provide cockpit control centering and feel for the stick and rudder pedals. These spring forces are phased out with increasing vector angle as the increasing velocities associated with higher vector angles generate enough dynamic pressure so that aerodynamic hinge moments provide stick forces.

The pilots requested that the longitudinal stick trim capability band be increased so that no force would be required to trim the vehicle in pitch at the most forward stick position required during transition.

To accomplish this, the pitch trim authority was changed until the aircraft could be trimmed in pitch hands off at 30° louver vector angle. This requirement and the hover spring gradient requirement set the spring gradient at all vector angles. The pitch spring gradient does not go to zero at 40 degrees vector, but the force gradient level at this point does not objectionably increase total stick force. At $\beta_V = 40°$, the stick grip trim button no longer actuates the spring package trim, but, as discussed previously, commands the horizontal tail.

3.4.7 Cross Coupling

Cross coupling of yaw control inputs into the roll axis, or roll control inputs into the yaw axis was not objectionable at any vector angle with or without stability augmentation.

3.4.8 Stability Augmentation

Stability augmentation turned out to be unnecessary above about 40 knots indicated airspeed.

Further, above 60 knots I.A.S., yaw position feedback, acting through roll/yaw coupling, stabilized the aircraft so completely in roll that the roll control available from the fans was not sufficient for maneuvering unless the yaw mode was in "maneuver."

Also, at velocities above those corresponding to vector angles of 45° a yaw/roll oscillation appeared at the stability augmentation settings determined to be optimum for hover.

To correct these characteristics, the yaw stability augmentation system was converted to a rate damping system. This was done by permanently shorting the capacitor in the amplifier input shaping network.

The effect of cutting out this capacitor is to remove the yaw channel "position memory". When inside the yaw pedal holding mode cutout switches, the system provides a maximum yaw rate feedback which is R/.03 times the maximum yaw rate feedback in maneuvering mode. Thus, two levels of rate gain can be chosen for feedback, through the yaw stability augmentation channel; a lower value for maneuvering and a higher value to keep the aircraft from developing large yaw rates when the rudder pedals are centered and the system is in holding mode. This modification was also incorporated into the SA pitch system. Since the pilot is continuously applying pitch control during transition, it was felt that the "holding" feature would not prove efficacious. The pitch axis has a large inertia, and is therefore less affected than the roll axis by external disturbances, which makes the position reference strictly a pilot option.

This system was re-evaluated in hover by the pilots and found to be completely satisfactory.

In transition flight the new system was also determined to be satisfactory. Not only was the roll control power restored to a reasonable level at all

velocities and vector angles, but the yaw/roll oscillation noted at $\beta_v = 45°$ disappeared, and pitch control was no problem.

3.4.9 Auxiliary Services

As part of the study made of the transition region, the following auxiliary services were performed by the flight simulation facility.

1. Aerodynamics and Performance:

   Checks of aircraft performance included determination of lift and drag totals for trimmed flight throughout the transition region, maximum lift attainable through the transition region, trimmed pitch stick positions, minimum single-engine sink rate in fan-powered flight at various vector angles, and checks of control power at various forward velocities.

   Runs were also made to determine aerodynamic damping and aircraft longitudinal natural frequencies through the transition flight regime.

2. Reliability:

   A rather comprehensive in-flight failure analysis study was run on the simulator. A summary of how this study was mechanized is presented in Section 3.7.

3. Flight Test:

   All portions of the flight test program which could be flown on the flight simulator were run. Shown below is a summary of the runs made. The summary includes runs made for hovering flight. The planned flight test program for the aircraft is presented in Reference 11.

RUN NO.	TEST CONDITION AND PROCEDURE	TEST PURPOSE	REF. 129
1	Hover trim $\beta_V = 0$, Mid-collective, constant engine RPM. Use collective lift for altitude control, evaluate autostab ability to maintain attitude.	Hover capability and attitude hold checks	2IIB and 2IIC p.33, 34
3	Hover over a fixed reference, yaw L&R to predetermined headings to evaluate directional control. Note any pitch or roll coupling, fan RPM change, etc.	"	"
4	Check autostab yaw hold by centering rudder pedals at a steady yawing velocity.	"	"
8	Hovering flight, constant RPM, make a series of small altitude changes and hold new altitude using collective lift only.	Effectiveness of using collective lift stick and/or fan RPM for altitude control	2IIB and 2IIC p.37, 38
9	Hovering flight, mid-collective, make a series of small altitude changes and hold new altitude using throttle control only.	"	"
10	Hovering flight, make a series of small altitude changes and hold new altitude, using combined collective and throttle control.	"	"

RUN NO.	TEST CONDITION AND PROCEDURE	TEST PURPOSE	REF. 129
11	Hover, mid-collective, lateral stick inputs	Altitude control, lateral control at extreme lift stick limits	2IIB and 2IIC p 39, 40
12	Hover, low collective, lateral stick inputs	"	"
13	Hover, full collective, lateral stick inputs	"	"
14	Constant Heading Square	Hover maneuvering characteristics	2IIB and 2IIC p 41, 42
15	Constant radius circle, A/C aimed at center	Hoever maneuvering characteristics	2IIB and 2IIC p 41, 42
16	Pirouettes	"	"
17	Hovering. Yaw SAS off. Turn right and left	Autostab inoperative evaluation	2IIB and 2IIC p 43, 44
18	Hovering. Yaw SAS ON, TURN PITCH SAS OFF. Hover steady state	"	"
19	Hovering. Pitch SAS OFF, TURN ROLL SAS OFF. Hover steady state	"	"
20	If Run 19 is O.K., TURN PITCH SAS OFF ALSO. Hover steady state	"	"
21	If Run 20 is O.K., TURN YAW SAS OFF & EVALUATE. If O.K., attempt a VTOL landing	"	"

RUN NO.	TEST CONDITION AND PROCEDURE	TEST PURPOSE	REF. 129
22	Trim at given vector angle, note trim A/S straight and level. Push to increase speed, stabilize, pull to decrease speed, stabilize. Note forces and control position	Translation, stability and control VTOL	1IIB and 2IIE p 47, 48
22a	β_V = 0° Note limit speed	20-243, 30-243, 30-246	"
b	5°	"	
c	10°	"	
d	15°	" " "	
g	30°	" " "	
i	40°	" " "	
j	45°	" " "	
23	Hover mid-collective, β_V = 0, trim. Vector to β_V = 5°, hold altitude w/collector. Note IAS, control position and force. DO NOT RE-TRIM. At β_V = 5° push to limit speed holding altitude. Decelerate to hover	Translation limit speed at 5° vector angle. Static longitudinal stability	1IIB and 2IIE p 49, 50
24	From β_V = 0, hover trim, accelerate to limit speed with β_V = 5° and attitude change. Hold attitude. Decelerate to hover at β_V = 0°	"	"

RUN NO.	TEST CONDITION AND PROCEDURE	TEST PURPOSE	REF. 129
25	Hover mid-collective, $\beta_v = 0$, trim. Vector to $\beta_v = 10°$, hold altitude with collective. Note IAS, control position and force. DO NOT RETRIM. At $\beta_v = 10°$, push to limit speed holding altitude. Decelerate to $\beta_v = 10°$ trim IAS, vector to zero	Static longitudinal stability	1IIB and 2IIE p 51, 52
26	Accelerate to Bv = 10° limit speed by combined vector and attitude change. Hold altitude. Decelerate to hover	"	"
27	From hover, vector rapidly to $\beta_v = 15°$, then slowly to $\beta_v = 20°$. When possible, vector at level attitude, then pitch to limit speed. Decelerate to Bv = 0 by continuous vectoring	Static longitudinal stability; behavior response with different vectoring rates	1IIB and 2IIE p 55, 56, 57
29	From hover, vector rapidly to 20°, then slowly to 25°	"	"
31	From hover, vector rapidly to 25°, then slowly to 30°	"	"
33	From hover, vector rapidly to 30°, then slowly to 35°	"	"
35	From hover, vector rapidly to 35°, then slowly to 40°	"	"

RUN NO.	TEST CONDITION AND PROCEDURE	TEST PURPOSE	REF. 129
37	From hover, vector rapidly to 40°, then slowly to 45°	Static longitudinal stability; behavior response with different vectoring rates	1IIB and 2IIE p 55, 56, 57
39	From hover, vector rapidly to 45°	"	"
41	β_v = 30° Level flight. Stability augmentation system on and off	Longitudinal evaluation of autostab at β_v = 30° Lateral evaluation of autostab at β_v = 30°	1IIB and 2IIE p 55, 56, 57
42	β_v = 30° Level flight. Stability augmentation system on and off	"	"
43	One engine β_v = 15°, stabilize rate of climb for 45 KIAS	Emergency Vertical Velocity Control VTOL	2IIF p 63, 64
44	One engine β_v = 15°, stabilize rate of climb for 55 KIAS	"	"
44b	One engine β_v = 15°, stabilize rate of climb for 60 KIAS	"	"
45	One engine β_v = 15°, stabilize rate of climb for 65 KIAS	"	"
45b	One engine β_v = 15°, stabilize rate of climb for 70 KIAS	"	"
47	One engine β_v = 20°, stabilize rate of climb for 55 KIAS	"	"

RUN NO.	TEST CONDITION AND PROCEDURE	TEST PURPOSE	REF. 129
47b	One engine $\beta_V = 20°$, stabilize rate of climb for 60 KIAS	Emergency Vertical Velocity Control, VTOL	2IIF p 63, 64
48	One engine $\beta_V = 20°$, stabilize rate of climb for 65 KIAS	"	"
49	One engine $\beta_V = 30°$, stabilize rate of climb for 45 KIAS	"	"
49b	One engine $\beta_V = 30°$, stabilize rate of climb for 50 KIAS	"	"
50	One engine $\beta_V = 30°$, stabilize rate of climb for 55 KIAS	"	"
50b	One engine $\beta_V = 30°$, stabilize rate of climb for 60 KIAS	"	"
51	One engine $\beta_V = 30°$, stabilize rate of climb for 65 KIAS	"	"
52	One engine $\beta_V = 40°$, stabilize rate of climb for 45 KIAS	"	"
53	One engine $\beta_V = 40°$, stabilize rate of climb for 55 KIAS	"	"
53b	One engine $\beta_V = 40°$, stabilize rate of climb for 60 KIAS	"	"

RUN NO.	TEST CONDITION AND PROCEDURE	TEST PURPOSE	REF. 129
54	One engine $\beta_v = 40°$, stabilize rate of climb for 65 KIAS	Emergency Vertical Velocity Control, VTOL	2IIF p 63, 64
54b	One engine $\beta_v = 40°$, stabilize rate of climb for 70 KIAS	"	"
101	One engine, $\beta_v = 15°$, push to increase IAS, Vector to 40°	"	"
55	Hover trim, $\beta_v = 0°$. Push to increase speed, release stick. Pull to decrease speed, release	Long period longitudinal stability, VTOL	1IIB p 79
56	Trim $\beta_v = 15°$, straight and level. Push to increase speed, release. Pull to decrease speed, release	Long period longitudinal stability	1IIB p 79
59	Hover trim, $\beta_v = 0°$ rapidly push stick and release. Rapidly pull stick and release	Short period longitudinal stability	1IIB p 81
60	Trim $\beta_v = 15°$, straight and level. Rapidly push stick and release. Rapidly pull stick and release	"	"
65	Trim $\beta_v = 15°$, straight and level. Perform constant heading sideslips; apply left rudder in 5° increments and bank opposite to maintain constant heading. Continue until rudder or aileron limit is reached	Static lateral-directional stability	1IIB p 83

RUN NO.	TEST CONDITION AND PROCEDURE	TEST PURPOSE	REF. 129
66	β_v = 15°, Right Rudder Sideslips	Static Lateral - Directional stability	IIIB - p 83
67	β_v = 30°, Left Rudder Sideslips	"	"
68	β_v = 30°, Right Rudder Sideslips	"	"
69	β_v = 45°, Left Rudder Sideslips	"	"
70	β_v = 45°, Right Rudder Sideslips	"	"
72	From Max. sideslip of 65 and 66, release controls	Dynamic Lateral - Directional Stability	IIIB p 85
73	From Max. sideslip of 67 and 68, release controls	"	"
74	From Max. sideslip of 69 and 70, release controls	"	"
75	Hover trim, β_v = 0, establish steady bank to left, roll rapidly to stabilized right bank, roll rapidly to stabilized left bank	Rate of roll and adverse yaw	IIIB p 87, 88
76	Trim at β_v = 15°, straight and level, repeat 75	"	"
77	Trim straight and level at β_v = 30°, repeat 75	"	"
78	Trim straight and level at β_v = 45°, repeat 75	"	"

RUN NO.	TEST CONDITION AND PROCEDURE	TEST PURPOSE	REF. 129
79	Preconvert CTOL mode, handling characteristics	Transition build-up, CTOL. Investigate low speed characteristics	2II-I p 61
80	From procedures of runs 27-42, determine optimum technique for accelerating to and decelerating from transition speed. Ease of control and pilot confidence are objectives	Transition build-up, VTOL	2IIIA p 67
81	Ascend VTOL, transition and convert CTOL, convert to VTOL and decelerate. Run "typical" transitions	Transition technique refinement	2IIIB, 2IIIC p 69, 70, 71, 72
82	Trim straight and level at $\beta_V = 40°$, vector rapidly to 45° and convert CTOL	Low speed conversion	
83	Hover $\beta_V = 0$, down collective. Long period longitudinal	Stability evaluation	
84	Hover $\beta_V = 0$, down collective. Short period longitudinal	"	
85	Hover $\beta_V = 0$, up collective. Long period longitudinal	"	
86	Hover $\beta_V = 0$, up collective. Short period longitudinal	"	
89	$\beta_V = 0°$, 10 KIAS trim. Longitudinal, lateral, directional upsets	Stability	

RUN NO.	TEST CONDITION AND PROCEDURE	TEST PURPOSE	REF. 129
90	$\beta_v = 0$, limit speed. Longitudinal, lateral, directional upsets	Stability	
91	$\beta_v = 5°$, trim level. Longitudinal, lateral, directional upsets.	Stability	
92	$\beta_v = 10°$, trim level. Longitudinal, lateral, directional upsets	Stability	

3.5 FLIGHT SIMULATOR CONVERSION STUDIES

The conversion sequence from fan-powered to conventional flight is as follows:

Initial Tail Incidence approximately 15° up.

1. At initiation of conversion, the tail starts toward full down immediately.

2. If tail is moving, the diverter actuates .3 sec. after start of sequence.

3. Wing fan closure doors start closing after the diverter has travelled its full stroke.

4. If the diverter does not begin motion within .5 sec. of tail first motion, the tail stops. and the wing fan closure doors remain open.

The conversion sequence from conventional to fan-powered flight is as follows:

1. The fan doors start open.

2. When the fan doors are 2/3 open (in about 1 sec.), the tail starts toward +10°, and at first tail motion the diverter starts.

3. If the diverter does not complete its stroke within .2 sec., the tail motion stops.

During the conversion cycle, the tail moves at 7.5 deg./sec. The conversion sequence is essentially the same as described in reference 1, and this portion of the simulation was a double-check on the previous work.

In general, conversions in either direction result in a transient variation of normal acceleration of about .5g. Conventional to fan results in a peak load factor of 1.5, and fan to conventional results in a minimum load factor of .5. It is felt that these figures will be improved upon under actual flight conditions because, in the simulator, the pilot must respond entirely to visual cues. While in the aircraft, the pilot will sense any load factor transients and make appropriate corrections.

Figures 167 through 170 includes recorder traces of a typical conventional to fan conversion. These traces are typical, and were not chosen to show more favorable results. In this conversion, a pilot-induced oscillation in normal acceleration occurred, but with peaks within ± .5g of lift equals weight. It is felt that these transients will be minimized by load factor cues in the actual airplane, whereas in the simulator, rate of climb is the highest derivative displayed.

Figures 171 thorugh 174 is a conversion from fan to conventional flight, and about the same characteristics are apparent.

These conversions were flown with the pilot directing most attention to the IVSI in an attempt to hold rate-of-climb to zero.

3. 5. 1 Time Histories

Figures 175 through 179 are time-history recordings of flight throughout the complete fan-powered and low-speed conventional flight regimes, including hover, transition and conversions in both directions.

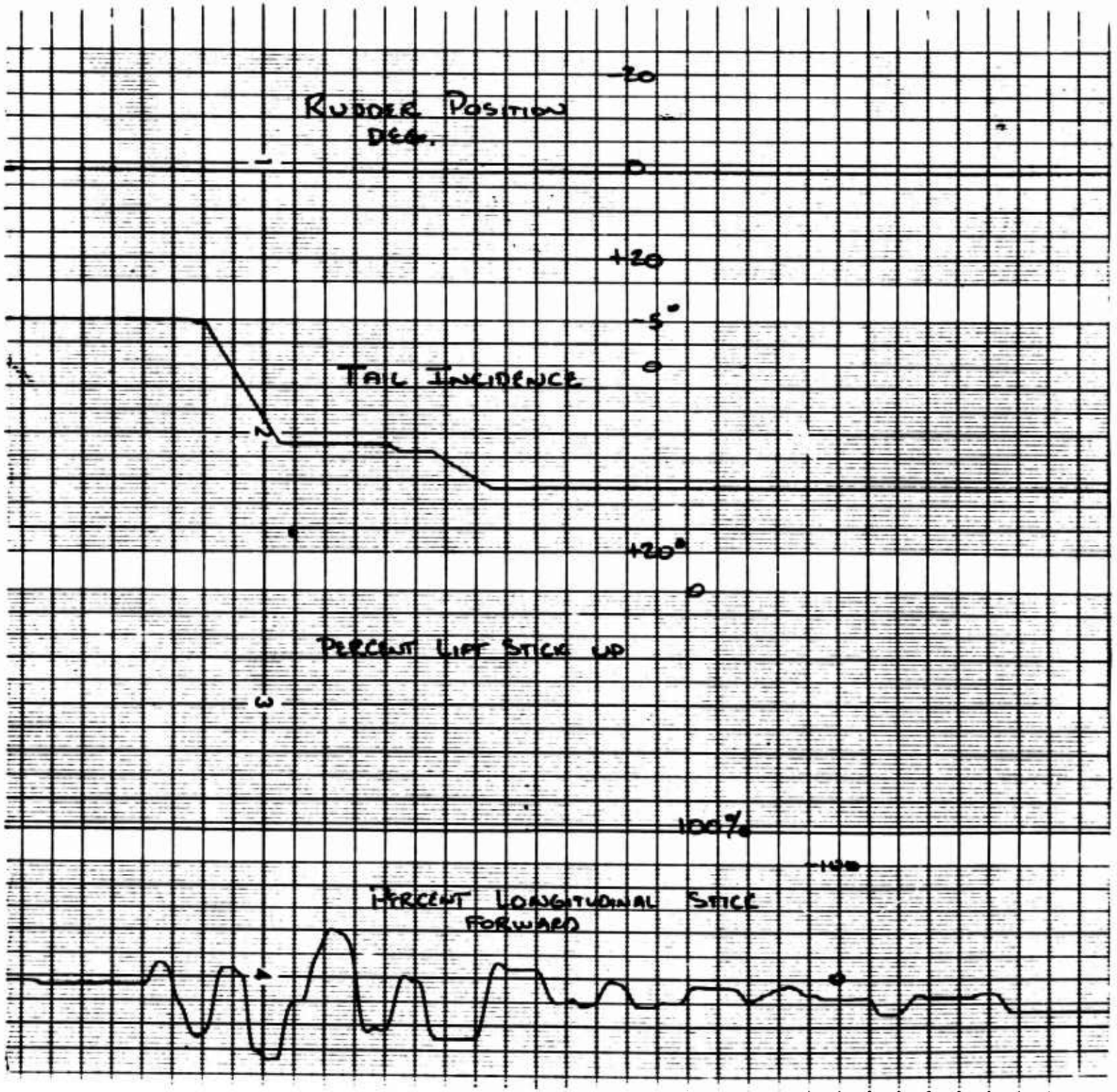
RUDDER POSITION
DEG.
-20
0
+20
TAIL INCIDENCE
-5°
0
+20°
0
PERCENT LIFT STICK UP
100%
-100
PERCENT LONGITUDINAL STICK
FORWARD

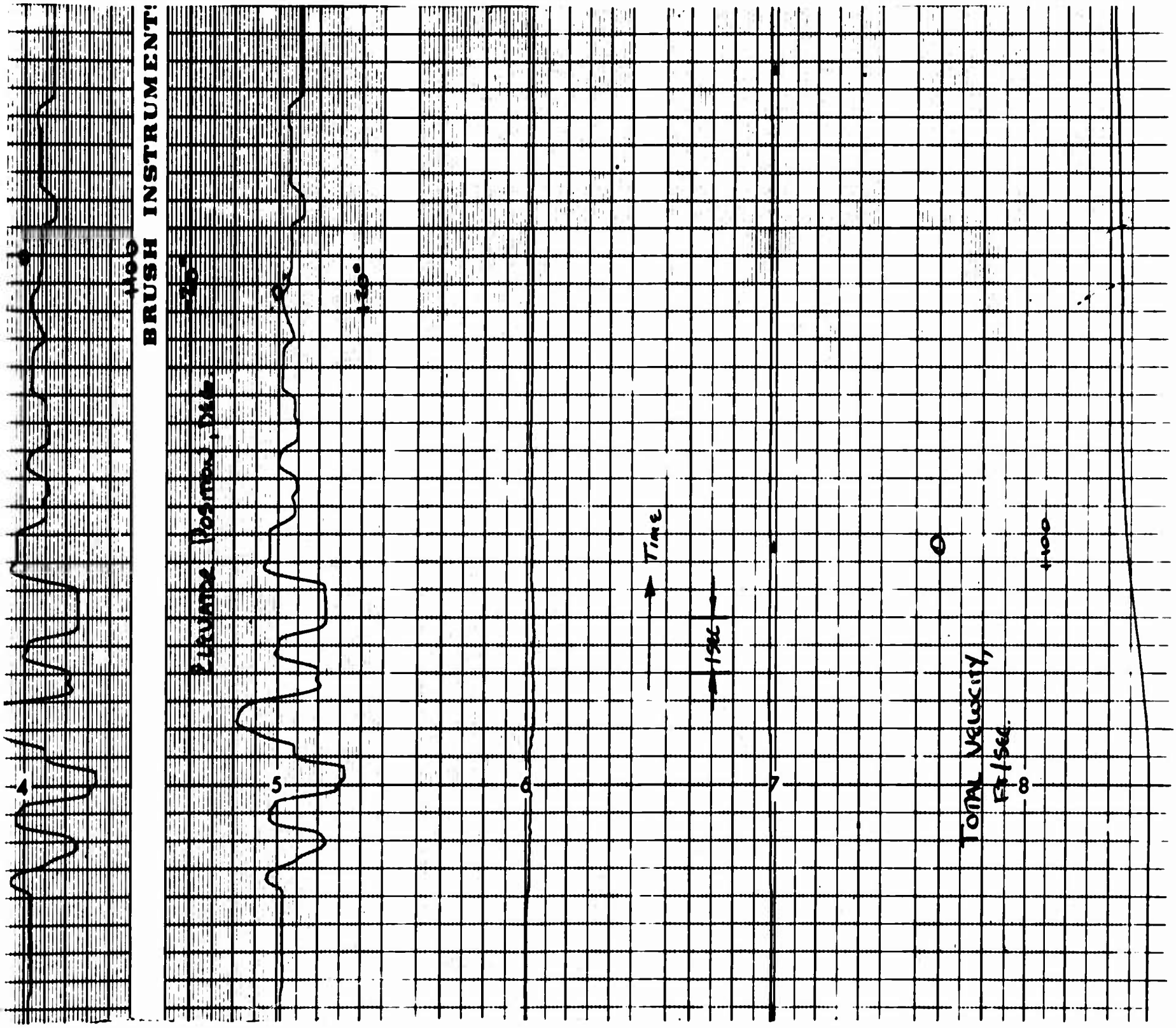

Figure 167 Conventional to Fan Conversion Time History, Pace 231R Brush Recorder

B

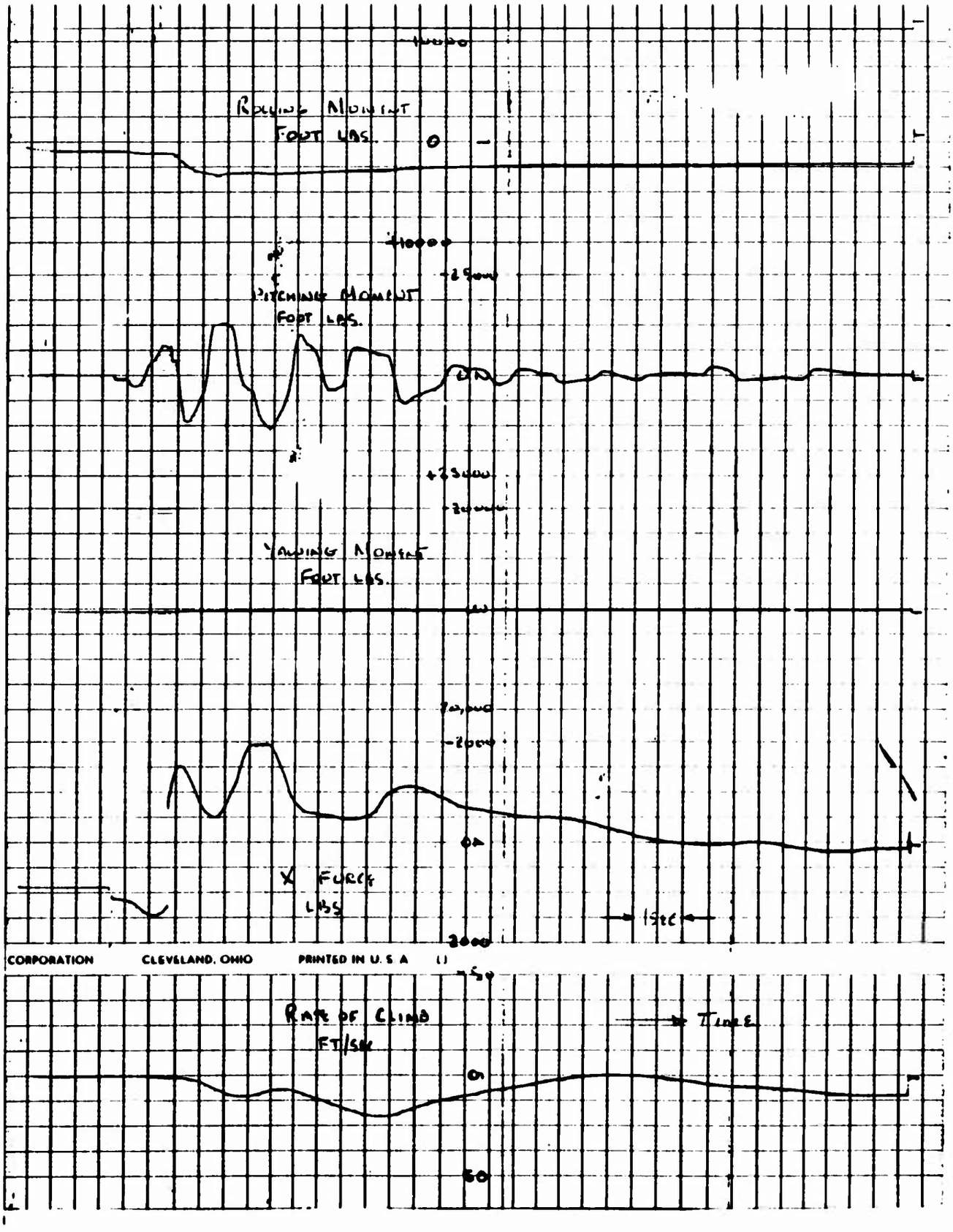

Figure 168 Conventional to Fan Conversion Time History, Pace 231R Sanborn Recorder

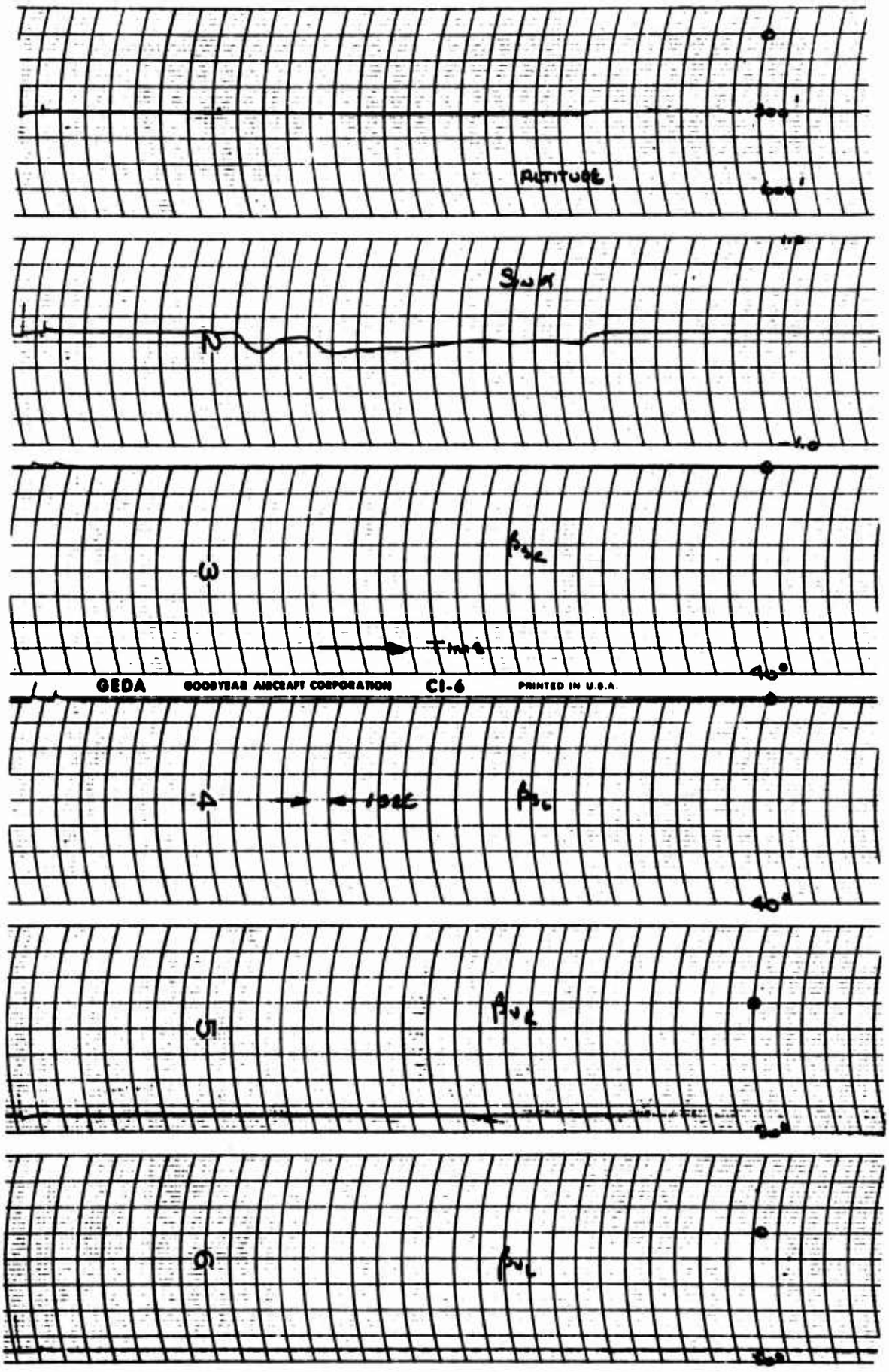

Figure 169 Conventional to Fan Conversion Time History, Pace D Recorder

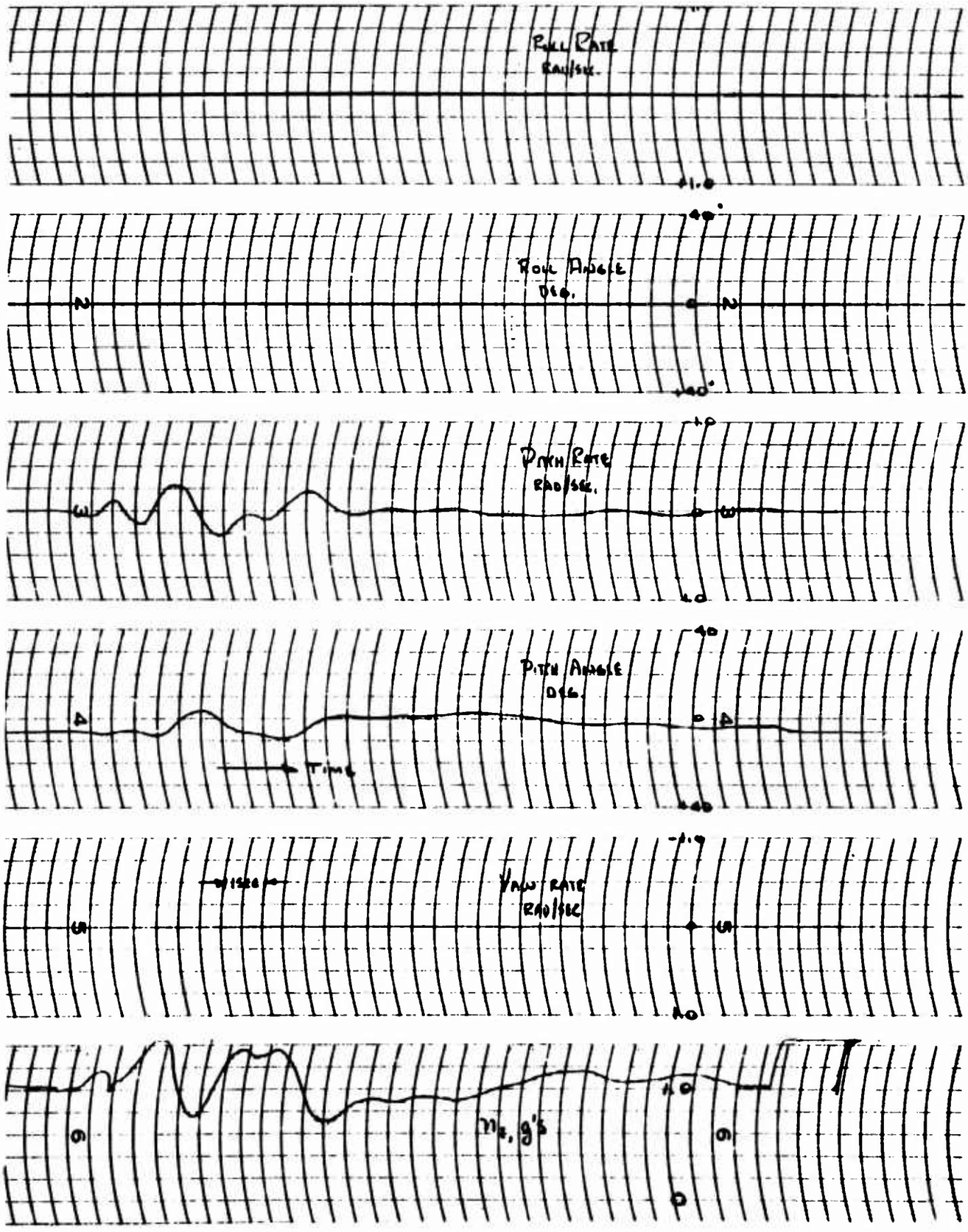

Figure 170 Conventional to Fan Conversion Time History, Pace E Recorder

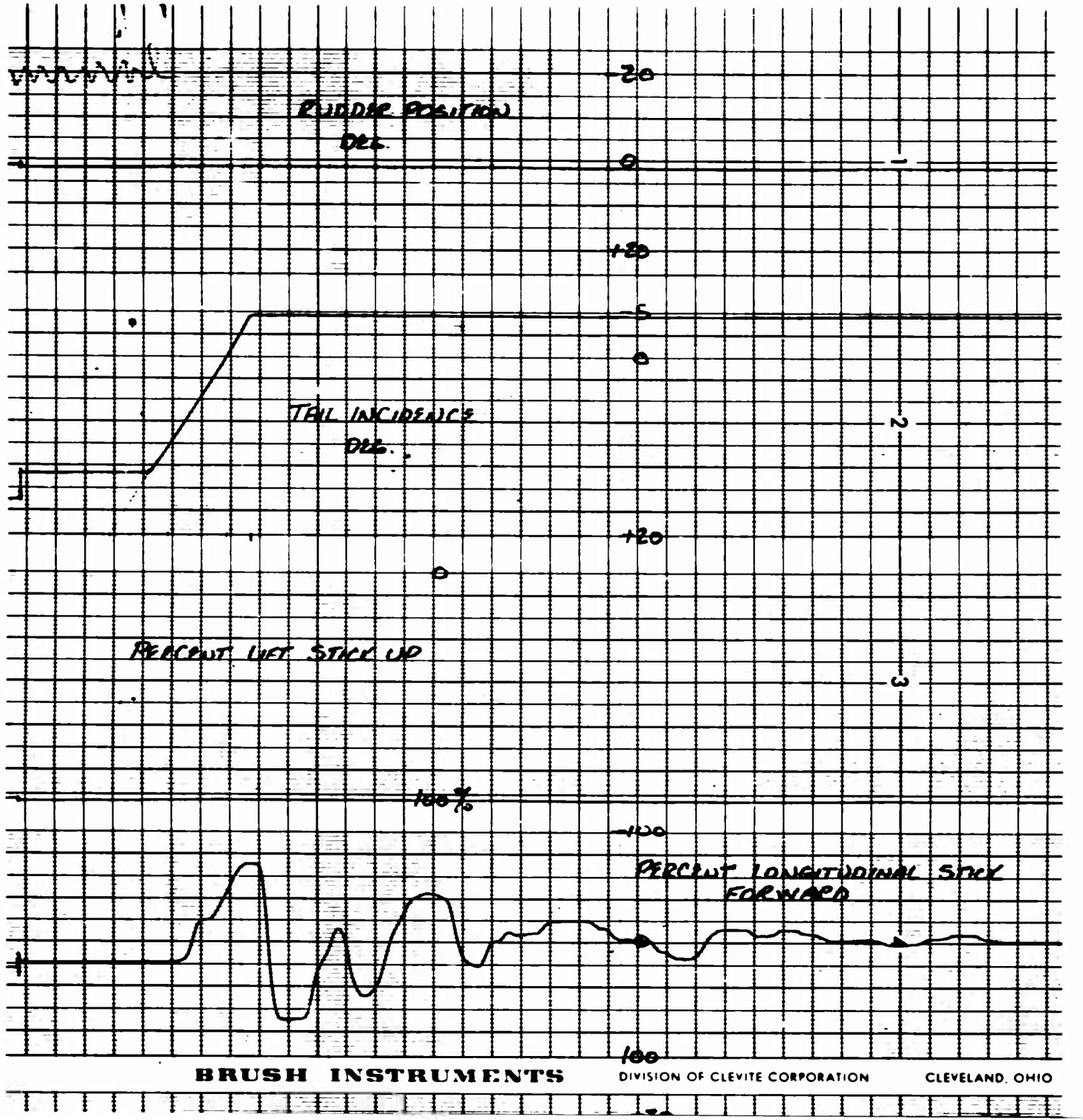
RUDDER POSITION
DEG.
-20
0
+20
TAIL INCIDENCE
DEG.
-5
0
+20
PERCENT LAT. STICK UP
100%
-100
PERCENT LONGITUDINAL STICK FORWARD
100
1
2
3
BRUSH INSTRUMENTS
DIVISION OF CLEVITE CORPORATION
CLEVELAND, OHIO

A

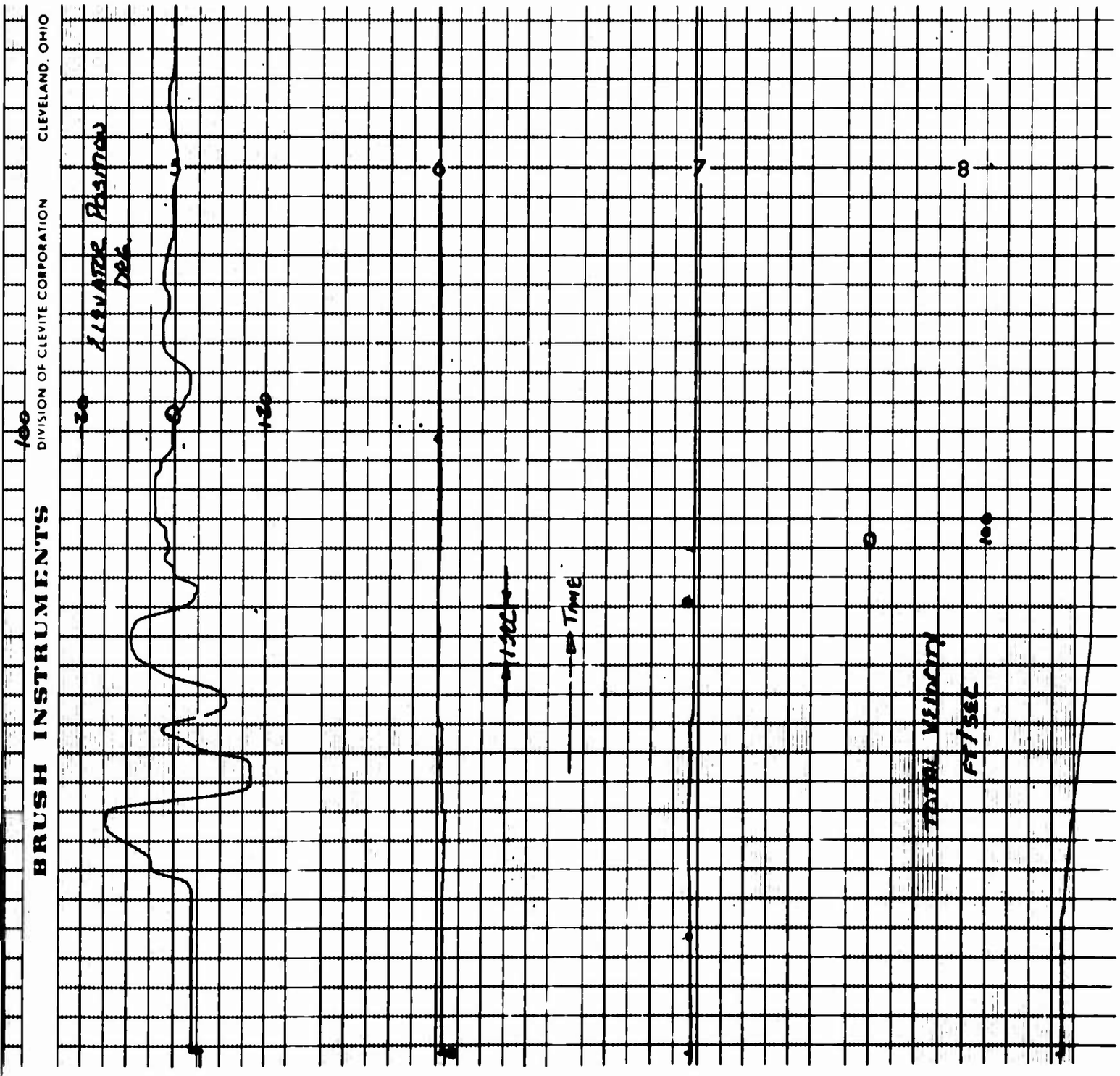

Figure 171 Fan to Conventional Conversion Time History, Pace 231R Brush Recorder

B

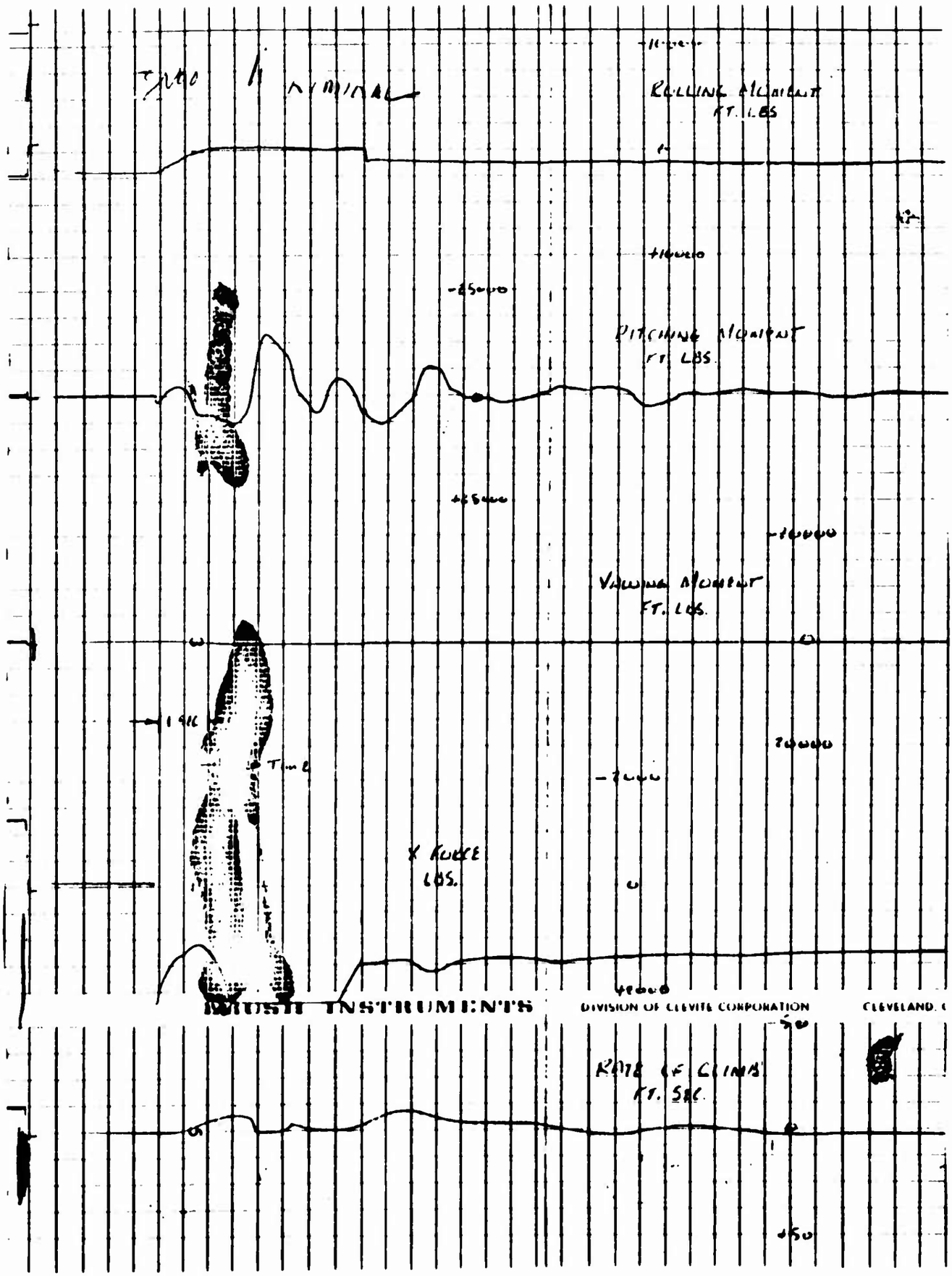

Figure 172 Fan to Conventional Conversion Time History, Pace 231R Sanborn Recorder

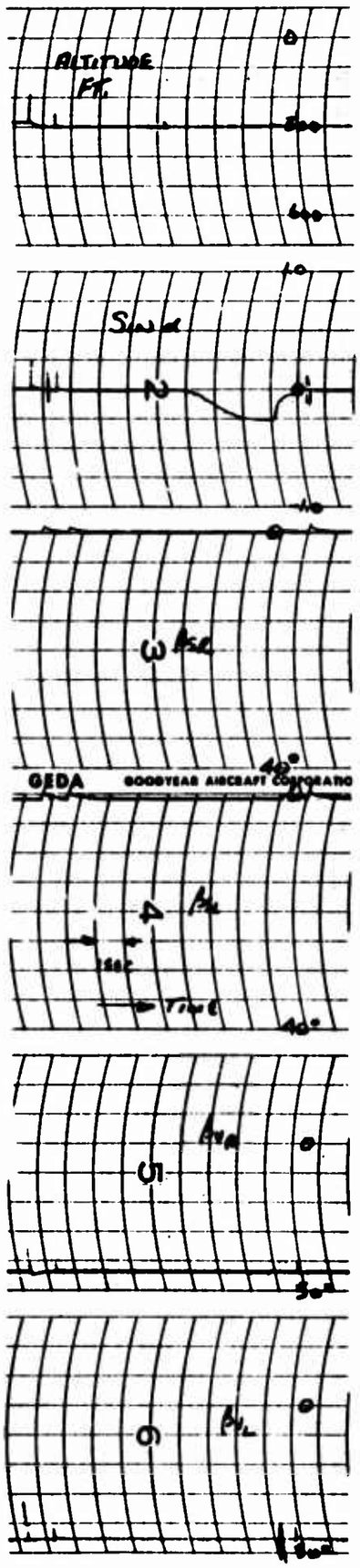

Figure 173 Fan to Conventional Conversion Time History, Pace D Recorder

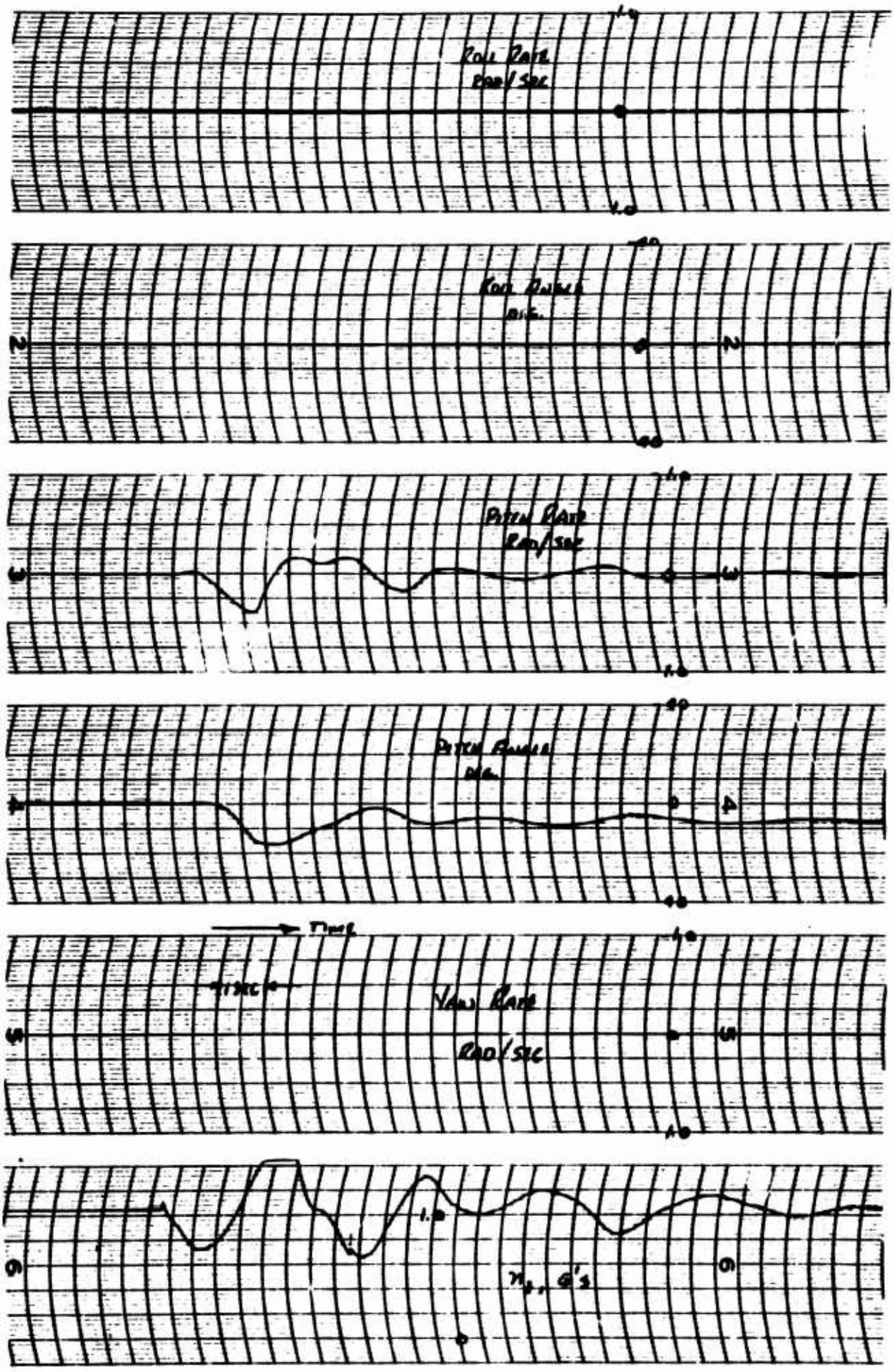

Figure 174 Fan to Convertional Conversion Time History, Pace E Recorder

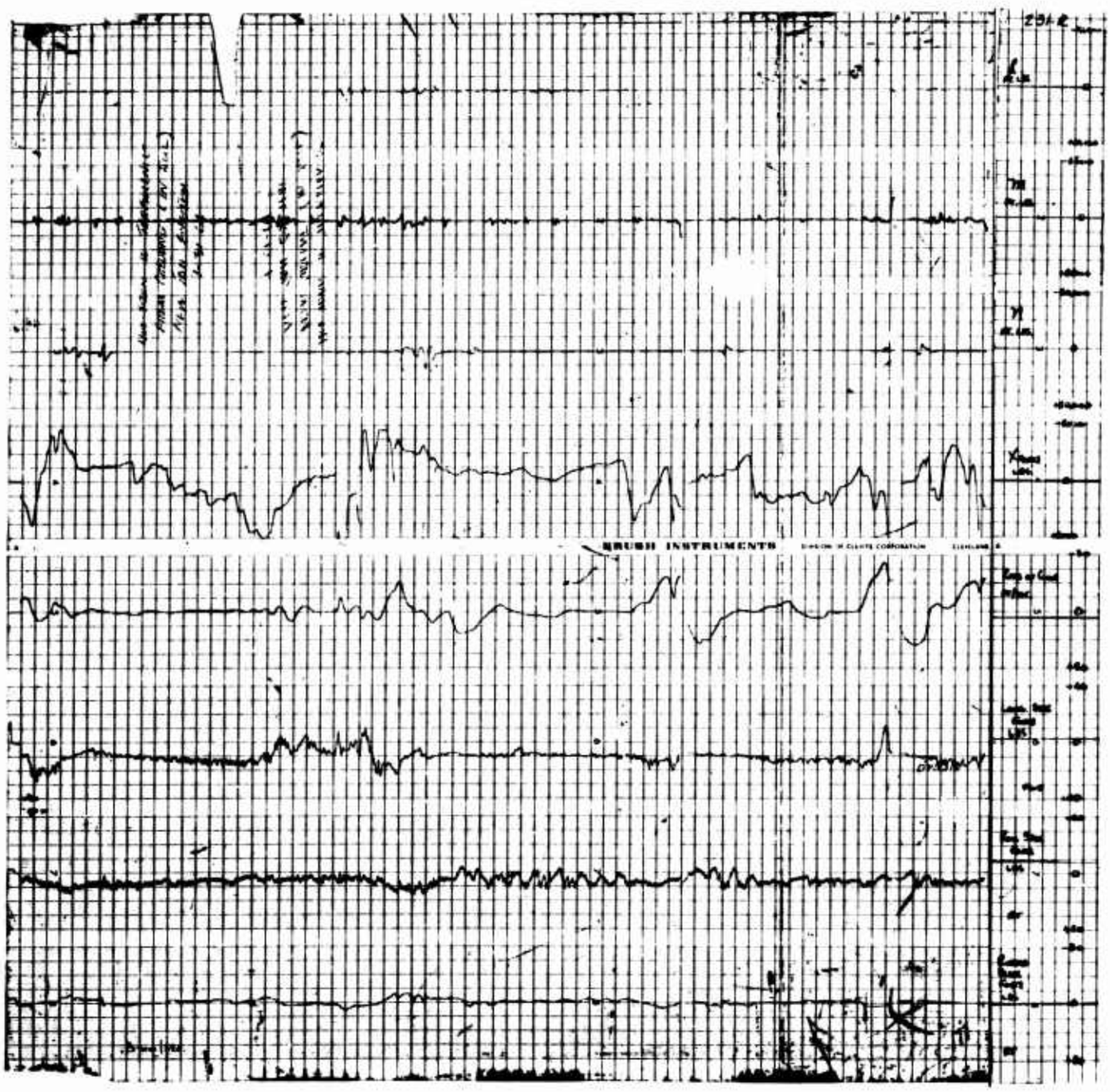

Figure 175 Hover, Transition and Conversion Time Histories, Pace 231R Sanborn Recorder

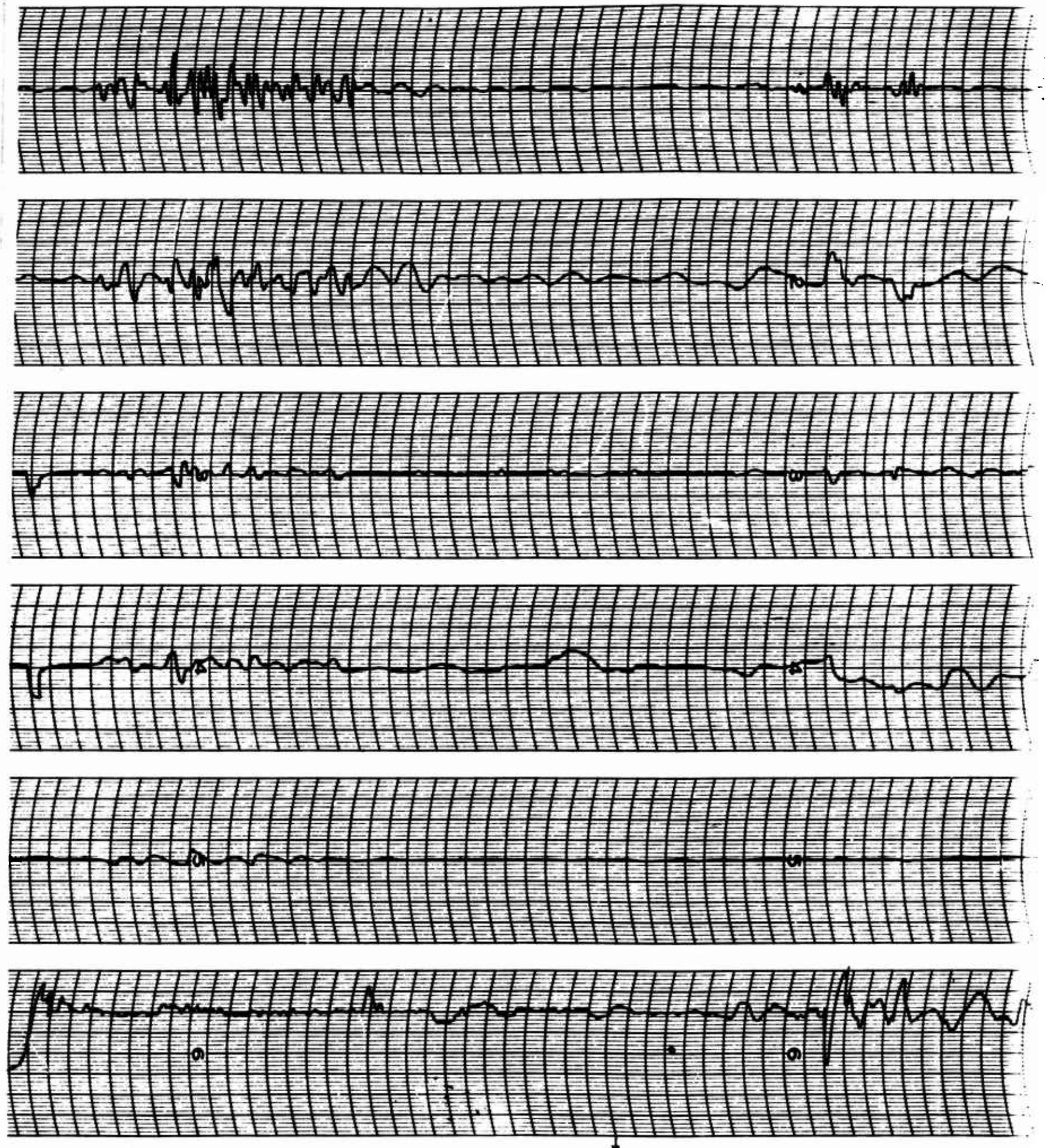

1 mm/s

CHART NO. RA 2961 30 **BRUSH INSTRUMENTS** DIVISION OF CLEVITE CORPORATION CLEVELAND OHIO

A

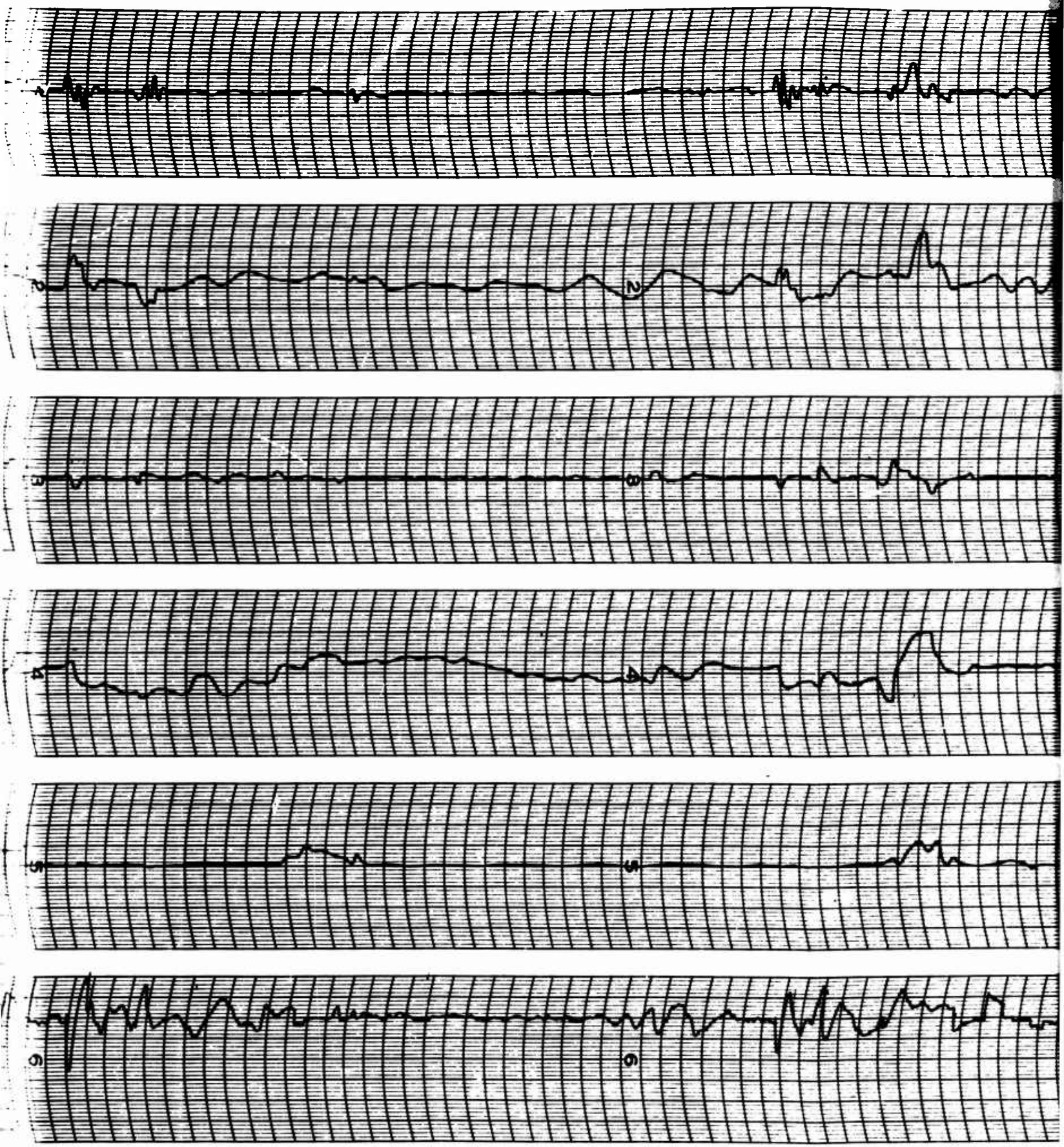

ITE CORPORATION CLEVELAND OHIO PRINTED IN U.S.A.

B

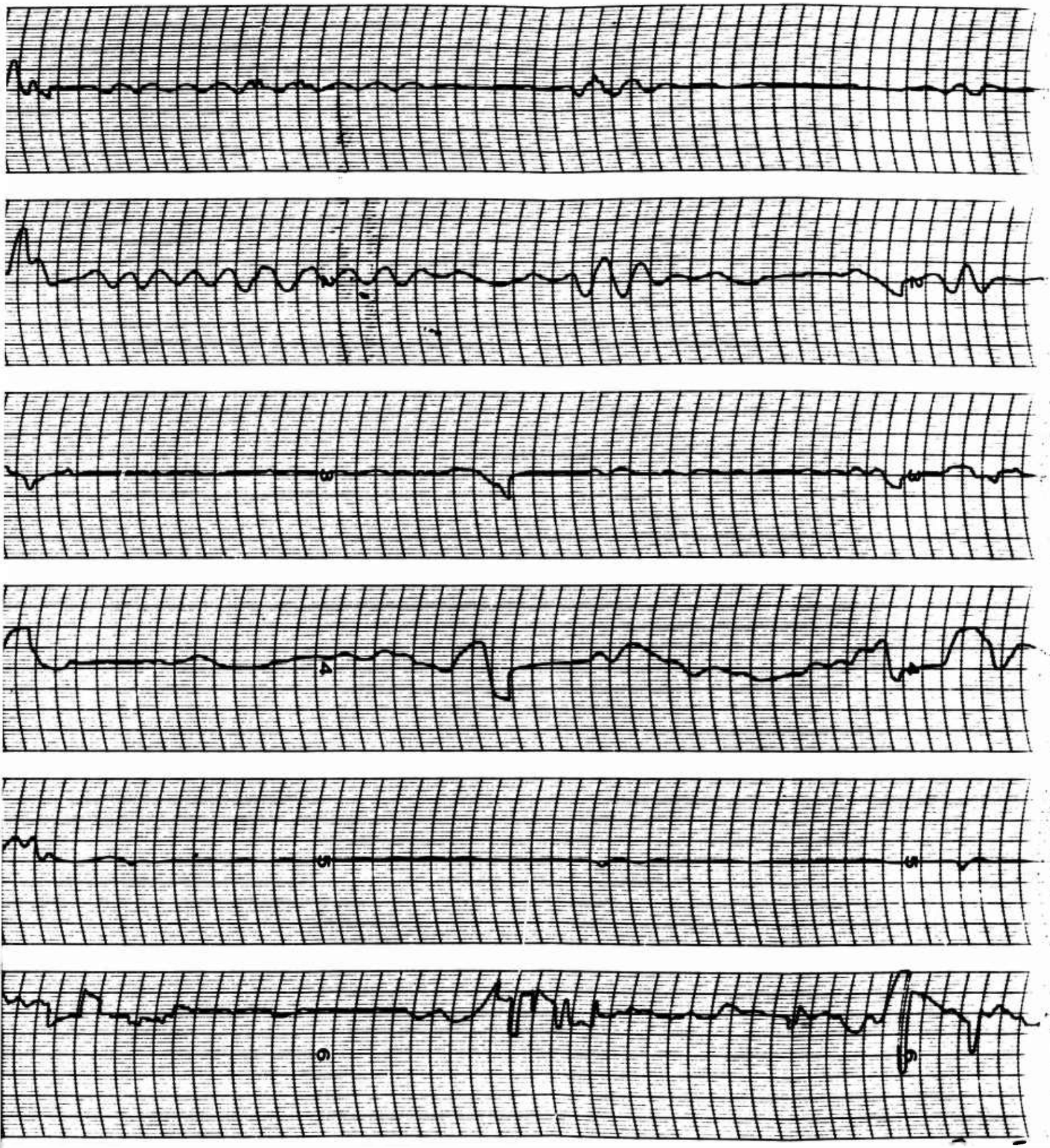

Figure 176 Hover, Transition and Conversion Time Histories,

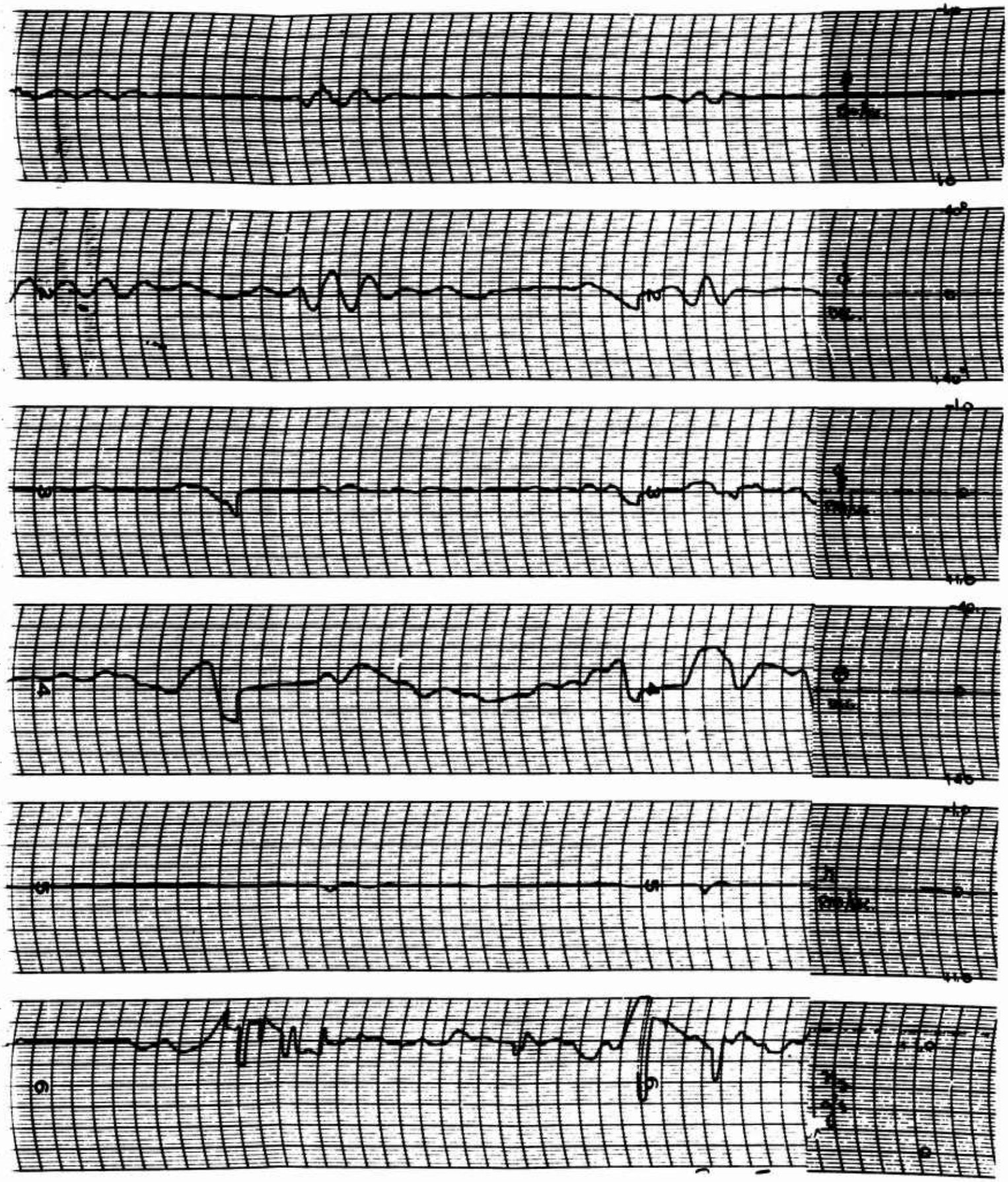

Figure 176 Hover, Transition and Conversion Time Histories, Pace E Recorder

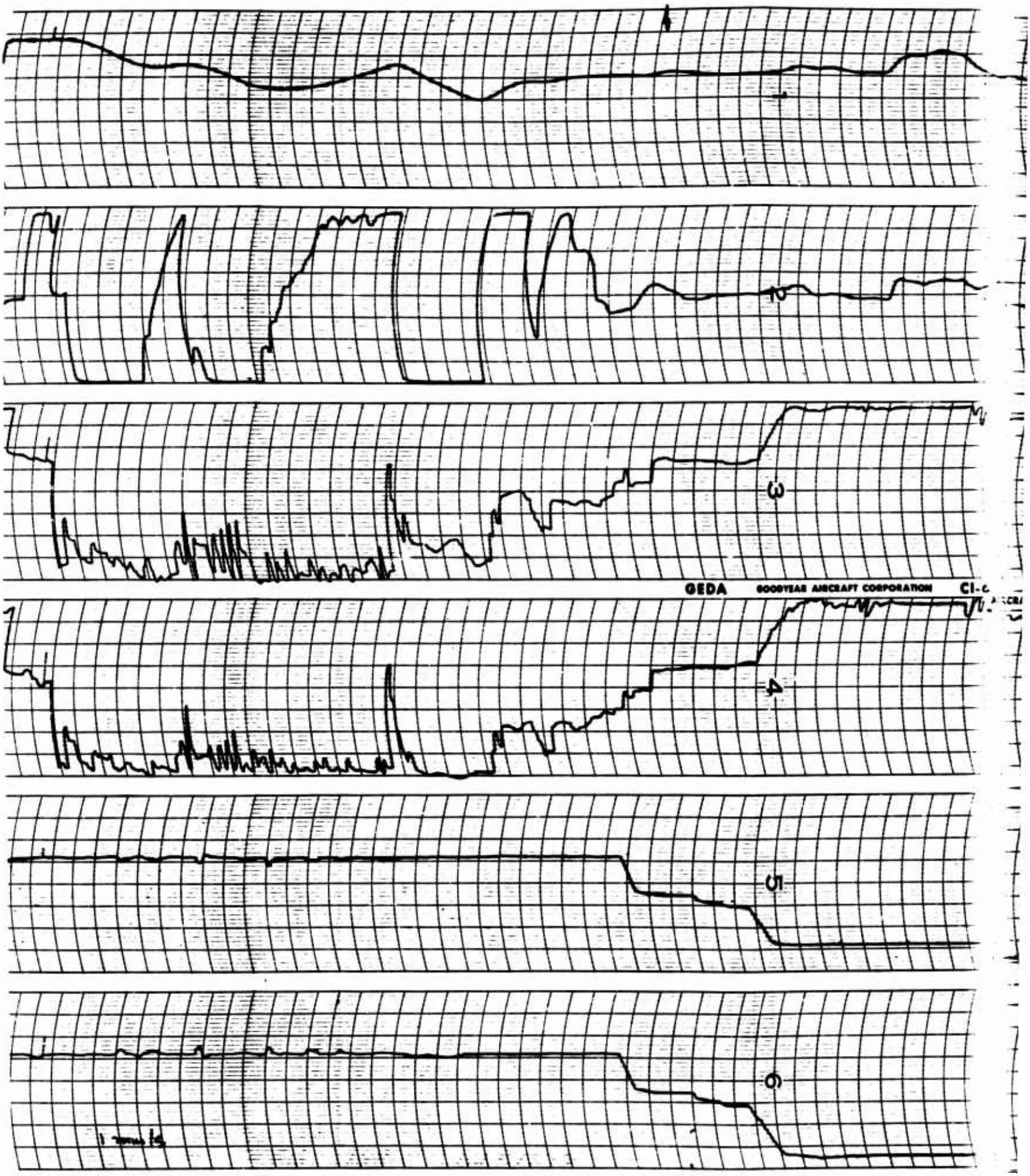

A

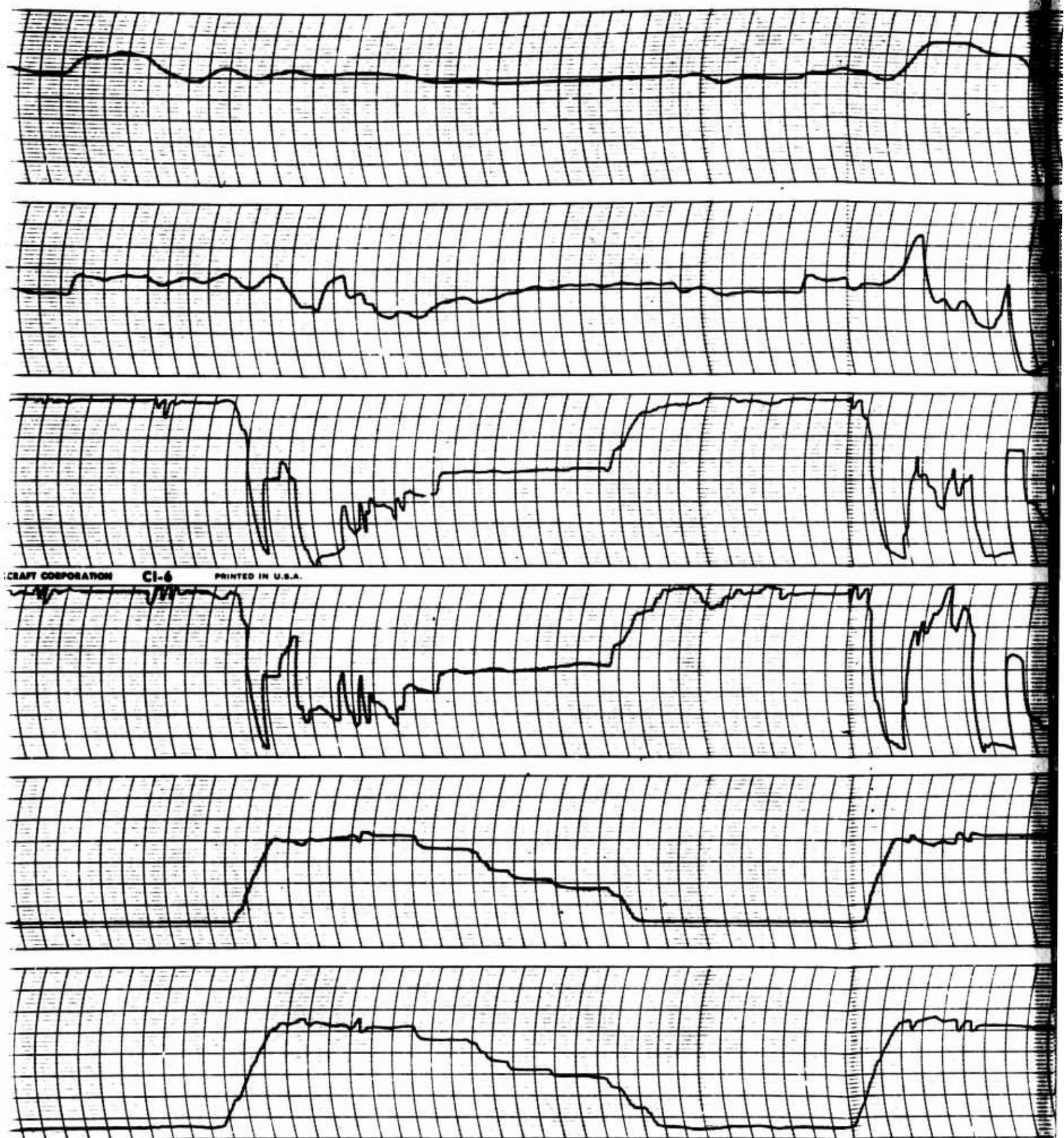
CRAFT CORPORATION
CI-6
PRINTED IN U.S.A.

Figure 177 Hover, Transition and Conversion Time Hist

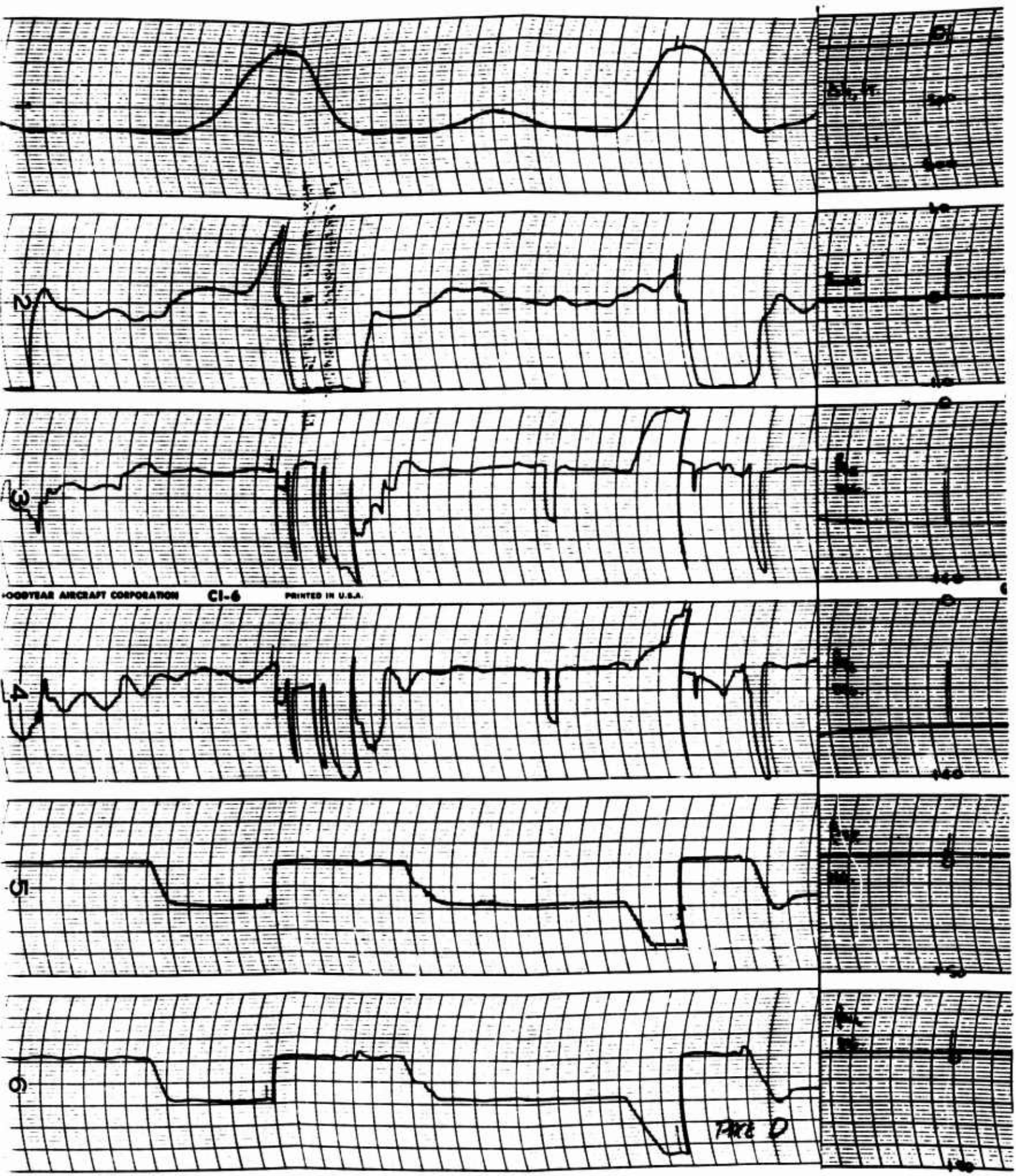

Figure 177 Hover, Transition and Conversion Time Histories, Pace D Recorder

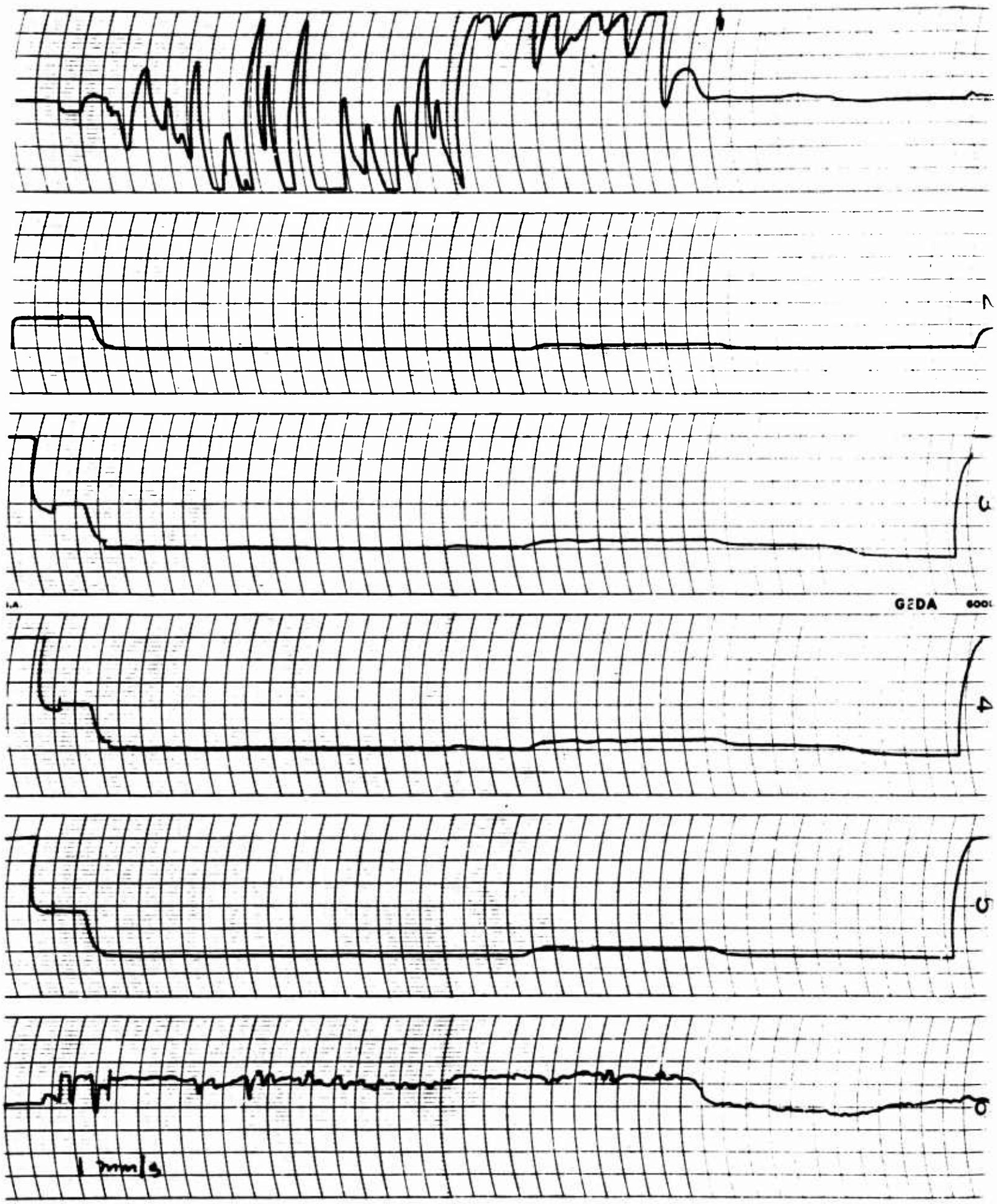

A

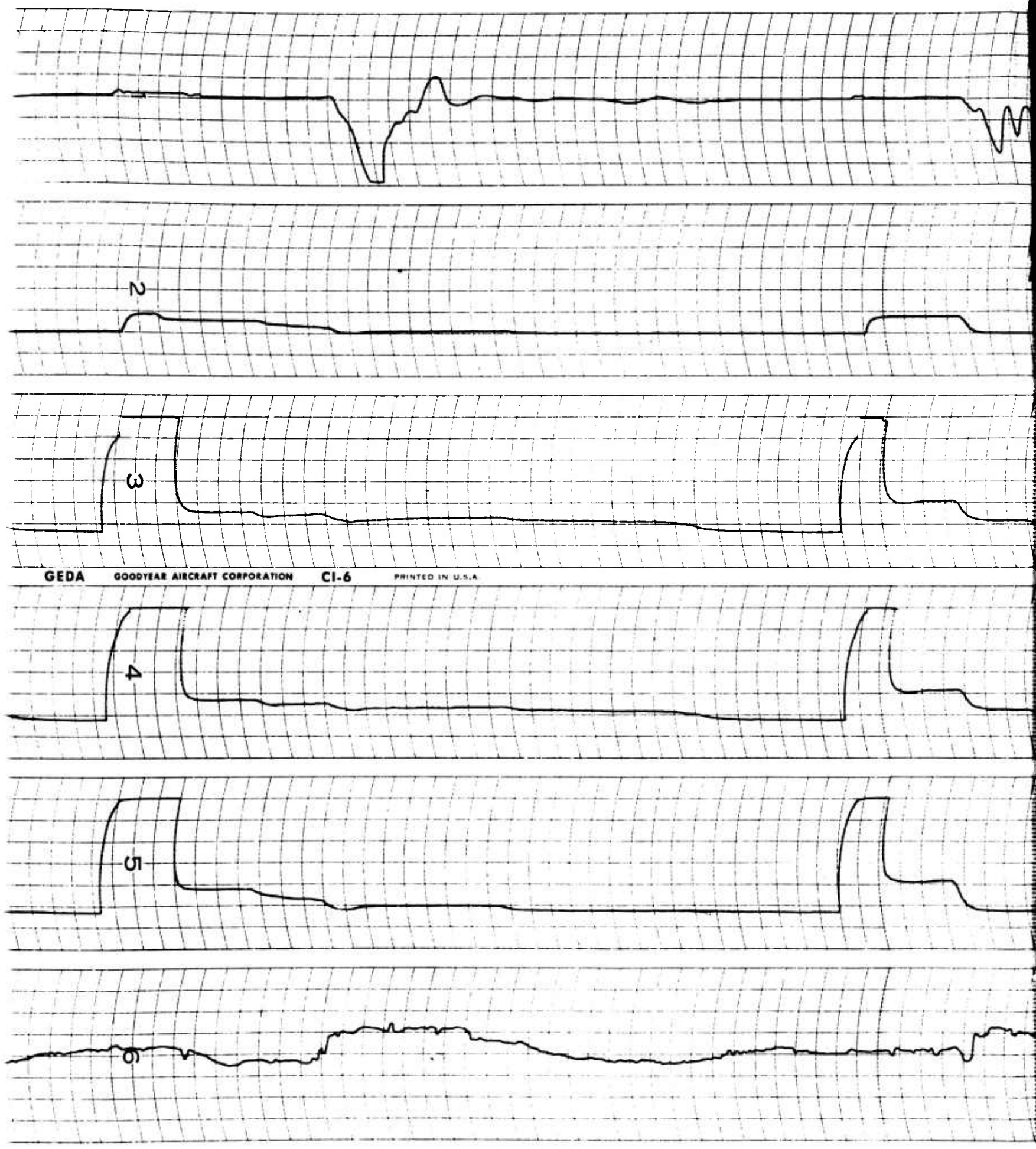
2
3
GEDA GOODYEAR AIRCRAFT CORPORATION CI-6 PRINTED IN U.S.A
4
5
6

B

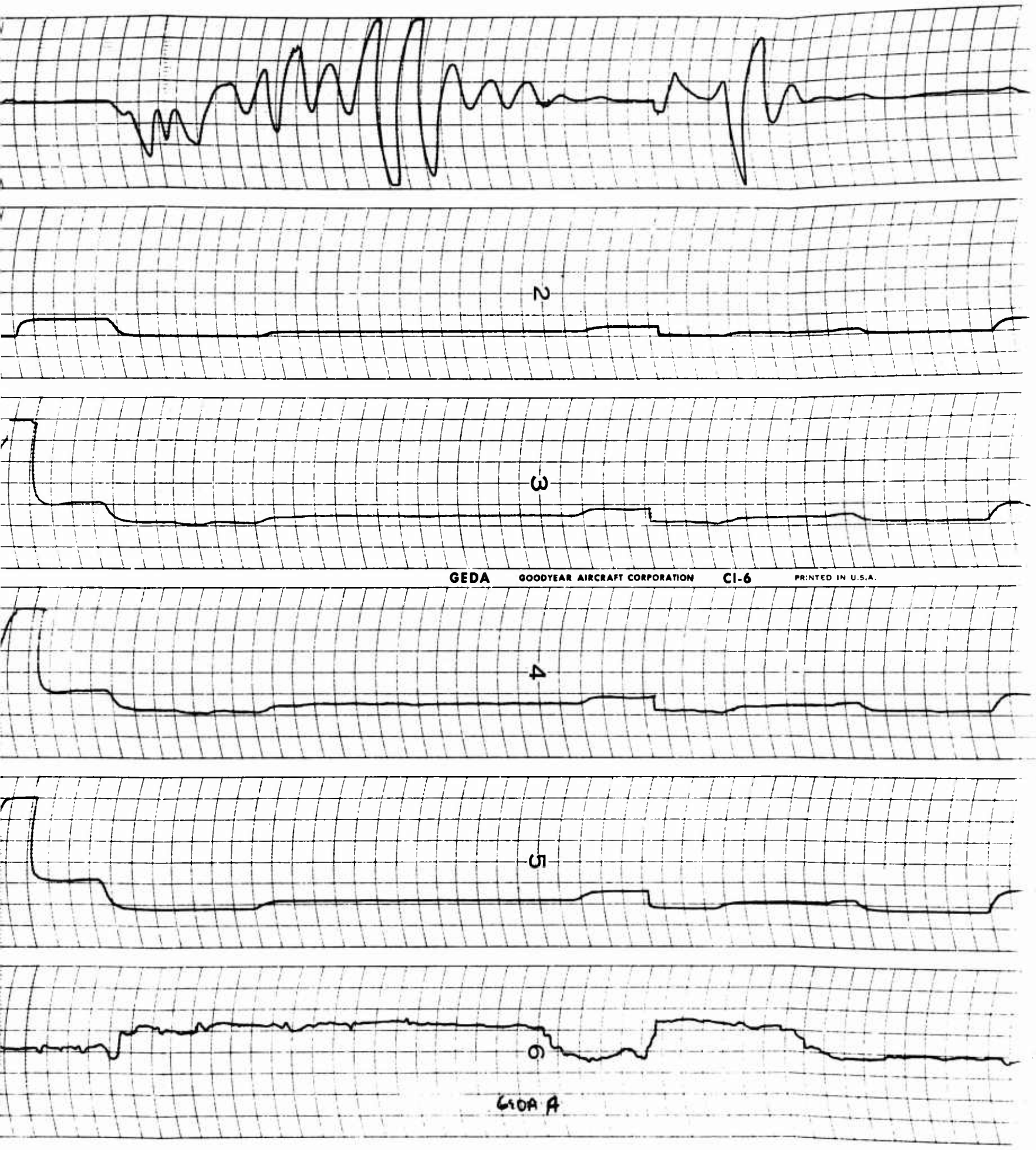

Figure 178 Hover, Transition and C

C

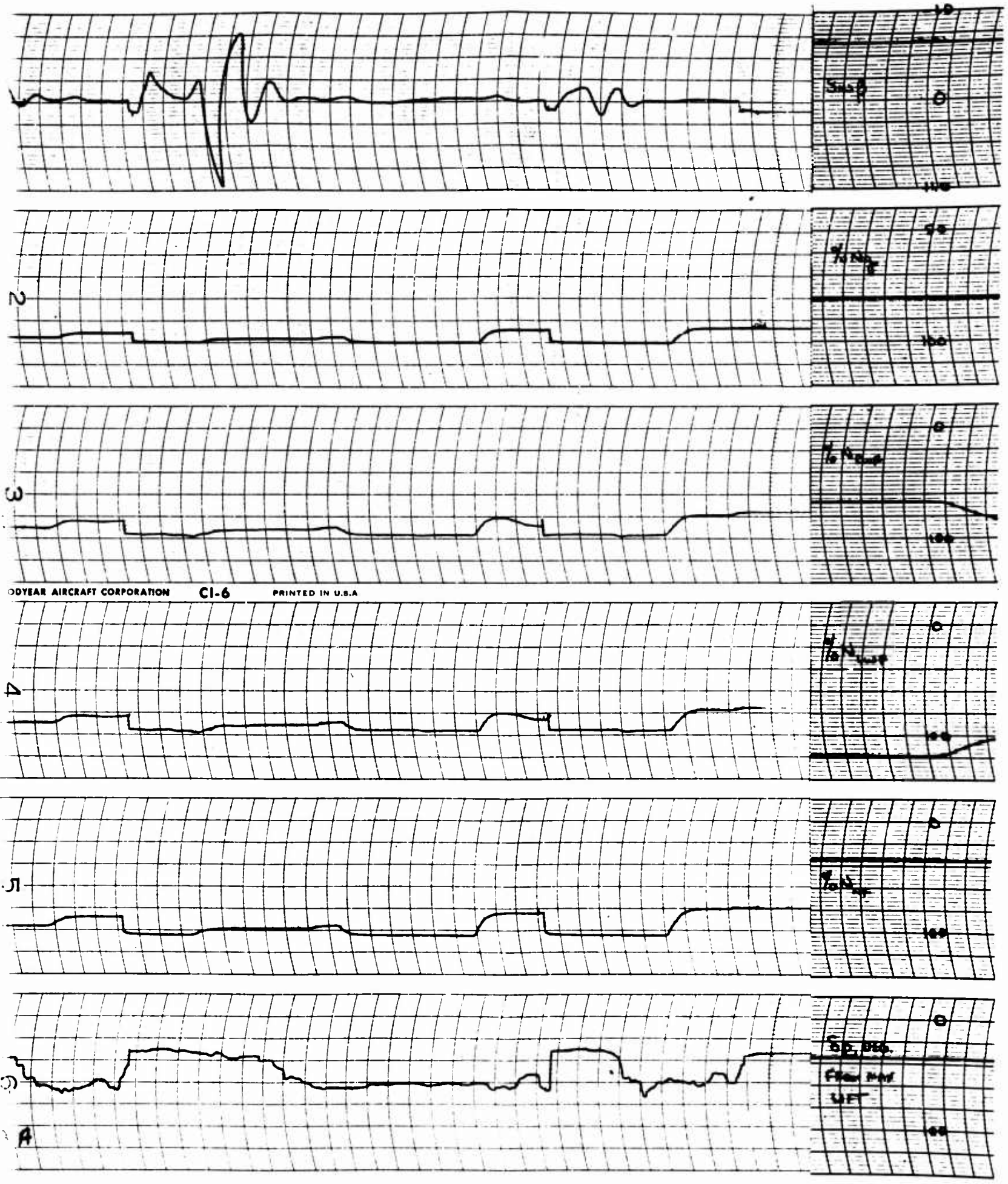

Figure 178 Hover, Transition and Conversion Time Histories, Geda A Recorder

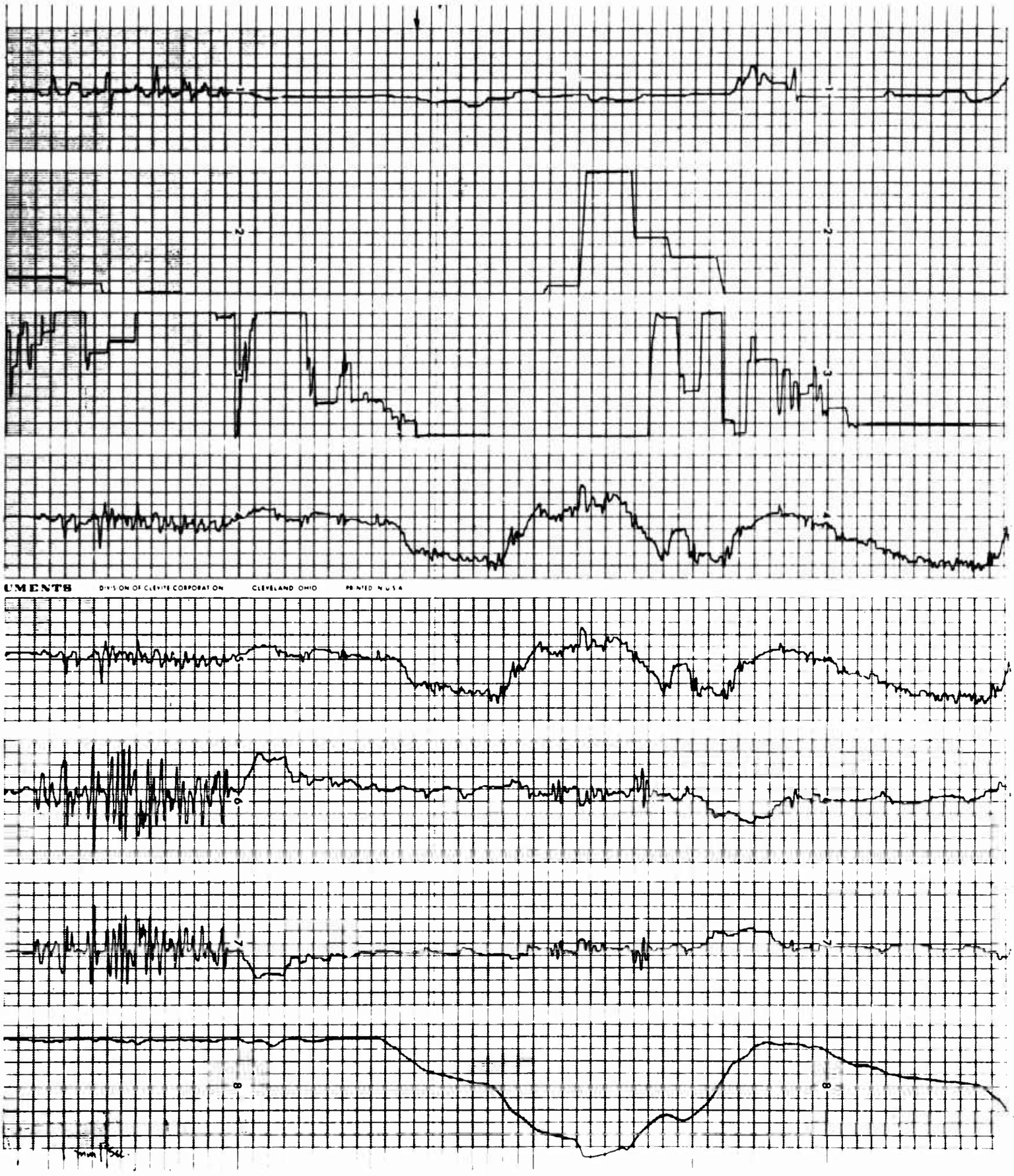
UMENTS
DIVISION OF CLEVITE CORPORATION
CLEVELAND OHIO
PRINTED IN U.S.A.

A

Figure 179 Hover, Transition
Pace 231R Brush

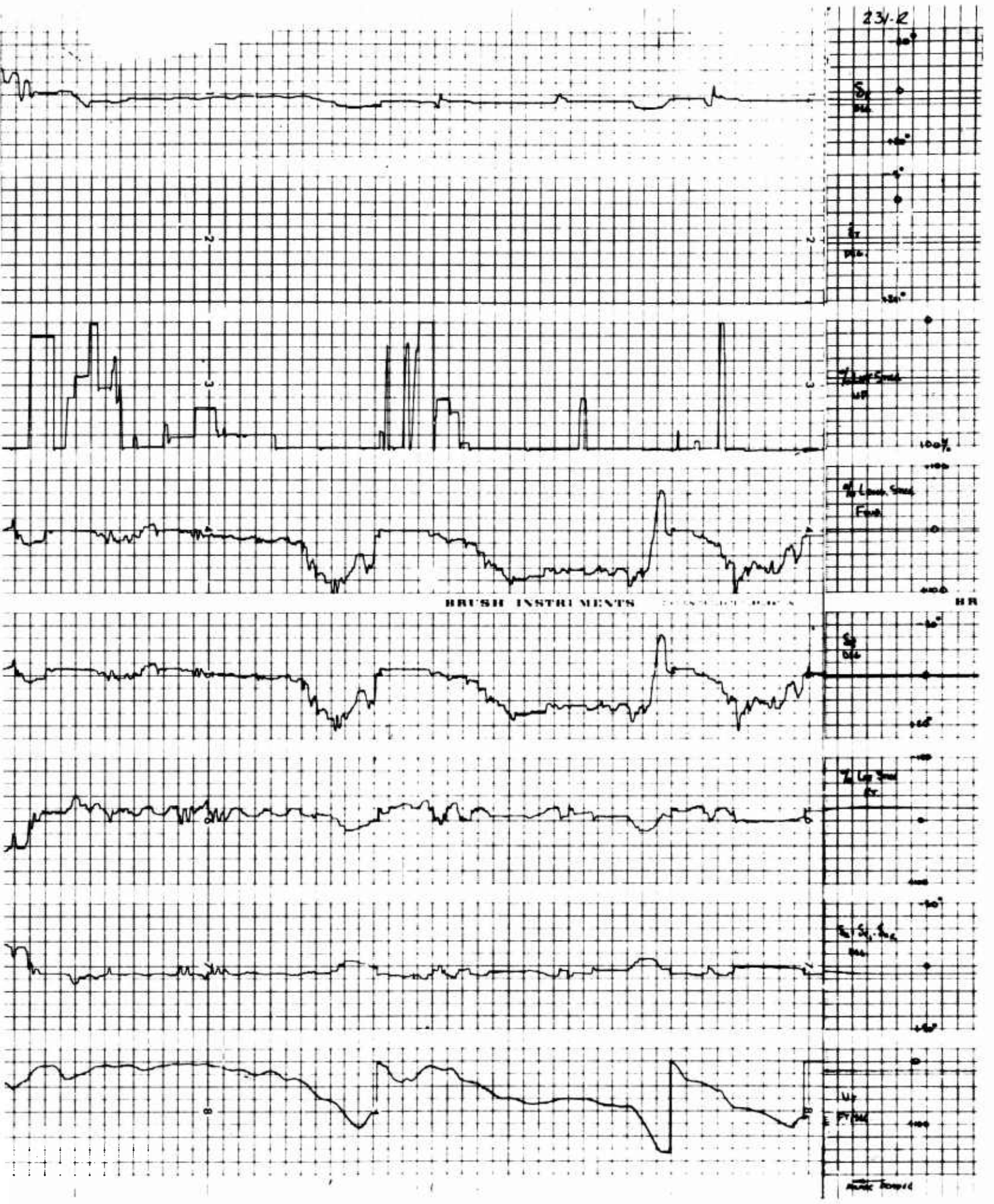

Figure 179 Hover, Transition and Conversion Time Histories, Pace 231R Brush Recorder

3.6 PILOTING METHODS

3.6.1 General

This section presents a summary of some of the piloting techniques developed during the flight simulator program.

The inclusion of some of the items may seem superfluous, but all the items included proved useful at some time in the program and may prove useful in later test phases of the lift fan program.

3.6.2 Hover and Low Speed Fan Flight Piloting Methods

Altitude Control

In attempting to control altitude, some pilots had a strong tendency to over-control the collective stick. This tendency could be overcome by the following piloting method:

> When reducing vertical velocity in either direction, approach the trim collective stick position (for lift equals weight) at the same rate as the rate of climb needle approaches zero. For instance, if the aircraft had an approximately steady rate of climb (stick above neutral), and the pilot wished to remove it - he went to a collective stick position below neutral, and then removed this negative stick position at the same rate that the rate of climb needle approached zero - i.e. removed x percent of the stick distance below neutral in the same time that x percent of the original vertical velocity was lost.

Forward Flight

When the aircraft is nosed down in pitch to develop forward velocity, the pitch stick passes through a set of switches located at the base of the stick and switches the stability augmentation system from holding to maneuvering mode.

When the holding mode is engaged, transients in pitch are caused. The aircraft when going from holding to maneuvering mode seems to "break loose", and in going in the reverse direction to "hang up". While this change in characteristics can be tolerated occasionally, at some forward velocity trim pitch stick position is right on the mode switch, and pitch

stick movements made to stabilize the aircraft are continuously passing through the mode switch. These continuous changes in pitch dynamics make the aircraft very unpleasant to fly.

To avoid this possibility, either the stability augmentation pitch channel capacitor can be shorted (in which case holding mode and maneuvering mode both are pure rate feedbacks and the transients encountered in passing from one to the other become negligible), or the stick-actuated mode switches can be removed to keep the system in one mode or the other at all times.

Sideways Flight

Because the aircraft builds up large fan induced rolling moments with side velocity, and because the stability augmentation system capability to remove energy from the system oscillating in roll is limited, some care must be used when recovering from a sideslip maneuver.

If the aircraft has a large side velocity and the roll stick is suddenly centered, the aircraft will oscillate violently in roll. This oscillation will last longer than the position of the dominant second order poles in roll would indicate. This is because the maximum roll rates are large enough to saturate the stability augmentation system almost continuously (for a recovery from a side velocity of 15 knots for example), and while operating saturated, the stability augmentation system is not removing as large a percentage of the system energy per cycle as when operating unsaturated.

To avoid large amplitude roll oscillations when recovering from a side velocity maneuver, the roll stick should be centered slowly, allowing the stability augmentation system to operate normally.

3.6.3 Transition Piloting Methods

Louver Vectoring and Pitch Control

The basic pitch control problem in transition is discussed in some detail in Section 3.4. The problem is that if a pilot vectors too far beyond the trim vector angle required for flight at a given velocity, it is possible to run out of down pitch control power.

To avoid this, the pilot must limit his "vector lead" to the value shown in Figure 165. A simple way to accomplish this is:

1. Vector to a maximum of 25 degrees vector at any vector rate (the aircraft will accelerate fast enough to follow the present maximum vector actuation rate in level flight).

2. As the aircraft accelerates, the pitch stick required will increase, reach a maximum and begin to slowly decrease.

3. As the pitch stick required begins to decrease, vector angle can be slowly added, 1 or 2 degrees at a time, holding the pitch stick position roughly constant.

4. When a vector angle of 30 to 35 degrees is reached by this method, high speed vectoring can be resumed.

3.6.4 Conversion Piloting Methods

The conversion area is the region of least certainty as to the validity of the aerodynamic data itself, as well as to the validity of the methods used to simulate the change from fan-powered to conventional flight, and vice-versa. The simulation has shown that the transients occurring are no larger than expected, and the main pilot task will be to achieve smooth rotation of the vehicle to the attitude required for the other mode of flight.

The conclusion is that all conversion simulation work to date has shown that a constant tail rate during the conversion transient results in disturbances well within the control capability of the pilot.

The piloting technique during conversion will evolve only as a result of flight tests, and any further discussion of the simulator results would be superfluous.

3.6.5 Piloting Methods Against Failures

The pilots were exposed to failures as summarized in Section 3.7. The results of this failure study will be discussed in the XV-5A Flight Worthiness Report. Included here, however, are the discussions of two of the most important failures.

Tail Runaway

Should the horizontal stabilizer run away during transition above a velocity of about 20 feet/second, and proceed any appreciable distance toward

its full down position, the pilot will quickly find himself out of pitch control moment.

To give the pilot warning of any such runaway, an aural and visual warning to indicate tail movement has been added to the aircraft.

If the warning sounds when the pilot is not commanding horizontal stabilizer movement, the pilot should immediately select "emergency trim."

If this does not correct the situation (and time permits), the circuit breakers for the tail actuator should be pulled. If all else fails, the pilot should consider departing the aircraft.

Single Engine Out - Fan Mode

For the conditions simulated, the aircraft cannot sustain level fan mode flight on one engine.

In the case of a single engine out, the pilot must perform a pushover, roundout and flare maneuver to land the aircraft.

Flight at less than the maximum allowable rate of sink (10 feet/sec) and less than stall angle of attack (20 to 22 degrees) will require a minimum of 57 knots, indicated air speed. If the aircraft has insufficient airspeed, altitude must be exchanged for velocity, with a flare at touchdown.

This "altitude or airspeed" requirement establishes a curve within which recovery of the aircraft is not possible at less than the 10 feet/second allowable sink rate. Should the pilot find himself within this curve with only one engine, he should consider departing the aircraft.

This curve is given in Figure 180 for a typical aircraft flight condition.

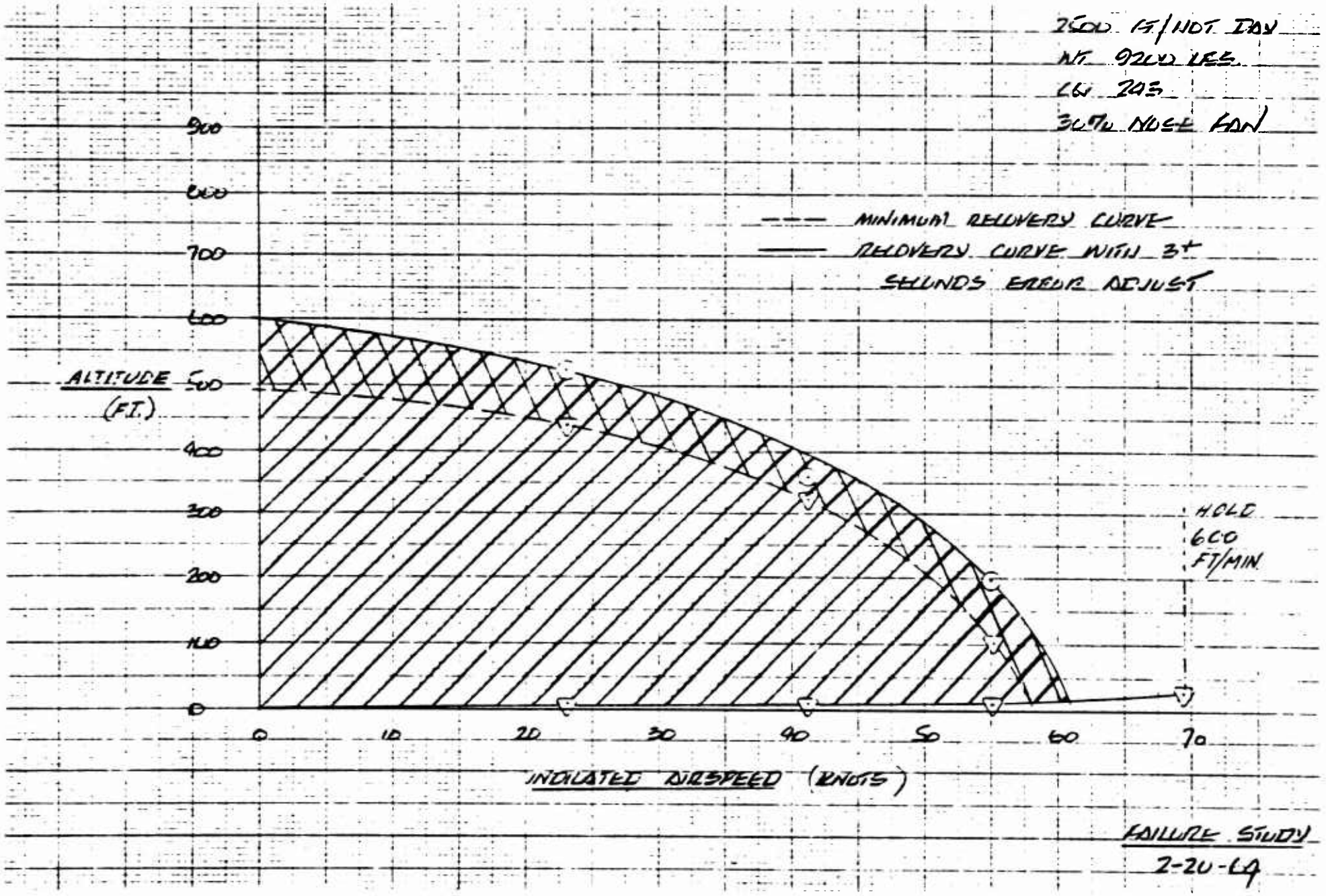

Figure 180 Single Engine Out Recovery Simulator Results

3.7 SIMULATION OF IN-FLIGHT FAILURES

A complete evaluation of the failure simulation program is presented under separate cover in the XV-5A Flight Worthiness Report.

This section deals only with an outline of the general modes of failure investigated, and the means used to mechanize the various failures. The failure modes investigated fell into the following eight categories:

1. Stability Augmentation Failures

2. Horizontal Stabilizer Control Failures

3. Fan Overspeed Warning/Cutback Failures

4. Single Gas Generator Failures

5. Vector Actuator Failures

6. Diverter Valve System Failures

7. Airspeed Indicator Failure

8. Mechanical Mixer Failures

Stability augmentation failures involved single-axis hard-over, single axis dead, all channels dead, and combinations of servo valve coil failures.

For this evaluation the pilot was directed to remain in the primary SA mode and attempt to "fly around" the failure. A small switch box was placed in series with the three channel inputs to enable dead or hard-over failures to be introduced. An additional switch box was fabricated to enable open or short-circuiting of either or both valve coils in a single servo.

Horizontal stabilizer control failures were introduced by means of a test box inserted in the wiring harness to the horizontal stabilizer actuator and associated hardware. Using this test box, all types of failures which could occur in the horizontal stabilizer system were investigated, including a few likely dual failures.

The fan overspeed warning/power cutback failures were accomplished by introducing transient and steady-state signals into the appropriate points in the fan overspeed simulation circuits.

Gas generator failures were introduced by simultaneously reducing the total gas generator power to the fan system to the single-engine equivalent and reducing one of the varidrive units to zero speed. This approach gave appropriate aural cues to the simulator pilot.

Vector actuator failures were introduced by means of a test box in series with the vector actuator harness such that vector actuator runaway and inoperative failures could be simulated, as well as vector actuator interlock circuit malfunctions.

Diverter valve system failures included the simulation of the diverter valve time delay inoperative and failed in the closed position.

The airspeed indicator was failed by removing the input.

Mechanical mixer failures were introduced by disconnecting various servo input torque tubes.

3.8 SUMMARY OF PROBLEMS ENCOUNTERED AND DESIGN CHANGES

Much of the material reviewed here is presented elsewhere, but it is felt valuable to review all changes which occurred within the control and stability augmentation systems in one section of the report. These are:

1. Modification of yaw and pitch SA system to provide rate damping only. (Discussed in Section 3.4.)

2. Inclusion of filtering on output of rate-gyro demodulators. (Discussed in Appendix I.)

3. Inclusion of a 15 cps notch network in all SA axes for elimination of structural feedback. (Discussed in Appendix I.)

4. Installation of viscous dampers on nose fan thrust reverser doors. (Discussed in Section 3.2.)

5. Increase of damping in aileron boost servo.

6. Modification of tail trim system so that tail is full up to 40° vector angle, and is controlled by the stick grip switch thereafter. (Discussed in Section 3.4.)

7. Extension of longitudinal trim range below 40° vector angle so that the stick may be trimmed to zero force at all regions of the transition regime. (Discussed in Section 3.4.)

8. Change of lateral stick travel to ±4" from original ±5" to afford clearance for the pilot's knees.

9. Change of stick force gradients in hover to 1.33 lb/inch in both roll and pitch.

10. Inclusion of a visual and aural signal to the pilot to signify tail motion.

11. Change of fan-powered flight regime horizontal tail trim rate from 4°/sec to 2.8°/sec. Discussed in Section 3.4.

12. Change of final tail incidence in the conventional to fan conversion to +10° from the original +12°.

13. Modification of the conversion sequence so that a conversion could be aborted at any time with no ill effects on the pilot or vehicle.

All except Items 5, 8, 9, 10, 12, and 13 are covered elsewhere.

Item 5 - Aileron Boost Servo Damping

The aileron boost servo as installed on the hydraulic simulator was marginally stable, in that a transient induced into the aileron tab would sometimes result in a continuous oscillation. This problem was solved by increasing the internal damping of the actuator.

Items 8 and 9 - Lateral Stick Sensitivity and Stick Force Gradients

Many simulator flights were made investigating the effects of changes in stick sensitivity and force gradients at near hover conditions.

The lateral stick originally had a full throw of ±5" at the grip, with provisions for reduction of the throw to as low as ±3". The longitudinal stick had similar throw adjustment provisions, and was originally set for ±6" of travel. The stick force gradients were arbitrarily set quite high, with provisions available to reduce the spring feel by the installation of weaker springs.

Both pilots finally agreed upon a lateral stick throw of ±4" because the original stick throw resulted in interference between the stick and the pilot's legs. The longitudinal stick throw was varied, but the original setting was deemed optimum. Several sets of feel springs were installed and evaluated, and the preload at neutral was reduced to reduce the breakout force requirements to a minimum. The value of 1.33 lb/inch was chosen as the optimum gradient for best stick feel.

Item 10 - Aural/Visual Tail Motion Warning

As a result of the failure simulation study, it was found that an uncommanded tail motion could result in a most serious flight condition. Even if the tail were moving at the normal transition tail rate of 2.8 deg/sec., the pilots in general did not recognize the malfunction in time to select emergency trim or pull the tail circuit breakers. To warn the pilot of such an event, a visual and aural signal was rigged in the simulator which greatly increased pilot/vehicle survival probability under runaway horizontal tail conditions. A system to provide this function has been incorporated into the aircraft.

Item 12 - Change of Final Tail Incidence Position at the Completion of the Conventional to Fan Conversion

Conversions were made from conventional to fan-powered flight at a number of different initial velocity points. The pilots felt that the best overall system was obtained when the horizontal tail was programmed to +10° at the completion of its up travel. This position will probably be modified as a result of flight tests.

Item 13 - Conversion Sequence Modification to Permit Rapid Abort of Conversion Attempt

It was found that a rapid fan to conventional and back to fan conversion command by the pilot could result in the tail being nearly full up while the diverter valve remained in the conventional mode. This was a catastrophic situation, and could have easily occurred for some reason the pilot decided to abort the fan to conventional conversion immediately after initiation. The conversion sequence has been modified so that there are no circumstances under which the pilot can get into trouble in this respect if all systems are working properly.

4.0 REFERENCES

1. "Preliminary Systems Analysis and Simulation", Report 127, September, 1963.

2. "Handbook of Geophysics", ARDC, 1960.

3. R. C. A'Harrah, MIAS, and S. F. Kwiatkowski, MIAS, "A New Look at V/STOL Flying Qualities", Aerospace Engineering, July 1961.

4. John Patierno, AIAS; James A. Isla, AIAS; "Instrument Flight Simulator Study of the VTOL Controllability - Control Power Relationship", Aerospace Engineering, March 1962.

5. George Cooper; "Understanding and Interpreting Pilot Opinion", Paper Presented at the Flight Testing Session, 25th Annual Meeting, IAS, N. Y., Jan. 28-31, 1957.

6. W. J. Klinar and S. J. Craig, Jr., "Gust Simulation as Applied to VTOL Control Problems", SAE Paper 370L, Delivered at the Summer Meeting, 1961.

7. O. Redlich and F. R. Watson, "On Programs for Tests Involving Several Variables", Aeronautical Engineering Review, June 1953.

8. C. J. Savant, "Basic Feedback Control System Design", McGraw-Hill Book Co., Inc., 1958.

9. J. G. Truxal, "Control System Synthesis", McGraw-Hill Book Co., Inc., 1955.

10. Seth B. Anderson, "An Examination of Handling Qualities Criteria for V/STOL Aircraft," NASA TN-D-331.

11. Moloney, J. E.; Harding, W. E. Jr; XV-5A Detailed Flight Test Program, Ryan Report 63B001B, 7 Feb. 1964.

5.0 CONCLUSIONS

Simulation and analysis of the XV-5A as described herein have produced the following results:

1. Stability augmentation (SA) system gains were optimized by piloted flight simulator evaluation of hovering under gusty wind conditions. A Cooper rating of 2.3 was derived for the aircraft with the selected gains. The final SA system configuration provides pitch and yaw rate damping without position reference. Both rate and position signals are used in roll with the position reference removed as a result of lateral stick control command. In the primary SA system, individual pitch, roll or yaw channels may be independently selected and gains are adjustable by the pilot. The secondary configuration is ground adjustable over the same range as the primary system.

2. While operation of the SA system poses no problems during transition, stability augmentation is unnecessary above 40 knots IAS.

3. For the 2,500 ft. hot day conditions simulated, the rapidity with which a constant altitude transition from hovering could be accomplished was limited by power available and, at the more aft c.g. locations when using a nose fan thrust reversal capability of 30%, by longitudinal trim capability. No power or control limitations appear to exist in a landing transition.

4. An automatic horizontal trim feature has been selected for transition which programs the tail to the full 20 degree incidence limit at all louver vector angles of 40 degrees or less. For vector angles greater than 40 degrees, tail trim may be manually commanded at 2.8 deg./sec.

5. Conversion between conventional and fan flight modes is accomplished by timed sequencing of the wing fan door opening and horizontal tail incidence change as a function of diverter valve motion. The introduction at the proper time of a constant horizontal tail trim rate of 7.5 deg./sec. programed to a preestablished end point was shown to permit smooth conversions over a range of initiation flight velocities.

6. Failure studies have shown that uncommanded tail motion could result in a dangerous flight condition. As a result, both aural and visual cockpit signals have been incorporated into the aircraft to indicate lack of commanded tail motion or tail runaway.

6.0 APPENDIX

6.1 STRUCTURAL FEEDBACK

In the work previously performed concerning pitch structural feedback problems, a second-order nose door response at 20 cps with .1 critical damping was assumed. This analysis indicated the need for a notch network to filter out frequencies around 15 cps, so that the airframe rigid body stability would be the limiting factor as far as maximum SA gain was concerned. It was felt at that time that the roll and yaw modes would exhibit no structural feedback problems.

As a result of airplane system tests with the airplane mounted on spring platforms, it was found that the nose door spring-mass system had a lightly-damped resonant peak at 14 cps, and it was further determined that the 15 cps notch network effectively eliminated pitch system structural feedback problems, while leaving the airplane rigid-body modes essentially unaffected. However, a roll "jitter" at 17 cps was noticed during these tests which caused continuous louver chatter.

The rate gyro bracket was found to be quite flexible in the roll axis, and to exhibit a natural frequency of about 20 cps. In addition, the wing exhibits a mode at 17 cps.

As a result of these tests, the rate gyro mount was stiffened, and the 15 cps notch network was included in both the roll and yaw channels, in addition to the pitch channel. Thus, all SA modules remain identical and interchangeable.

A problem arose during the incorporation of the parallel "T" notch network into the SA system. The rate gyro output is double-sideband suppressed carrier amplitude modulation, with a carrier frequency of 400 cps. This signal is full-wave demodulated at the gyro output to provide a DC signal for use with the input compensation network. Since the "T" network only attenuates the DC component of the demodulated rate gyro signal, the AC components go straight through the system and result in a very poor notch. A 1 mfd capacitor was placed across the demodulator output to ground, and with the demodulator output resistance of 3K Ω gave a filter down 3DB at 50 cps, while affording a theoretical 24 DB of attenuation of the 800 cps component of the demodulated rate gyro output

signal. As actually measured the notch was down 27 DB from the low frequency gain value.

For this reason, the 1 mfd filter capacitor was incorporated in all SA channels.

As a point of interest, the airplane system tests were performed both with the airplane completely buttoned up, and with the engine cowl and canoe removed. Although the cowl and canoe are not structural, they had a definite effect on the test results.

The tests consisted of energizing the input of a single SA channel with a variable frequency sine wave, and measuring the resulting output from all three rate gyros. Since this was done with the hydraulic systems energized, the amount of structural feedback to the rate gyros from roll, pitch and yaw inputs was measurable.

The yaw rate gyro showed negligible response to excitation by inputs to any axis.

The roll rate gyro showed a response at 17 cps, and this frequency was present over the whole range of input frequencies to the roll SA channel.

The pitch rate gyro showed strong responses to inputs to the pitch SA channel. With the cowl and canoe removed, the first major response occurred at 9 cps, and the second at 14 cps, the frequency of the nose-door resonant peak. Since the first symmetrical body mode was previously measured at 12 cps, it was concluded that the 9 cps response was the first body mode without the cowl and canoe. The test was repeated with the cowl and canoe installed, and the previous 9 cps response was not evident, but the body 12 cps as well as the nose door 14 cps responses were obtained.

During ground engine/fan tests, the lightly-damped nose-door second order response was excited by the nose fan door efflux to such an extent that large door oscillation amplitudes were noticed at near full-power runs.

Hydraulic dampers were installed on the nose doors which were calculated to increase the damping to . 2 critical or greater. This modification served to further redu e the possibility of structural feedback in the pitch mode.

6.2 ELEVATOR NOSE-DOOR FEEDBACK

Summary

During the ground tests of the XV-5A, it was found that the elevator had a stick-fixed resonance at 9 cps which fed into the nose-door system through the base of the locked stick.

Since the nose-doors themselves had a 14 cps natural frequency (which caused feedback through the SA system), and two airframe symmetric modes were in the same region, it was felt that there could be a possible problem of the elevator-nose-door combination setting up a sustained oscillation through the flexible airframe.

The data taken during the ground vibration tests was used to determine the first two symmetric flexible body modes, and the aircraft mass distribution and measured mode shapes were used to calculate the generalized mass of the first two modes, as well as the intermodal mass of the same modes. The intermodal mass determines the coupling between the modes and is a measure of the orthogonality of the measured modes. If the measured modes were actual normal modes, the intermodal generalized masses would be zero.

The effect of the intermodal generalized mass on the first two modes was calculated and determined to be negligible.

The equations of motion for the springy elevator, rigid airframe and flexible airframe combination were developed and set up on the analog computer after a futile try at hand calculation.

The simulation showed that a 20:1 increase in gain through the elevator-nose door system could be tolerated before instability occurred.

Calculation of Generalized Masses for the First and Second Symmetric Modes

As described in Reference 1, the motion of the flexible airframe can be described by means of the normal vibration modes of the vehicle. The problem was arbitrarily simplified to include only the effects of the first two symmetric modes, which have frequencies of 71.7 and 88 radians per second, respectively.

The generalized masses of the first two modes were calculated using the latest vehicle mass distribution in conjunction with smoothed modal

displacement data obtained from the ground shake tests. Where the displacement data was obtained at different points than the locations of the incremental masses, graphs were drawn to accurately determine the vehicle displacements at the incremental mass points. These vehicle displacements were then normalized and used to calculate m_{11}, m_{22}, and m_{12}, the intermodal mass.

The values in slug ft^2 are:

$$m_{11} = 8.22$$

$$m_{22} = 19.49$$

$$m_{12} = 1.52$$

As a check on the calculation of the generalized masses, data on the maximum vehicle amplitude in the first mode during the vibration test was utilized. The transient response of the 1st symmetric mode was recorded on an oscillograph, thus enabling the damping of the first mode to be measured. The damping ratio of the first mode was determined to be . 02. In addition, the shaker forces and shaker attach point displacements were known. To determine the maximum displacement, $q^{(1)}$, of the first body mode, we make use of the relationship, assuming no intermodal coupling:

$$q^{(1)} = \frac{\sum_{s=1}^{i} F_s \phi_s^{(1)}}{m_{11}(S^2 + 2\xi_1 \omega_{11} S + \omega_{11}^2)} \qquad (1)$$

where the F_s values are the shaker forces exciting the first mode.

If we let $S = j\omega$, thus assuming the shaker forces are sinusoidal, the transfer function becomes:

$$q^{(1)} = \frac{\sum F_s \phi_s^{(1)}}{m_{11}\left(\omega^2 - \omega_{11}^2 + 2j\omega\omega_{11}\xi_1\right)} \qquad (2)$$

and if we further "tune" the exciting frequency so that $\omega = \omega_{11}$, we obtain the expression for the value of $q^{(1)}$:

$$q^{(1)} = \frac{\sum_{s=1}^{i} F_s \phi_s^{(1)}}{m_{11}\left(2j\omega_{11}^2 \xi_1\right)} \tag{3}$$

Now, as $q^{(1)}$ and ξ_1 have been determined, a check on m_{11} is made possible.

In the case of the first mode, eight shakers were applied, and the amplitudes and normalized displacements of the shaker inputs are given below in Table 12 along with the generalized force components:

TABLE 12

SHAKER NUMBER	F_s, PEAK SHAKER FORCE	$\phi_s^{(1)}$	$F_s \phi_s^{(1)}$
1	3	.75	2.25
2	5.7	.75	4.27
3	4.4	.415	1.83
4	-7.0	-.227	1.59
6	-10.2	-.410	4.18
7	-2.5	-.209	.523
8	-1.14	-.209	.239
		$\sum F_s \phi_s^{(1)} \rightarrow$	16.13

We can now use equation (3) to solve for $q^{(1)}$:

$$q^{(1)} = \frac{\Sigma F_s \phi_s^{(1)}}{m_{11}\left(2j\omega_{11}^2 \xi_1\right)} = \frac{16.13}{8.22\ (2 \times .02 \times 5126)} \tag{4}$$

$$q^{(1)} = .00956 \text{ ft} = .1147 \text{ in.} \tag{5}$$

Now, the maximum acceleration measured on the vehicle during this test was .94 g's. At a frequency of 71.7 radians per second, this acceleration is equal to a .0059 ft or .0708 in. peak displacement. Thus the measured displacement, .0708 in., compares fairly well with the calculated displacement using smoothed mode shape data.

The effect of the intermodal mass, m_{12}, can be determined by writing the differential equation for the response of the first two modes:

$$m_{11}\ddot{q}^{(1)} + m_{12}\ddot{q}^{(2)} + k_{11}q^{(1)} = \Sigma F_j q_j^{(1)} \tag{6}$$

$$m_{22}\ddot{q}^{(2)} + m_{21}\ddot{q}^{(1)} + k_{22}q^{(2)} = \Sigma F_j q_j^{(2)} \tag{7}$$

Taking the Laplace transform of (6) and (7)

$$q^{(1)}\left(S^2 m_{11} + k_{11}\right) + S^2 m_{12} q^{(2)} = \Sigma F_j q_j^{(1)} \tag{8}$$

$$S^2 m_{12} q^{(1)} + q^{(2)}\left(S^2 m_{12} + k_{22}\right) = \Sigma F_j q_j^{(2)} \quad , \tag{9}$$

and solving for $q^{(1)}$:

$$q^{(1)} = \frac{\Sigma F_j q_j^{(1)}\left(S^2 m_{22} + k_{22}\right) - \Sigma F_j q_j^{(2)} S^2 m_{12}}{\left(S^2 m_{11} + k_{11}\right)\left(S^2 m_{22} + k_{22}\right) - S^4 m_{12}^2} \tag{10}$$

The effect of m_{12} on the response of $q^{(1)}$ is evident, in that the roots of the characteristic equation are modified.

If we add the effect of structural damping to equation 10, then

$$q^{(1)} = \frac{\Sigma F_j q_j^{(1)}\left(S^2 m_{22} + SD_{22} + k_{22}\right) - \Sigma F_j q_j^{(2)} S^2 m_{12}}{\left(S^2 m_{11} + SD_{11} + k_{11}\right)\left(S^2 m_{22} + SD_{22} + k_{22}\right) - S^4 m_{12}^2} \tag{11}$$

If the structural damping is approximately equal to $\xi = .02$, then $D_{11} = 23.57$, and $D_{22} = 68.6$. Substituting values of m_{11}, D_{11}, k_{11}, m_{22}, D_{22}, k_{22} and m_{12}, we obtain a new characteristic equation, which is:

$$157.89\,(S^4 + 6.48\,S^3 + 13.028 \times 10^3\,S^2 + 40.756 \times 10^3\,S + 40.13 \times 10^6) = 0 \qquad (12)$$

The solution of this equation results in two new modal frequencies, with values of 70.7 and 89.55 radians per second, respectively. Since the uncoupled frequencies were 71.7 and 88 radians per second, the effect of m_{12} was considered to be negligible.

In order to include the nose-door dynamic effects on the fuselage, the characteristics of the nose fan thrust-reverser doors including the turning vanes were calculated. Since the vertical reaction on the vehicle is caused by vertical motion of the nose-door c.g., the nose door c.g. location must be known with respect to the door hinge line.

Table 13 lists the nose door and turning vane c.g. location.

TABLE 13

	ONE NOSE DOOR	ONE TURNING VANE
$\bar{x}$	57.3	57.89
$\bar{y}$	15.94	10.9
$\bar{z}$	83.0	86.4
Weight	23 lbs	8.87 lbs

Solving for the total c.g.:

$$\bar{x} = \frac{8.87\,(57.89) + 23(57.3)}{31.87} = 57.46 \qquad (13)$$

$$\bar{y} = \frac{8.87\,(10.9) + 23(15.94)}{31.87} = 14.53 \qquad (14)$$

$$\bar{z} = \frac{8.87\ (86.4) + 23\ (83.0)}{31.87} = 83.95 \qquad (15)$$

In addition, the I_x of the vane parts about the vane c.g. = 116 lb in^2.

The inertia about the hinge line of one door alone was measured to be 1702 lb in^2.

By a geometric construction the moment arm of the turning vanes about the nose door hinge lines was found to be 6.8".

The total vane inertia about the hinge line is thus:

$$I_{x_{\text{hinge line}}} = 116 + 6.8^2 \times 8.87 = 526 \text{ lb in}^2 \qquad (16)$$

The addition of the turning vanes thus increases the inertia of a single nose door from 1703 lb in^2 to 2228 lb. in^2. The increase of inertia lowers the nose-door spring-mass natural frequency to about 77 rad/sec.

By means of the same construction the moment arm of the door c.g. about the hinge line was found to be 3.5". At zero nose fan thrust, corresponding to 45° β_V, the nose door plus vane c.g. rotation has a tangent at 35° from the vertical.

The vertical acceleration of the door c.g. is thus:

$$\ddot{z}_{c.g.} = r\dot{\omega}\cos 35° = 3.5\ \ddot{\delta}_p (.82) \text{ in/sec}^2 \qquad (17)$$

The force necessary to accelerate the door c.g. is thus:

$$F_{VERT} = m_{door} (.82 \times 3.5\ \ddot{\delta}_p) \qquad (18)$$

$$F_{VERT} = 2.87\ m_{door}\ \ddot{\delta}_p \qquad (19)$$

The mass of one door with vanes $= \frac{31.87}{386} = .0825 \frac{\text{lb sec}^2}{\text{in}}$. Therefore, the vertical reaction due to a positive door angular acceleration is:

$$F_{React.} = 02.87 \times .0825 \ddot{\delta}_p = -.236 \ddot{\delta}_p$$

$$= -.236 S^2 \delta_p \text{, per door.} \tag{20}$$

In addition, the nose door actuator body moves with the nose doors, and has a gain of 2.74 inches per radian of δ_p.

The moving parts of the actuator weigh about 6 lbs, so the reaction on the vehicle due to servo acceleration is:

$$F_{React._{Servo}} = \frac{2.74 \times 6}{386} \ddot{\delta}_p = -.0426 S^2 \delta_p \tag{21}$$

We must now compute the total forces exerted on the vehicle by both sides of the nose doors plus the servo. Therefore, using a gradient of -1300 lbs per radian of δ_p for static nose fan thrust:

$$F_{\delta_{p_{TOT}}} = -1300 \delta_p - 2 \times .236 \delta_p S^2 - .0426 \delta_p S^2 \tag{22}$$

$$F_{\delta_{p_{TOT}}} = \delta_p \left[-1300 - (.472 + .043) S^2\right] \tag{23}$$

$$F_{\delta_{p_{TOT}}} = -1300 \delta_p \left[1 + \frac{S^2}{2520}\right] \tag{24}$$

The effect of the nose door mass therefore puts a second order zero at $S = \pm j 50.1$ radians/second.

The effect of the flexibility of the system between the servo and the doors themselves can now be added as below, where $\xi_{\text{nose door}}$ has been increased to about .2 critical by the addition of fluid dampers:

$$F_{\delta_p} = \frac{-1300 \delta_p \left[1 + \frac{S^2}{2520}\right]}{\left(\frac{S^2}{77^2} + \frac{2 \times .2 S}{77} + 1\right)} \tag{25}$$

If we now add the effect of the nose door servo actuator response, which is a 1/20 sec. time lag, we obtain:

$$\frac{F_{\delta_p}}{\delta_{p_{command}}} = \frac{-1300\left(1 + \frac{S^2}{2520}\right)}{\left(\frac{S^2}{77^2} + \frac{.4S}{77} + 1\right)\left(\frac{S}{20} + 1\right)} \tag{26}$$

This is the equation, then, for the net force on the airframe due to nose door input command.

The elevator system is connected to the nose door system through the pitch mixer. At $\beta_V = 45°$, the gain of the nose door rotation to elevator position is equal to .69. We can then write:

$$\frac{F_{\delta_p}}{\delta_e} = \frac{-897\left(1 + \frac{S^2}{50.1^2}\right)}{\left(\frac{S^2}{77^2} + \frac{.4S}{77} + 1\right)\left(\frac{S}{20} + 1\right)} \tag{27}$$

We must now derive the relationships governing the elevator and rigid-body dynamics.

If we define pitch angle, θ, in the usual sense, the position of the elevator with respect to the tail, δ_e, is:

$$\delta_e \triangleq \theta_\epsilon - \theta_T \tag{28}$$

where:

θ_T = Tail pitch angle

θ_ϵ = Elevator pitch angle

In our analysis we will assume the stick is fixed in the cockpit. Any elevator deflection from neutral will be opposed by both the hinge moment due to elevator deflection and tail angle of attack, and the spring constant of the elevator system. In our elevator system the elevator inertia is

equal to .173 slug ft^2, and the elevator spring mass system natural frequency, stick fixed, is equal to 55.2 rad/sec. The elevator system spring constant is thus equal to 525 ft lbs/rad. We can thus write the equation relating elevator torque to elevator acceleration:

$$I_\epsilon S^2 \theta_\epsilon = -K_s \delta_\epsilon + H_\epsilon \tag{29}$$

$$I_\epsilon S^2 \theta_\epsilon = -K_s (\theta_\epsilon - \theta_T) + H_\epsilon \tag{30}$$

where K_s is the elevator spring constant, referred to the elevator hinge line. We may expand H_ϵ

$$H_\epsilon = q S_\epsilon \bar{c}_\epsilon \left[C_{h_{\epsilon_{\delta_e}}} \delta_\epsilon + C_{h_{\epsilon_{\alpha_\tau}}} \alpha_\tau \right] \tag{31}$$

where the various terms are as defined in the list of symbols and definitions.

For this vehicle:

$$C_{h_{\epsilon_{\delta_e}}} = -.006/\text{deg.} = -.3438/\text{rad} \tag{32}$$

$$C_{h_{\epsilon_{\alpha_\tau}}} = -.0012/\text{deg.} = -.069/\text{rad} \tag{33}$$

$$S_\epsilon = 11.97 \text{ ft}^2 \tag{34}$$

$$\bar{c}_\epsilon = 1.11 \text{ ft} \tag{35}$$

If we let $\gamma = 0$, then $\alpha = \theta$, so:

$$H_\epsilon = q S_\epsilon \bar{c} \left[-.3438 \delta_\epsilon - .069 \theta_T \right] \tag{36}$$

or, using equation 28:

$$H_\epsilon = q S_\epsilon \bar{c}_\epsilon \left[-.3438 \, (\theta_\epsilon - \theta_T) - .069 \, \theta_T \right] \tag{37}$$

$$H_\epsilon = q S_\epsilon \bar{c}_\epsilon \left[-.3438 \, \Delta\theta_\epsilon + .27 \, \Delta\theta_T \right] \tag{38}$$

In this case, we define:

$$\theta_T = \theta_{T_{RB}} + \theta_{T_{BT}} \tag{39}$$

where:

$\theta_{T_{RB}}$ = Incremental variation of tail pitch angle due to rigid body rotation.

$\theta_{T_{BT}}$ = Incremental variation of tail pitch angle due to rotation of the tail under flexible body bending.

We also write the equations relating the rigid body motions of the vehicle to elevator deflections and angle of attack variations:

$$I_y S^2 \theta_{RB} = L_{NF} \bar{x}_{NF} - L_T \bar{x}_T \tag{40}$$

where:

L_{NF} = nose fan lift variation due to elevator deflection, shown in equation (27).

L_T = tail lift variation due to elevator deflection and angle of attack variations.

The tail lift terms may be expanded as below:

$$L_T = q K_T \eta_T \left[C_{L_{\alpha_t}} (\alpha - \epsilon) + C_{L_{\delta_\epsilon}} \delta_\epsilon \right] S_t$$

$$+ \rho \frac{V_T S_w \bar{c}}{4} C_{L_q} \dot{\theta} \tag{41}$$

Substituting values into eq. (41) and letting $\gamma = 0$, we obtain:

$$L_T = q \left\{ 144.6\, \theta_T - 50.6\, \theta_{RB} + 62.8\, \delta_\epsilon \right\} + 2171\, \rho\, V_T \dot{\theta} \qquad (42)$$

Using eq. (28), we rewrite eq. (42):

$$L_T = q \left\{ 81.8\, \theta_T - 50.6\, \theta_{RB} + 62.8 \theta_\epsilon \right\} + 2171\, \rho\, V_T \dot{\theta} \qquad (43)$$

All of the data are now at hand to determine the stability of the system.

The nose fan and tail lift values are used to determine the generalized forces for the first two flexible body modes, and these in turn will determine $q^{(1)}$ and $q^{(2)}$, which in turn will determine θ_T, and so on.

The complete differential equations to be solved, in operator form, are given below.

The analog computer mechanization for these equations is shown in Figure 181.

It was found that a 20:1 increase in gain around the loop was required to cause any instability for this system. The conclusion was that there will be no problem due to coupling of the nose-doors and elevator at high vector angles.

$$I_y S^2 \theta_{RB} = L_{NF} \bar{x}_{NF} - L_T \bar{x}_T \qquad (44)$$

$$I_\epsilon S^2 \theta_\epsilon = -K_s \delta_\epsilon + q S_\epsilon \bar{c}_\epsilon \left[-.3438\, \theta_\epsilon + .275\, \theta_T \right] \qquad (45)$$

$$\delta_\epsilon = \theta_\epsilon - \theta_T \qquad (46)$$

$$\theta_T = \theta_{T_{RB}} + \theta_{T_{BT}} \qquad (47)$$

$$\theta_{T_{BT}} = q^{(1)} \sigma_T^{(1)} + q^{(2)} \sigma_T^{(2)} \qquad (48)$$

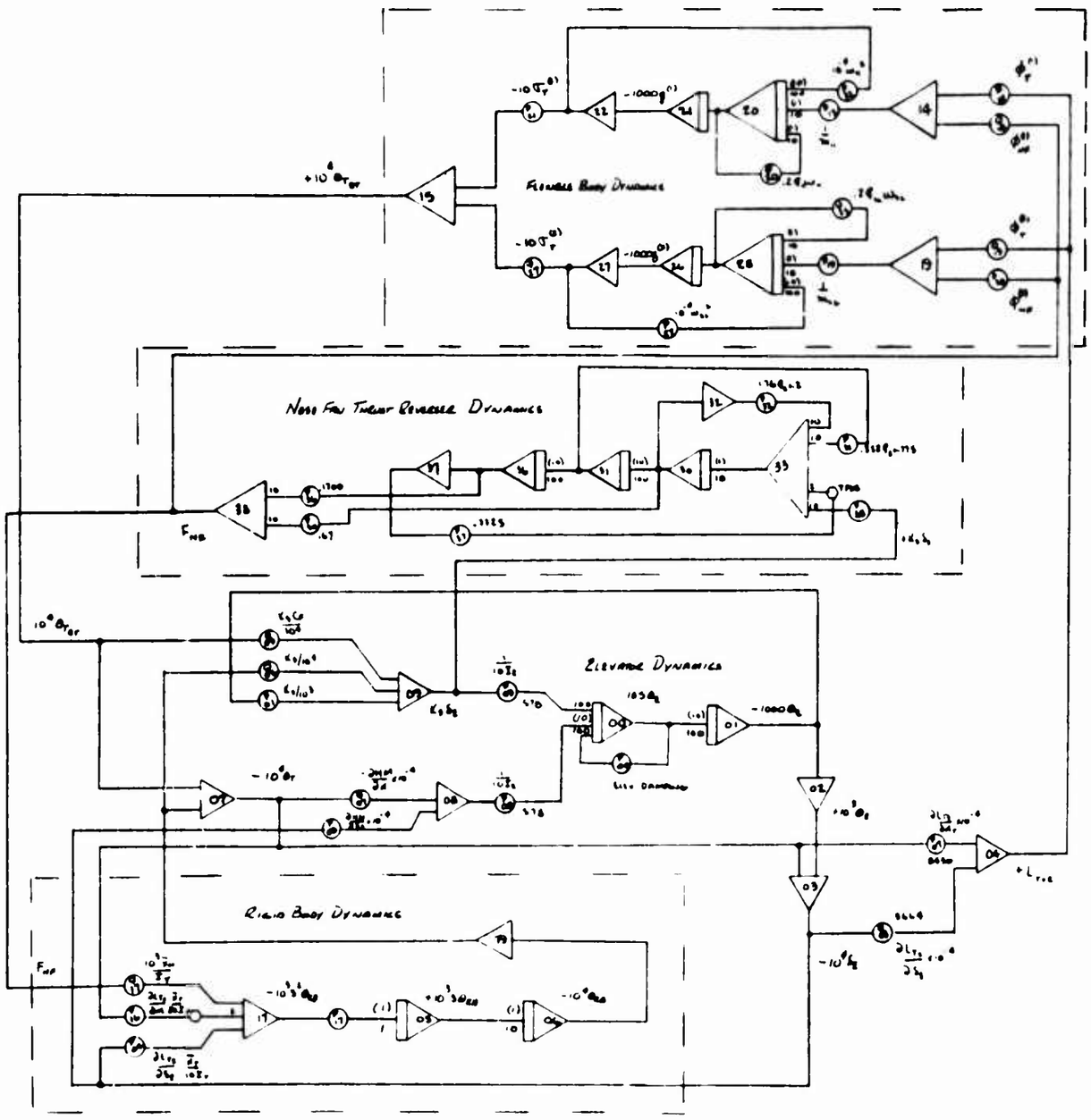

Figure 181 Elevator-Nose Feedback, Analog Computer Setup, Rigid Body Plus First Two Flexible Body Modes

$$q^{(1)} = \frac{L_{NF}\,\phi_{NF}^{(1)} + L_T\,\phi_T^{(1)}}{m_{11}\left(S^2 + .04\,S\omega_{11} + \omega_{11}^2\right)} \tag{49}$$

$$\dot{\sigma}^{(2)} = \frac{L_{NF}\,\phi_{NF}^{(2)} + L_T\,\phi_T^{(2)}}{m_{22}\left(S^2 + .04\,S\omega_{22} + \omega_{22}^2\right)} \tag{50}$$

$$L_{NF} = \frac{-897\,\delta_\epsilon\left(1 + \dfrac{S^2}{50.1^2}\right)}{\left(\dfrac{S^2}{77^2} + \dfrac{.4S}{77} + 1\right)\left(\dfrac{S}{20} + 1\right)} \tag{51}$$

$$L_T = q\left[81.8\,\theta_T - 50.6\,\theta_{RB} + 62.8\,\theta_\epsilon\right] + 2171\,\rho\,V_T\dot{\theta}$$

For use with equations 48, 49, and 50, the following values for θ and T obtain:

$$\phi^{(1)}_{NF} = .28 \qquad \phi^{(2)}_{NF} = +.50$$

$$\phi^{(1)}_{T} = +.46 \qquad \phi^{(2)}_{T} = +.54$$

$$\sigma^{(1)}_{T} = -.0369 \qquad \sigma^{(2)}_{T} = -.6830$$

In the solution used for this study, the effect of the torque developed at the elevator hinge line on the flexible body modes is neglected.

6.3 WINDS

It was desired to enable the insertion of steady and gusty winds into the simulation, to permit a more realistic evaluation of the vehicle handling qualities.

The inclusion of a wind vector in the simulation requires the modification of the generation of u, v, w, V_T, and their derivative functions, such as α, β, q, etc.

Referring to equations 1, 2, and 3 of the equations of motion, it is seen that the u, v, and w components of the first two terms of each equation are inertial velocities measured with respect to the earth. However, the relative velocity affects the calculation of forces and moments.

Thusly, two velocities are computed for each of the linear degrees of freedom. In the case of u, the inertial value of u, called simply u, is used in the body dynamic equation and u_a, the effective aerodynamic u, is computed by adding the wind u, u_w, to u.

Or

$$u_a = u + u_w$$

Then:

$$v_a = v + v_w \tag{29}$$

$$w_a = w + w_a \tag{30}$$

If we assume the surface wind acts only in the horizontal plane, and only affects the airplane x - y plane, we can write, assuming a wind of V_w fps is blowing from a direction Ψ_w:

$$u_w = V_w \cos (+ \Psi + \Psi_w) \tag{31}$$

$$v_w = V_w \sin (- \Psi + \Psi_w) \tag{32}$$

$$w_w = 0 \tag{33}$$

and in the vertical plane:

$$w_w = w_w \tag{34}$$

Where V_w and w_w have the correct spectral densities to simulate the desired wind characteristics.

In our work, to conserve equipment, the wind mass was assumed to be blowing from the $\Psi = 0$ direction, with no variation in direction.

It is thus possible to simulate winds from any direction by simply rotating the vehicle in yaw to the desired heading.

If the wind comes from the $\Psi = 0$ direction, then

$$u_w = V_w \cos \Psi$$

$$v_w = V_w \sin \Psi$$

$$w_w = w_w \text{ (w_w is assumed independent of the distribution of } V_w)$$

Thusly, the velocities to be used in calculating the aerodynamic terms are subscripted "a" and are:

$$u_a = u + u_w$$

$$v_a = v + v_w$$

$$w_a = w + w_w$$

Once the method of inserting winds into the problem is determined, the structure of the wind must be determined, and a means must be developed to generate this wind structure.

The method chosen was to determine a gust spectral density and then operate on a white-noise signal with the appropriate transfer function to attain this spectral density.

The only available information on surface gusts was obtained from Reference 2, and was taken on Long Island at a height of 300'. It was felt that this data would be sufficiently general to be useful in this simulation.

Table 14 is a listing of $10^4 \frac{\Delta v^2}{w_m^2}$ versus the gust frequency in cycles per hour:

TABLE 14

f, cycles/hr	6	8	10	20	40	60	80	100	200	400
$10^4 \frac{\Delta v^2}{W_m^2}$	-	-	-	68	66	52	38	32	16	7

Δv is defined as the eddy velocity, and W_m is defined as the mean wind.

If this gust spectrum is considered valid when in proximity to the ground and applicable to the California desert area, it is only necessary to generate this spectrum and set the gust level at a point deemed reasonable from local observations.

In lieu of better data, observations taken at a local yacht club have formed the basis for setting gust levels. In general, over a period of several years, it has been noted that a mean wind of 15 knots will fluctuate between 25 knots and 10 knots. If we can assume the velocities normally distributed, then the 15 knot peak-peak variation can be assumed to be the plus or minus 3 σ variation, or 6 σ is 15 knots or 25.4 fps. The RMS value of the gust is then σ, or 15/6 = 2.5 knots.

With this in mind, the gust spectrum was shaped based on the ARDC information, and added to a steady wind in varying proportions.

Now, the spectral density of the output of a filter driven with white noise is:

$$\phi_{on-on}(j\omega) = \left|G(j\omega)\right|^2 \phi_{nn}(j\omega),$$

where $\phi_{nn}(j\omega)$ is a constant, given as volts^2/cps, and $G(j\omega)$ is the frequency response of the filter.

A first order filter was used to fit the gust spectrum of Table 14, and the data of this table along with the resultant of white noise into a first order filter is shown in Figure 182 for three filter time constant values.

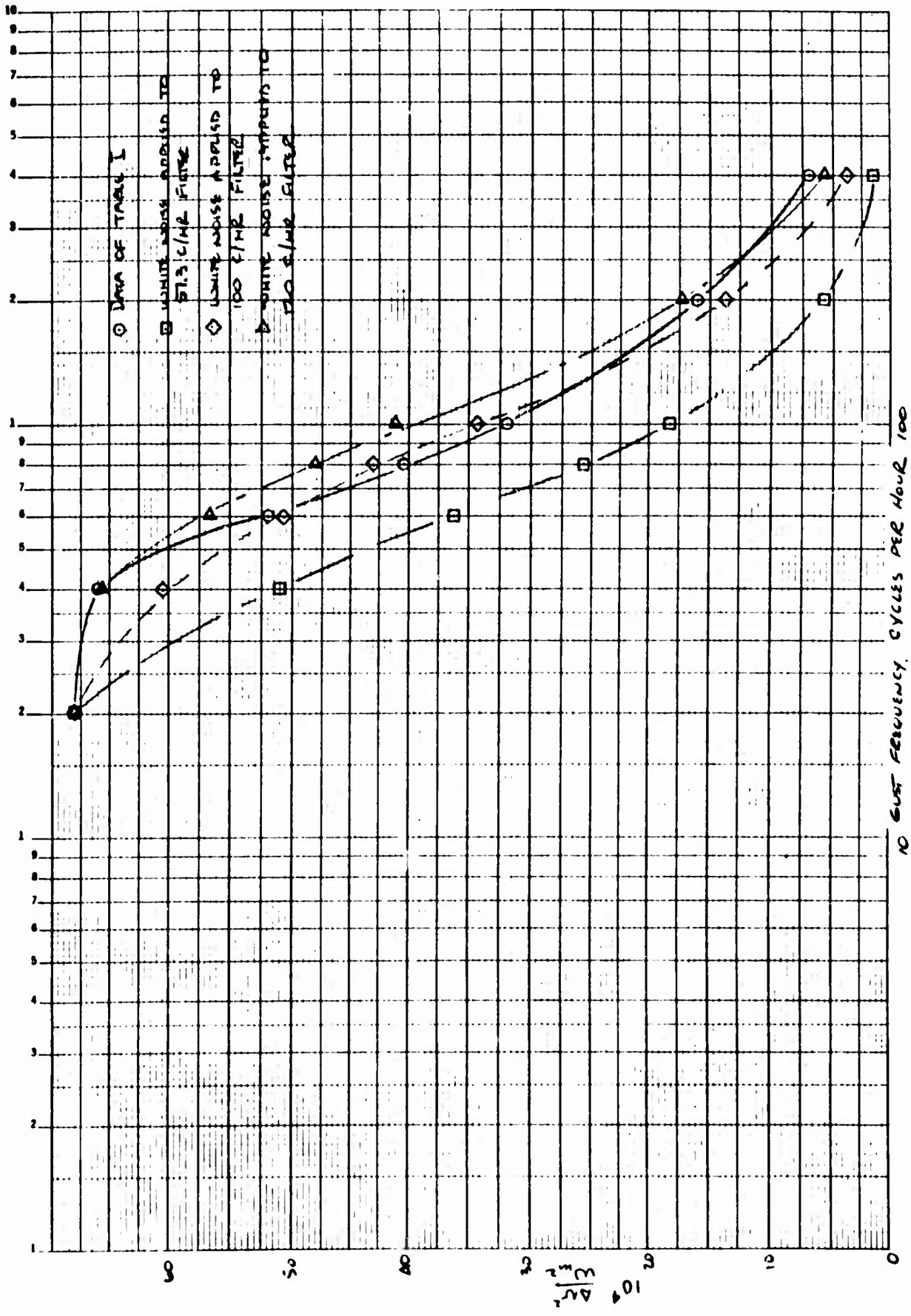

Figure 182 Gust Velocity Distribution

For no particular reason, the 57.3 cycle/hour filter was chosen to generate the gust spectrum for this study. The RMS gust level was set as high as 50 per cent of the steady wind for handling qualities evaluations, and no problems were apparent.

In the case of vertical winds, absolutely nothing was known about the expected effects of fan exhaust impingement and re-ingestion.

Since the vehicle is most sensitive in roll, the output of a white noise generator equivalent to an RMS rolling moment of 7500 ft/lbs was applied to the vehicle. The noise generator had a bandwidth of from DC to 120 cps, and the airframe provided the filtering.

With the worst condition of rolling moment noise and no pilot roll control the SA system held the aircraft to within plus or minus 8° bank angle. Altitude control was precise enough at this time to successfully land the vehicle in this noise environment.

6.4 LOUVER SERVO TESTS

Since the roll-yaw bridge concept for the exit louver servo electrical inputs was untested until the XV-5A hydraulic simulator became available, several tests were performed to determine the cross-coupling from roll to yaw and vice versa, as well as to verify the predicted operation in the presence of valve coil failures.

The roll-yaw bridge is designed such that each of the two electrical input coils for an actuator is located in an opposite bridge leg. If the SA amplifiers had infinite output resistance, there would be no effect for a single open coil.

When the simulator was first turned on, an open coil was discovered in the aft right louver servo, and the data for roll and yaw inputs is presented in Table 15 following.

The input was adjusted so the forward left louver had a plus or minus 1° amplitude, for both roll and yaw inputs.

TABLE 15

EFFECT OF SINGLE OPEN VALVE COIL

LOUVER FUNCTION	FWD LT	AFT LT	$\beta_{s_{LT}}$	$\beta_{v_{LT}}$	FWD RT	AFT RT	$\beta_{s_{RT}}$	$\beta_{v_{RT}}$
Yaw Input	±1°	±.43°	±.57°	±.715	∓.65°	∓.4°	∓.25°	∓.525
Roll Input	±1°	.45°	±1.45	±.275°	±.425°	∓.7°	∓1.125°	∓.1375°

Using the definitions:

$$\beta_s = \beta_2 - \beta_1 ,$$

$$\beta_v = \frac{\beta_2 + \beta_1}{2} ,$$

We calculate β_s and β_v for right and left fans in Table 15.

As is mentioned in the failure analysis section, fan-powered flights were made with both open and shorted valve coils, and with the two coils in a single servo open and shorted simultaneously.

These failures and the associated coupling as shown in Table 15 have been determined to have essentially no effect on flying qualities when introduced during the failure simulation program.

Frequency response runs were made on installed louver and nose fan door servos on the hydraulic simulator, and are presented in Figures 183 thru 187, along with linear fits to the data.

A further cross-coupling effect was noted which didn't cause flying problems, but is of interest.

It was found that cross-coupling occurred from roll-yaw and yaw-roll which varied with hydraulic oil temperature. Measurements were made with sufficient roll or yaw SA inputs to cause saturation of the servo electrical input, and the resulting vector and stagger changes were noted. These are given in Table 16.

TABLE 16

COLD OIL	$\beta_{s_{RT}}$	$\beta_{s_{LT}}$	$\beta_{v_{RT}}$	$\beta_{v_{LT}}$
+ Yaw Rate	+27.03°	+27.8°	+1.10°	-4.62°
- Yaw Rate	28.06°	27.18°	-6.06°	+2.72°
+ Roll Rate	+34.76°	+20.4°	-2.06°	- .82°
- Roll Rate	+20.6°	+34.7°	-2.33°	-1.07°
WARM OIL (190° F)				
+ Yaw Rate	+26°	+27.15°	- .09°	-5.42°
- Yaw Rate	+28.05°	+26.35°	-6.95°	+1.73°
+ Roll Rate	+33.38°	+19.8°	-3.54°	-1.69°
- Roll Rate	+21.0°	-33.5°	-3.00°	-2.2°

As originally specified, the louver deflection for full electrical input was plus or minus 3.4°. Thus, a full roll signal affords 6.8° of stagger on each wing (3.4 + 3.4), and a full yaw signal affords 3.4° of vector on each wing $\left(\frac{3.4 + 3.4}{2}\right)$.

6.5 GYROSCOPIC COUPLING

There are five major rotating components in the XV-5A which can cause gyroscopic coupling effects. These are the two J-85 gas generators and the three lift fans. Since the wing fans counter-rotate, the major part of wing fan angular momentum is eliminated, and the only angular momentum arising from the wing fans is due to fan speed differential.

Table 17 is a listing of the various angular momentum values for the engines and fans.

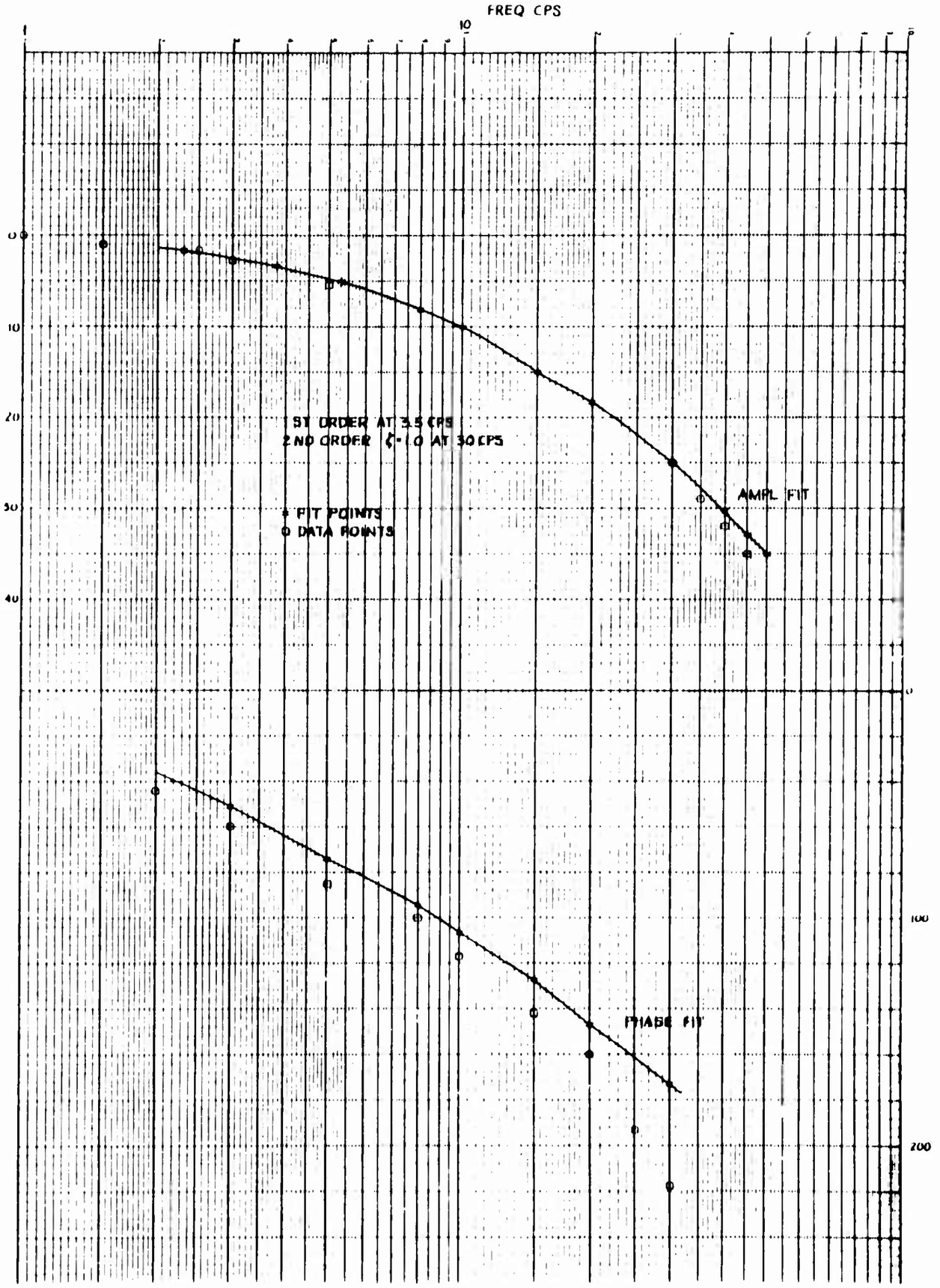

Figure 183 L. H. Forward Louver Servo Test

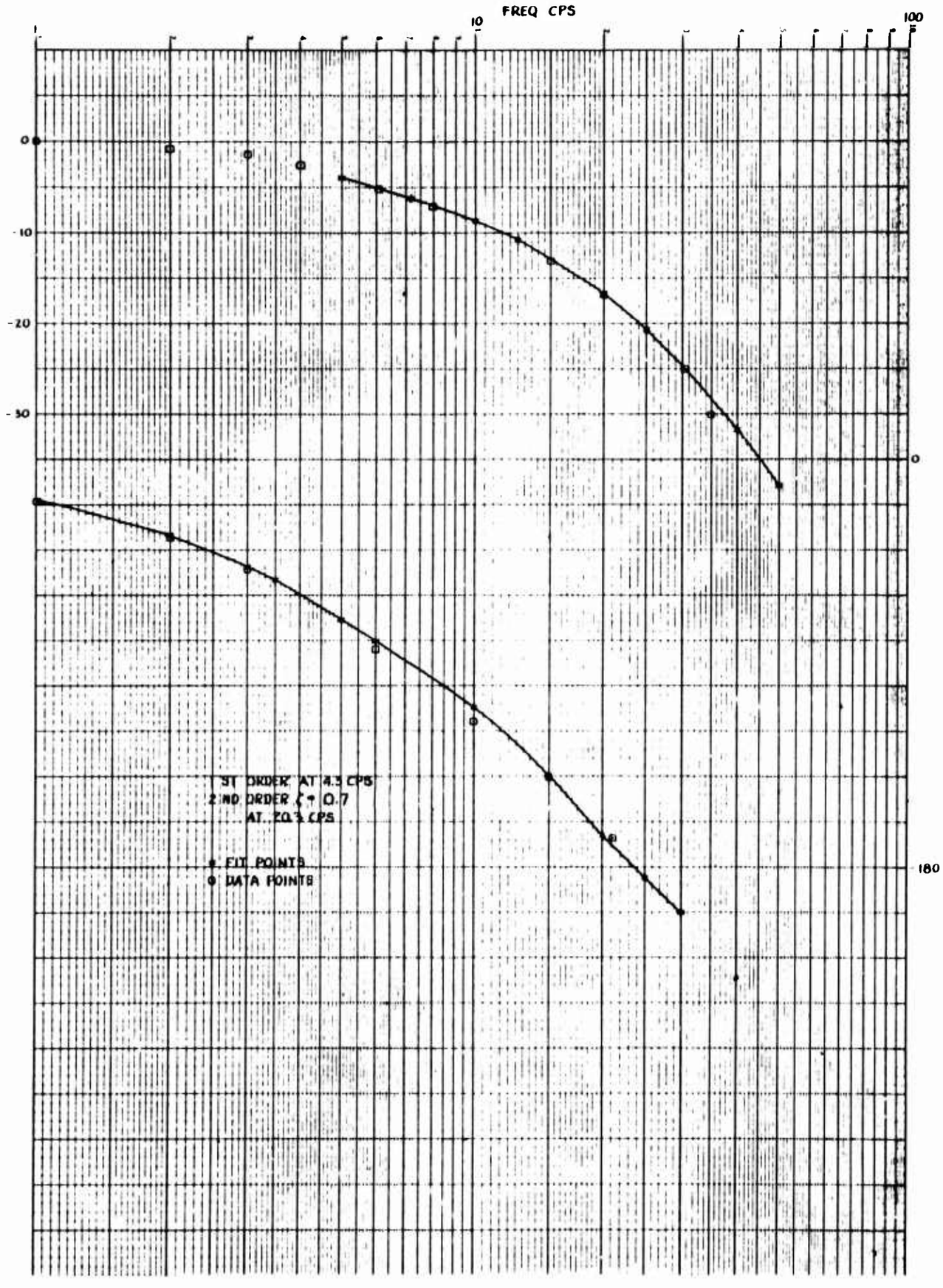

Figure 184 Louver Servo Test ± 4ma Electrical Input

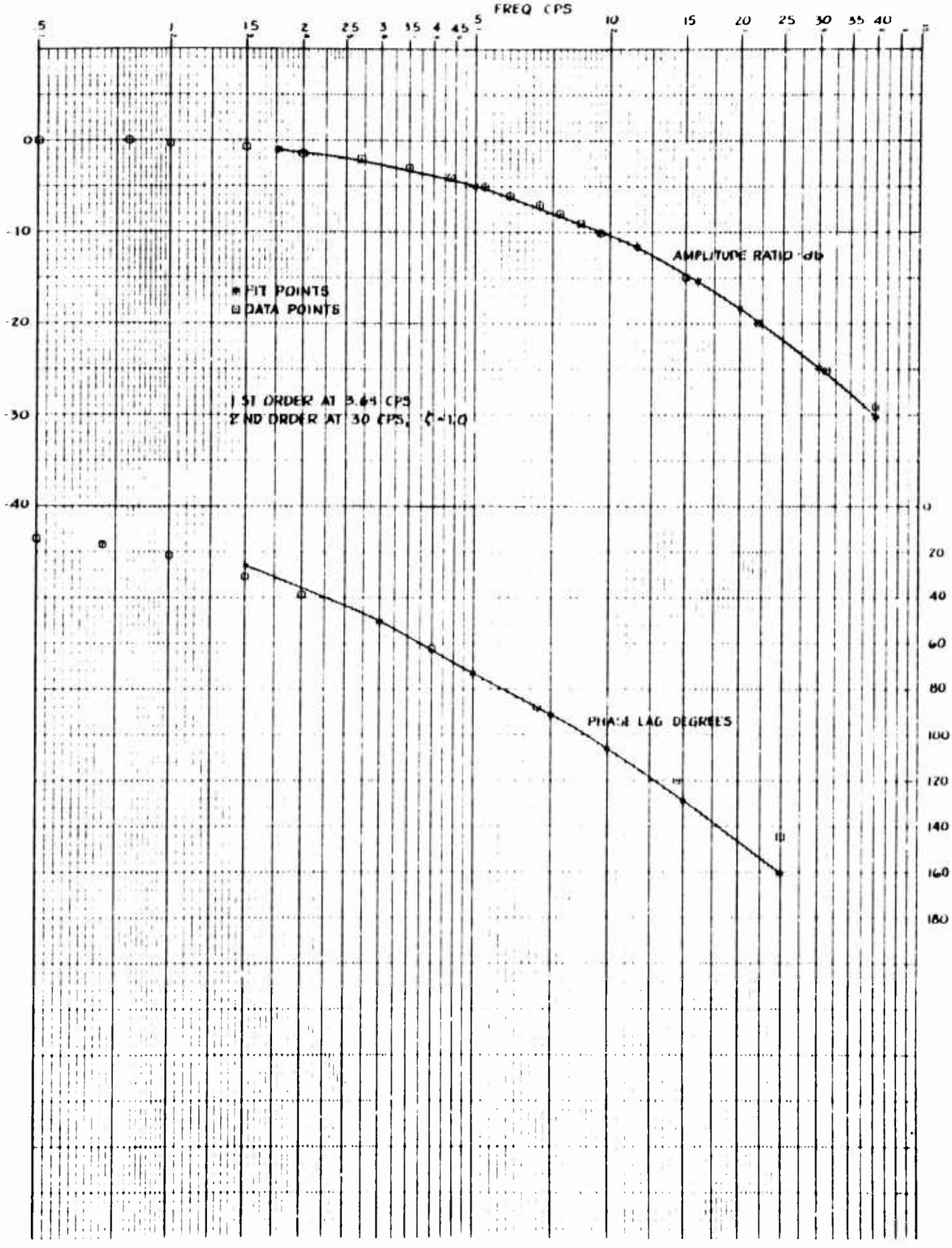

Figure 185 Louver Servo Test + 2ma Electrical Input

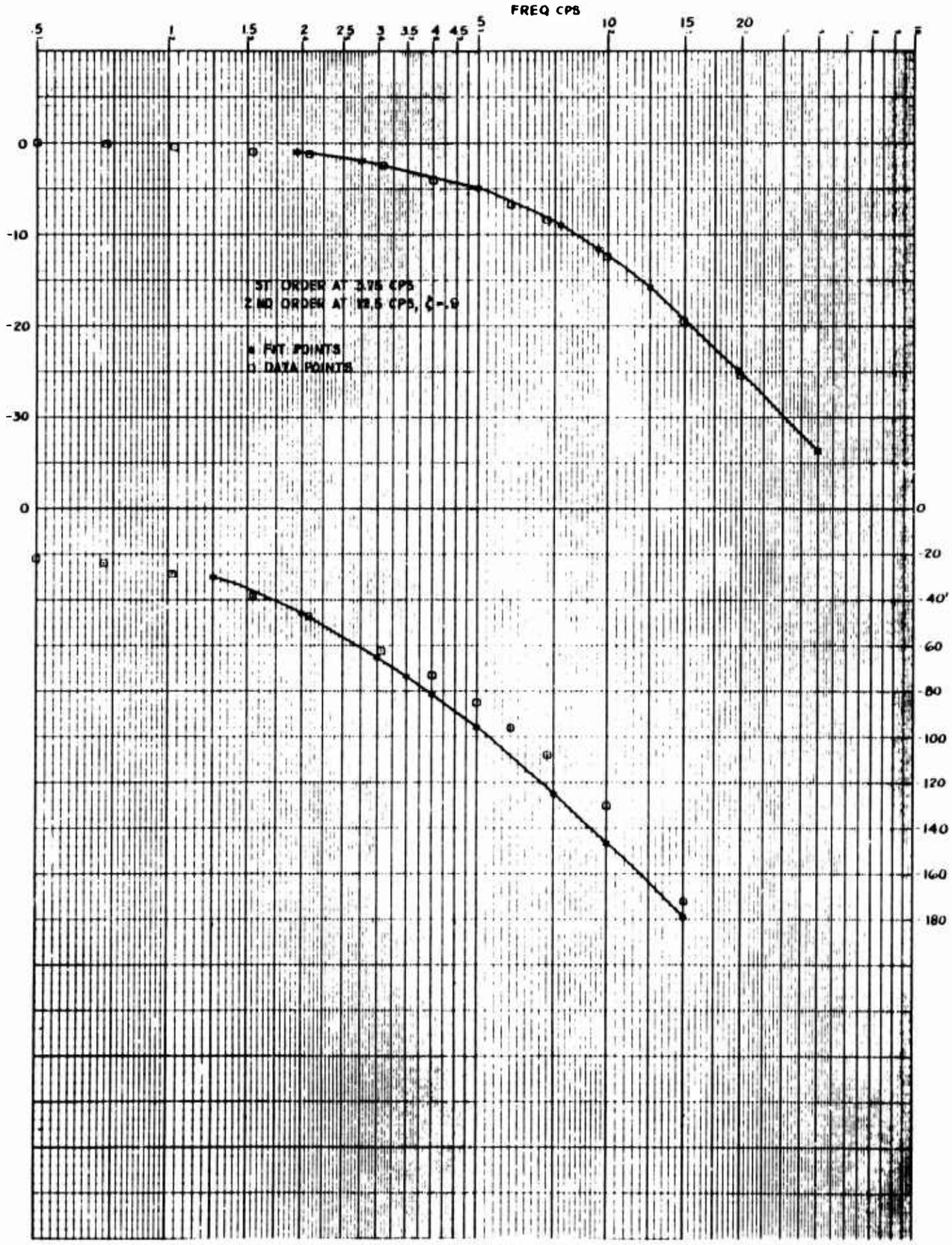

Figure 186 Louver Servo Test ± 1ma Electrical Input

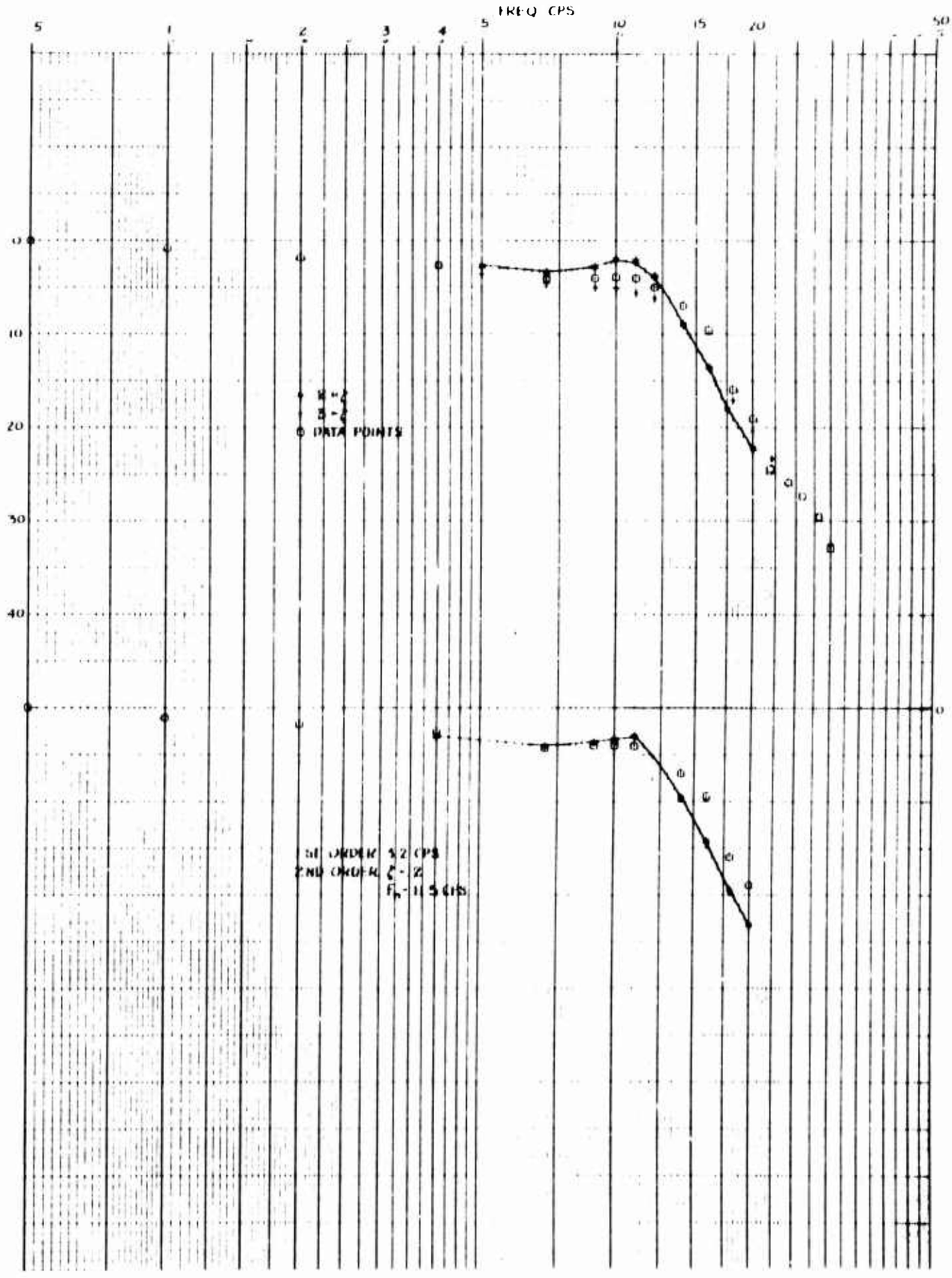

Figure 187 Noise Fan Thrust Reverser Servo Test

TABLE 17

		DIR. OF ROT.	RPM @ 100%	POLAR MOM. OF INERTIA	ANG. VEL. AT 100%, RAD/SEC
1.	RT J-85	cw from rear	16,500	.512	1730
2.	LT-J-85	cw from rear	16,500	.512	1730
3.	Nose fan	ccw from top	4,074	1.293	426
4.	Rt. wing fan	cw from top	2,640	30.2	276
5.	Lt. wing fan	ccw from top	2,640	30.2	276

	ANG. MOM. AT 100%	ROTATION AXIS LOCATION	H_x	H_y	H_z
1.	885	5° up from x	882	0	- 77.1
2.	885	5° up from x	882	0	- 77.1
3.	- 552	z	0	0	- 552
4.	8350	z	0	0	8350
5.	-8350	z	C	0	-8350

As can be seen, the angular momentums from the wing fans will normally cancel. However, the case of full roll control will be investigated because the fan speed on the wing fans will differ appreciably. It is possible to have this condition in the case of hovering in a sidewind, for example.

At full gas generator power, 2500' hot day, with full right roll commanded in the hover mode, the right and left wing fan RPM can be computed from the following relationships:

$$C_p^s(\beta_v, \beta_s) = \frac{P_F \rho^{1/2}}{\left(\frac{T_{ooo}}{A_F}\right)^{3/2} A_F} \tag{1}$$

and

$$\frac{T_{ooo}}{A_F} = 291 \left(\frac{N_F}{100}\right)^2 \tag{2}$$

In our case, $C_p^s = 1.0$ at hover and $\beta_s = 0$, and P_F at 100% $N_g = 3.64 \times 10^6$.

If we command full roll control at nominal lift, the left wing stagger will be 14°, and the right wing stagger will be 40°. In this case, assuming $\beta_v = 0$, the ΔC_p^s due to β_s will be -.12 on the right wing and -.014 on the left wing. Thus $C_{p_{RT}}^s = .88$, and $C_{p_{LT}}^s = .986$.

Solving Eq. (1) for T_{ooo}/A_F, with $\rho = .00205$, we obtain,

$$\frac{T_{ooo}}{A_F}_{RT} = \left(\frac{3.64 \times 10^6 (.00205)^{1/2}}{.88 \times 42.6}\right)^{2/3} = 271 \tag{3}$$

$$\frac{T_{ooo}}{A_F}_{LT} = \left(\frac{3.64 \times 10^6 (.00205)^{1/2}}{.986 \times 42.6}\right)^{2/3} = 253 \tag{4}$$

Then,

$$N_{RWF} = 100\sqrt{\frac{271}{291}} = 96.6\% \tag{5}$$

$$\omega_{RWF} = .966 \times 276 \text{ rad/sec} = 267 \text{ rad/sec} \tag{6}$$

$$N_{LWF} = 100\sqrt{\frac{253}{291}} = 93.3\% \quad (7)$$

$$\omega_{LWF} = .933 \times 276 = 257.5 \text{ rad/sec} \quad (8)$$

We may calculate the airplane angular momentums in this configuration, assuming $N_{NF} \approx 100\%$.

TABLE 18

	ω, RAD/SEC.	I	Iω	H_x	H_y	H_z
Total J-85	1730	1.024	1770	1764	0	-154.2
Nose Fan	426	1.293	-552	0	0	-552
Rt Wing Fan	267	30.2	8070	0	0	8070
Lt Wing Fan	257.5	30.2	-7780	0	0	-7780
		TOTAL H RT ROLL		1764	0	-416.2

For a full left roll, the wing fan situation is reversed, and the angular momentum differential is of the opposite sign. For this case:

TABLE 19

$H_x = 1764$

$H_y = 0$

$H_z = -996.2$

To judge the effect of this angular momentum upon the vehicle, we can write the equations of motion for the angular degrees of freedom of the vehicle and determine the frequency of nutation associated with these constants. As the period of the nutation increased, the pilot would find

it harder and harder to detect, and it would finally be lost in the normal vehicle maneuver motions.

Assuming the vehicle to be just angular momentum and inertia, we can write from the laws of mechanics,

$$I\dot{\omega} + \omega \times H = \Sigma \text{ moments applied} \tag{12}$$

where

$$\dot{\omega} = \dot{p}\hat{i} + \dot{q}\hat{j} + \dot{r}\hat{k} \tag{13}$$

$$I = I_x\hat{i} + I_y\hat{j} + I_z\hat{k} \tag{14}$$

$$\omega = p\hat{i} + q\hat{j} + r\hat{k} \tag{15}$$

$$H = H_x\hat{i} + H_y\hat{j} + H_z\hat{k} \tag{16}$$

we can now expand equation (12) as follows:

$$I_x\dot{p}\hat{i} + I_y\dot{q}\hat{j} + I_z\dot{r}\hat{k} = -(p\hat{i} + q\hat{j} + r\hat{k}) \times \left(H_x\hat{i} + H_y\hat{j} + H_z\hat{k}\right) \tag{17}$$

$$I_x\dot{p}\hat{i} + I_y\dot{q}\hat{j} + I_z\dot{r}\hat{k} = -\Big[+ pH_y\hat{k} - pH_z\hat{j} - qH_x\hat{k} + qH_z\hat{i} + rH_x\hat{j} - rH_y\hat{i} \Big] \tag{18}$$

We can group the $\hat{i}$, $\hat{j}$ and $\hat{k}$ values, and since $H_y = 0$,

$$I_x\dot{p} = -qH_z \tag{19}$$

$$I_y\dot{q} = -rH_x + pH_z \tag{20}$$

$$I_z\dot{r} = qH_x \tag{21}$$

Now, $I_x \approx 4250$, $I_y \approx 15000$, and $I_z \approx 17000$, so, using these values and the values for the angular momentums from Table 19, we write

$$4250\,\dot{p} = 996\,q \tag{22}$$

$$15000\,\dot{q} = -1764r + 996\,p \tag{23}$$

$$17000\,\dot{r} = 1764\,q \tag{24}$$

Taking the Laplace transform and dividing by the inertia values

$$Sp = .235\,q \tag{25}$$

$$Sq = -.118r - .067\,p \tag{26}$$

$$Sr = .104\,q \tag{27}$$

or

$$Sp - .235\,q + 0 = 0 \tag{28}$$

$$.067p + Sq + .118r = 0 \tag{29}$$

$$0 - .104q + Sr = 0 \tag{30}$$

Solving for the characteristic equation,

$$S^3 + .067\,(.235)S + .118\,(.104)S = 0 \tag{31}$$

$$S^3 + S\,(.028) = 0 \tag{32}$$

$$S\,(S^2 + .028) = 0 \tag{33}$$

$$S\,(S^2 + .167^2) = 0 \tag{34}$$

Equation 34 shows a nutational natural frequency of .167 rad/sec, or a period of 37.6 seconds. This period is so long that the pilot would not notice it, and the gyroscopic coupling terms were thus eliminated from the equations of motion.

6.6 SHEAR NOMOGRAPH

This nomograph is useful in relating free stream dynamic pressure, air density, fan RPM and thrust coefficient. During flight test all of these variables except thrust coefficient, $T_C{}^S$, will be available, and this chart allows the quick computation of $T_C{}^S$. The chart solves the equation:

$$T_c^s = \frac{\frac{T_{ooo}}{A_F}}{\frac{\rho V_T^2}{2} + \frac{T_{ooo}}{A_F}} \qquad (1)$$

Now, T_{ooo}/A_F is the fan disc loading which would occur if suddenly V_T, β_V and β_S were reduced to zero, which means that T_{ooo}/A_F is a function only of fan speed and the density of the air.

For the XV-5A main fans, the fan disc loading can be accurately expressed as:

$$\frac{T_{ooo}}{A_F} = 338\sigma\left(\frac{N_F}{100}\right)^2 \qquad (2)$$

This can also be written:

$$\frac{T_{ooo}}{A_F} = 338\left(\frac{N_F\sqrt{\sigma}}{100}\right)^2 \qquad (3)$$

In this form, a "corrected" fan RPM is used in calculating T_{ooo}/A_F.

These data are taken into account in the construction of Figure 188

6.7 LOADED PARALLEL T NETWORK

In general, a parallel T notch network is used to provide attenuation of an undesired frequency in a servo amplifier or an audio amplifier, where the main consideration is that the network have good rejection at the notch frequency. Further, in many cases the loading of the network can be made negligible, as well as the effect of the impedance of the circuit driving the network. In general, the undesired frequencies are far enough separated from the normal signals so the notch network has no effect on the normal signals.

In our case, however, the network is fed by an impedance not negligibly small, and drives an impedance not negligibly large.

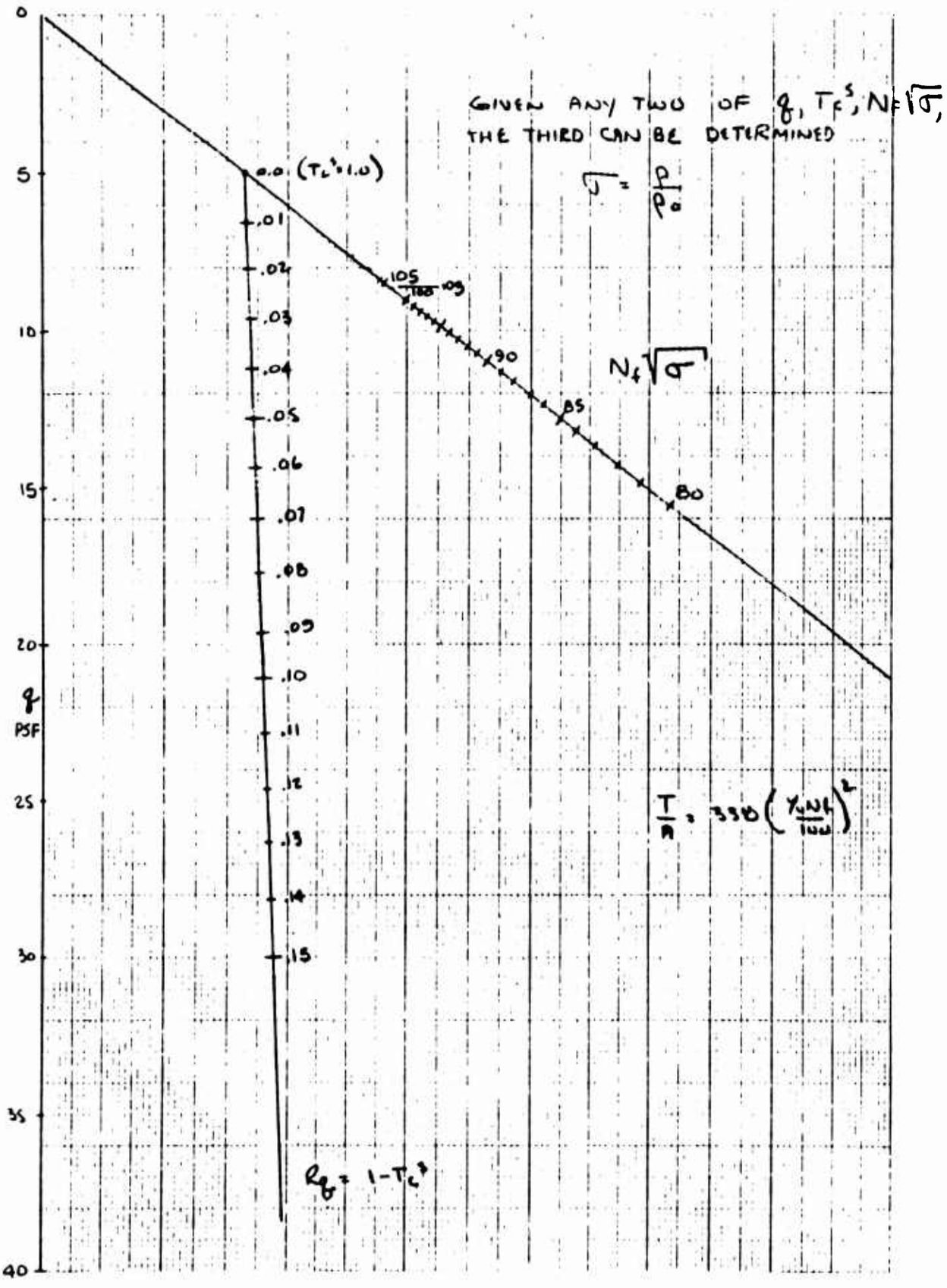

Figure 188 Shear Nomograph

It will be shown that the frequency of the null is independent of the source or load impedance, but that the network response above and below the notch is affected.

Figure 189 following is a diagram of the notch network with source and load impedance:

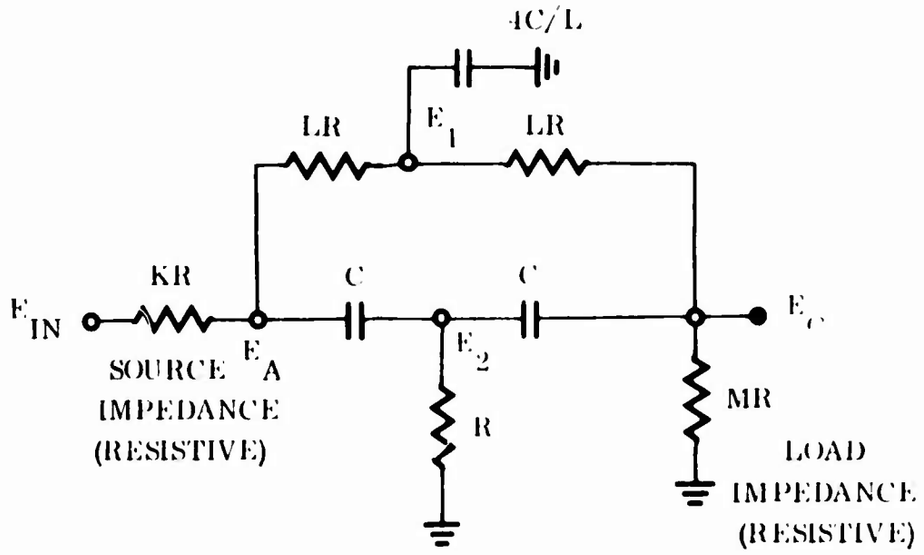

Figure 189 Parallel Tee Notch Network

For this circuit, ω_0, the frequency of maximum attenuation is given as:

$$\omega_o = \frac{1}{\sqrt{2L}\ RC} \qquad (1)$$

For simplicity, we make the substitution,

$$Z = \frac{S}{\omega_o},$$

and the transfer function of the network can be written:

$$\frac{E_O}{E_{IN}} = \frac{(1 + Z^2)\,\frac{2ML^3}{\sqrt{2L}}}{\left[ML^2\sqrt{2L} + KML^2\sqrt{2L} + 2KML\sqrt{2L} + KL^2\sqrt{2L}\right]}$$

$$\left[Z^2 + \frac{\left[4L^3 + 2ML^3 + 4ML^2 + 4KL^2 + 4KML + 2KML^2 + 2KL^3\right] Z}{ML^2\sqrt{2L} + KML^2\sqrt{2L} + 2KML\sqrt{2L} + KL^2\sqrt{2L}} \right.$$

$$\left. + \frac{\left[2L^3 + ML^2 + KL^2\right]}{ML^2 + KML^2 + 2KML + KL^2} \right] \qquad (2)$$

If we let K = 0 and M = ∞, we get the relationships for a conventional unloaded notch network:

$$\frac{E_O}{E_{IN}} = \frac{\frac{2L^3}{\sqrt{2L}}(1 + Z^2)}{L^2\sqrt{2L}\left[Z^2 + \frac{(2L^3 + 4L^2)}{L^2\sqrt{2L}} Z + 1\right]} \qquad (3)$$

$$\frac{E_O}{E_{IN}} = \frac{1 + Z^2}{Z^2 + \frac{2L+4}{\sqrt{2L}} Z + 1} \qquad (4)$$

This response has the characteristics of a complex zero pair at $Z^2 = -1$ and a complex pole pair with $\omega_N = \omega_O$, and with a damping ratio determined by L.

We solve for the value of L which results in a minimum damping ratio:

$$2\xi = \frac{2L+4}{\sqrt{2L}} \qquad (5)$$

$$\frac{2d\xi}{dL} = (2L+4)(-1/2)(2L)^{-3/2}(2) + 2(2L)^{-1/2} \qquad (6)$$

The minimum occurs at $\frac{d\xi}{dL} = 0$, or,

$$\frac{-(L+2)}{(2L)^{3/2}} + \frac{1}{(2L)^{1/2}} = 0 \tag{7}$$

$$\frac{L+2}{(2L)^{3/2}} = \frac{1}{(2L)^{1/2}} \tag{8}$$

$$\frac{L+2}{2L} = 1 \tag{9}$$

$$L+2 = 2L \tag{10}$$

$$L = 2 \tag{11}$$

Thusly, the minimum damping for the denominator term occurs at L = 2, and is:

$$\xi_{min} = \frac{L+2}{\sqrt{2L}} = \frac{4}{\sqrt{4}} = 2 \tag{12}$$

we can now solve for the location of the roots of the denominator:

$$Z^2 + 4Z + 1 = 0 \tag{13}$$

$$Z = \frac{-4 \pm \sqrt{16-4}}{2} = -3.732,\ -.268 \tag{14}$$

The second order denominator is then composed of a real root at $S = -.268\,\omega_o$ and a real root at $S = -3.732\,\omega_o$.

In our case, we were mainly interested in keeping the phase lag below the notch frequency as low as possible so that the least possible effect on the airframe rigid body would result. The calculation of the values of K, M, and L to attain minimum low frequency phase lag was not attempted due to lack of time.

The network may be designed, however, so that the ratio of gain below the notch to the gain above the notch can be any desired value. If the gain is higher at high frequencies, the notch characteristics will exhibit

a leading (or less lagging) phase characteristic when compared to the network with equal high and low frequency gain.

Since we desire the higher frequencies to have at least no more response than the low frequencies, and the lowest possible phase lag at low frequencies, L = 2 was picked for this case.

If we desire the ω_N of the denominator to be ω_o, or greater, we see, from equation 2, that:

$$\omega_N^2 = \omega_o^2 \left(\frac{2L^3 + ML^2 + KL^2}{ML^2 + KML^2 + 2KML + KL^2} \right) \tag{15}$$

$$\omega_N^2 = \omega_o^2 \left(\frac{2L^2 + ML + KL}{ML + KML + 2KM + KL} \right) \tag{16}$$

or,

$$\frac{2L^2 + ML + KL}{ML + KML + 2KM + KL} \geq 1 \tag{17}$$

We also see that if equation 17 is equal to 1, the condition for equal high and low frequency gains is met.

Thus

$$2L^2 + ML + KL = ML + KML + 2KM + KL \tag{18}$$

$$2L^2 = KML + 2KM \tag{19}$$

$$\frac{2L^2}{L+2} = KM \tag{20}$$

If we let L = 2 (an arbitrary choice here),

$$\frac{8}{4} = KM, \text{ or } KM = 2 \tag{21}$$

Since the source resistance, R_0, is 3K Ω and the load resistance, R_L, is 100K Ω in our system,

$$R_0 R_L = KMR^2 \tag{22}$$

$$300 = 2R^2 \quad (\text{in K } \Omega) \tag{23}$$

$$R^2 = 150 \tag{24}$$

$$R = \sqrt{150} = 12.2\text{K } \Omega \tag{25}$$

in this case, $L = 2$, $K = \frac{3}{12.2} = .248$, $M = \frac{100}{12.2} = 8.2$.

The high and low frequency gains are thus:

$$\text{GAIN} = \frac{2ML^3}{\sqrt{2L}} \times \frac{1}{\sqrt{2L\left[ML^2 + KM^2 + 2KML + KL^2\right]}} \times \frac{\left[ML^2 + KML^2 + 2KML + KL^2\right]}{\left[2L^3 + ML^2 + KL^2\right]} \tag{26}$$

$$= \frac{2ML^3}{2L\left[2L^3 + ML^2 + KL^2\right]} \tag{27}$$

$$= \frac{2ML^3}{2L^3\left[2L + M + K\right]} = \frac{M}{2L + M + K} \tag{28}$$

$$= \frac{8.2}{4 + .248 + 8.2} = \frac{8.2}{12.448} = .66 \tag{29}$$

We can further substitute these values into equation (2) to determine the damping ratio of the denominator.

Thus:

$$2\xi = \frac{4x8 + 16.4x8 + 4x8.2x4 + 4x.248x4 + 4x2x.248x8.2 + 2x.248x8.2x4 + 2x.248x8}{8.2x8 + 2x4x2 + 2x2x2x2 + .248x8} \quad (30)$$

$$2\xi = \frac{334.3}{99.6} = 3.35 \quad (31)$$

$$\xi = 1.67 \quad (32)$$

The response of the notch used thus becomes:

$$\frac{E_O}{E_{IN}} = \frac{.66\,(1 + Z^2)}{Z^2 + 3.35Z + 1} \quad (33)$$

$$\frac{E_O}{E_{IN}} = \frac{.66\,(1 + Z^2)}{(.335Z + 1)\,(3.015Z + 1)} \quad (34)$$

The effect of the notch on the root locus plots is nearly negligible, except for the static gain loss.

Development of transfer function for parallel T notch network

Referring to Figure 189 we can write the nodal equation for the network;

$$E_A\left[\frac{1}{KR} + \frac{1}{LR} + CS\right] + E_1\left[-\frac{1}{LR}\right] + E_2\left[-CS\right] + 0 = \frac{E_{IN}}{KR} \quad (35)$$

$$E_A\left[-\frac{1}{LR}\right] + E_1\left[\frac{1}{LR} + \frac{1}{LR} + \frac{-4CS}{L}\right] + 0 + E_O\left[-\frac{1}{LR}\right] = 0 \quad (36)$$

$$E_A\left[-CS\right] + 0 + E_2\left[CS + CS + \frac{1}{R}\right] + E_O\left[-CS\right] = 0 \quad (37)$$

$$0 + E_1\left[-\frac{1}{LR}\right] + E_2\left[-CS\right] + E_O\left[-\frac{1}{MR} + \frac{1}{LR} + CS\right] = 0 \qquad (38)$$

Now, let $\omega_o = \frac{1}{\sqrt{2L\ RC}}$, or, $C = \frac{1}{\sqrt{2L\ R\omega_o}}$ and also let $\frac{S}{\omega_o} = Z$,
and we can rewrite equations 35 thru 38 as below:

$$E_A\left[\frac{1}{KR} + \frac{1}{LR} + \frac{Z}{R\sqrt{2L}}\right] + E_1\left[-\frac{1}{LR}\right] + E_2\left[-\frac{Z}{R\sqrt{2L}}\right]$$

$$+ 0 = \frac{E_{IN}}{KR} \qquad (39)$$

$$E_A\left[-\frac{1}{LR}\right] + E_1\left[\frac{2}{LR} - \frac{4Z}{RL\sqrt{2L}}\right] + 0 + E_O\left[-\frac{1}{LR}\right] = 0 \qquad (40)$$

$$E_A\left[-\frac{Z}{R\sqrt{2L}}\right] + 0 + E_2\left[-\frac{2Z}{R\sqrt{2L}} + \frac{1}{R}\right] + E_O\left[-\frac{Z}{R\sqrt{2L}}\right] = 0 \qquad (41)$$

$$0 + E_1\left[-\frac{1}{LR}\right] + E_2\left[-\frac{Z}{R\sqrt{2L}}\right]$$

$$+ E_O\left[\frac{1}{MR} + \frac{1}{LR} + \frac{Z}{R\sqrt{2L}}\right] = 0 \qquad (42)$$

It is then possible to solve the above simultaneous equations to arrive at equation (2).

6.8 STABILITY AUGMENTATION SYSTEM HARDWARE MEASUREMENTS

Figure 190 is a schematic diagram of the final stability augmentation system configuration.

The system is identical for all channels, primary and standby, with the one exception that the 330 MFD capacitor is permanently shorted by means of a jumper in the primary pitch and yaw modes, as shown by the dashed line.

The rate gyro 400 CPS double sideband suppressed carrier output signal is demodulated to separate the rate information from the carrier components, and this signal is fed to the SA shaping network. The carrier harmonics are removed by the 1MFD capacitor placed at the junction of the 27K and 1.5K resistors, and the resulting rate signal is shaped by the network. This filtering was necessary because without filtering of the gyro demodulator output the 400 CPS harmonics were transmitted through the notch network with small attenuation, to be remodulated into "signal", which acts to degrade the 15 CPS notch network action upon the rate signal.

The gain of the notch network used is .57 at frequencies above and below the notch frequency, and this reduces the overall system gain somewhat. Since the system is operated below maximum gain, this is no restriction.

The output of the notch network is remodulated and fed through the amplifier to the servo valves.

The transfer function of the standby-system and primary roll system shaping network is a lag-lead with the lead time constant set at any of six values, as determined by the "Ratio" switch setting for primary roll. The standby system ratio can be varied, but is not a cockpit variable. The transfer function is: (neglecting the effect of the 1MFD filter capacitor, which results in 3DB attenuation at 50 CPS)

$$\frac{E_O}{E_{IN}} = \frac{1 + 10RS}{1 + 10S} \qquad (1)$$

The circled numbers in Figure 190 refer to the "ratio" switch positions, and Table 20 relates the value of R with the switch position:

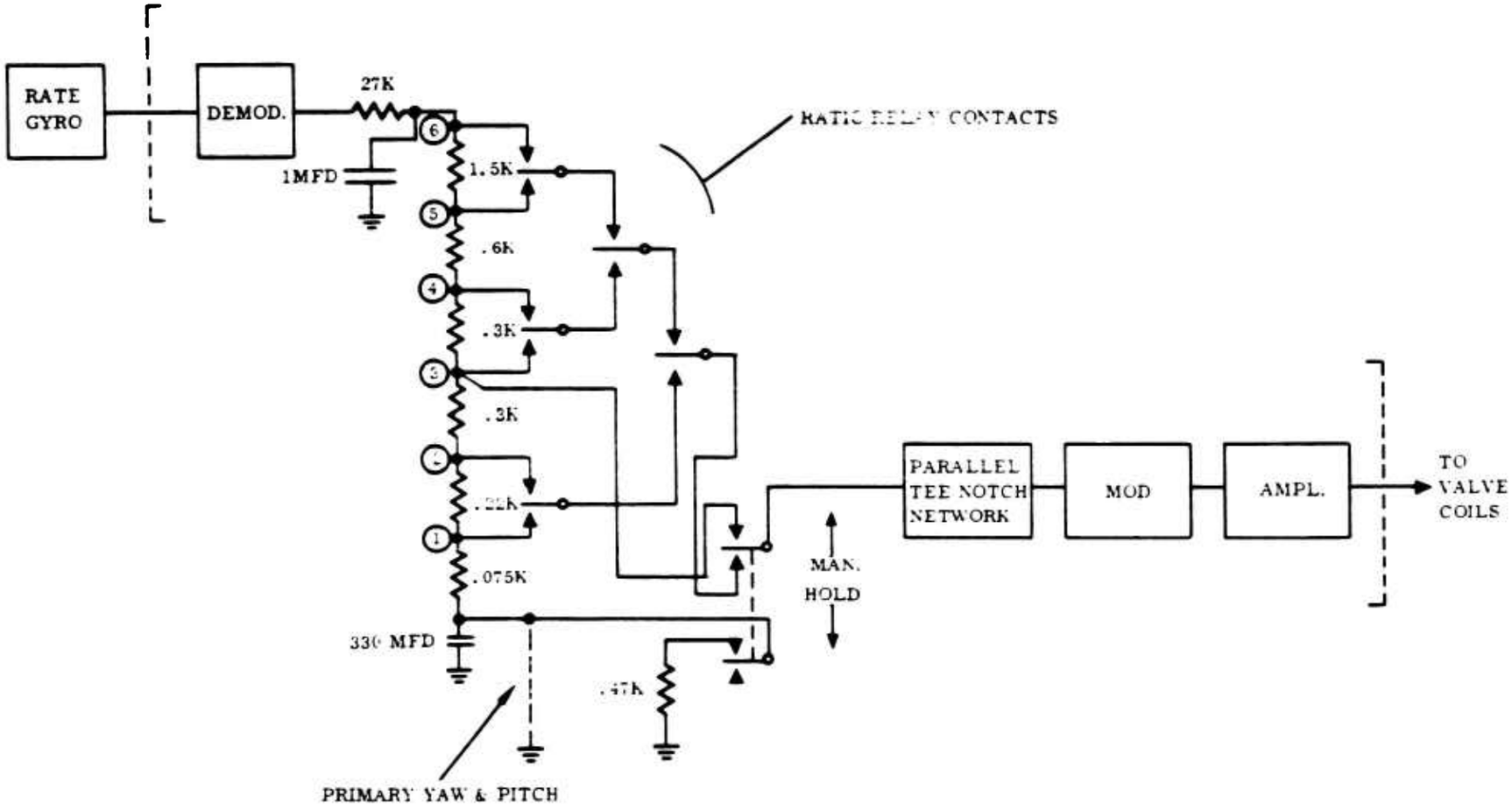

Figure 190 Stability Augmentation System - Block Diagram

TABLE 20

RATIO SWITCH POSITION	R	10R
1	.0025	.025
2	.01	.1
3	.02	.2
4	.03	.3
5	.05	.5
6	.1	1

If we consider frequencies such that 10S>>1, equation (1) becomes:

$$\frac{E_O}{E_{IN}} = \frac{1 + 10RS}{10S} = \frac{1}{10S}(1 + 10RS) \qquad (2)$$

Now, if a rate signal, S, is applied at the input, we have:

$$E_O = \frac{1}{10}(1 + 10RS) \qquad (3)$$

It can be seen that this is the familiar form of rate plus position feedback, where the coefficient of S, 10R, is equal to the ratio of rate gain to position gain.

If R = .1 is chosen, the coefficient of S is unity, and we have a system equivalent (at least if 10S>>1) to a rate plus position feedback with equal rate and position gains.

The "ratio" switch thus enables the selection of any of 6 values of rate/position ratio, as shown in the "10R" column of Table 20.

In the case of primary yaw and pitch, simulator flights indicated that improved handling qualifies were obtained using the shorting jumper of Figure 190, which eliminates the effect of the capacitor. With this jumper installed, the effect of the shaping network is nothing more than as a variable attenuator in the holding mode: When the Ratio switch in primary yaw and pitch is in position 3, and the maneuvering and holding gain pots

in these two channels are set to the same value, there is no effect when the maneuver switches are energized.

The system exhibits rate feedback only, and the holding and maneuvering gains are identical. This modification thus allows the use of two separate rate gains in the primary pitch and yaw modes. The SA system standby channel retains the holding feature in all axes, so that both configurations can be tested in actual flight. In the "Maneuver" mode, the primary roll and standby SA channels have the following transfer function:

$$\frac{E_O}{E_{IN}} = .03S \frac{(1 + .0865\ S)}{(1 + .153\ S)} \qquad (4)$$

This is essentially a rate gain, due to the short numerator and denominator time constants involved.

Figure 191 is a plot of the normal stability augmentation system frequency response taken from the rate gyro output to the valve coil input for ratio position 6 in the holding mode without the notch network.

Figure 192 is a plot of the frequency response of the same system configuration with the notch network installed.

Figure 193 is a plot of the frequency response of the system in the normal maneuvering mode without the notch network. The effect of the lag-lead of equation (4) is noted.

Later work revealed that the effect of the lag-lead in the maneuvering mode was not negligible, and the 470 Ω resistor used to discharge the 330 MFD capacitor was changed to 47 Ω.

6.9 LOUVER SERVO CHANGE ANALYSIS

The first VTOL hover flight attempt showed that roll control power was not adequate for flight. This was due to the fact that the louver airloads were much higher than anticipated, and consequently the louver servos were stalling.

New servos were designed which delivered the required louver stagger deflections. The time constants for the new servos are:

Fwd Servos: τ .07 sec.

Aft Servos: τ .09 sec.

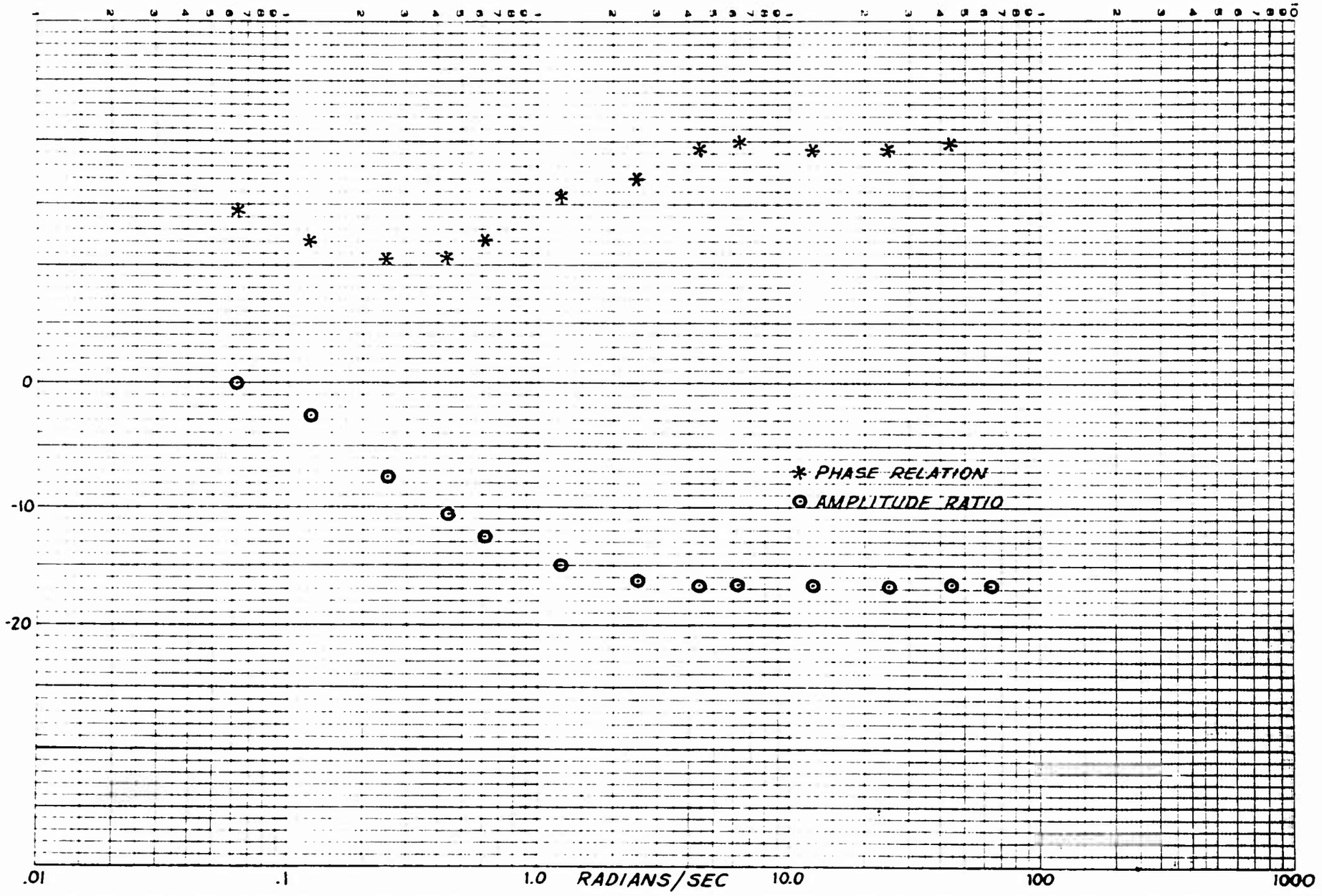

Figure 191 Stability Augmentation System Frequency Response Holding Mode without Notch Network (R = .1)

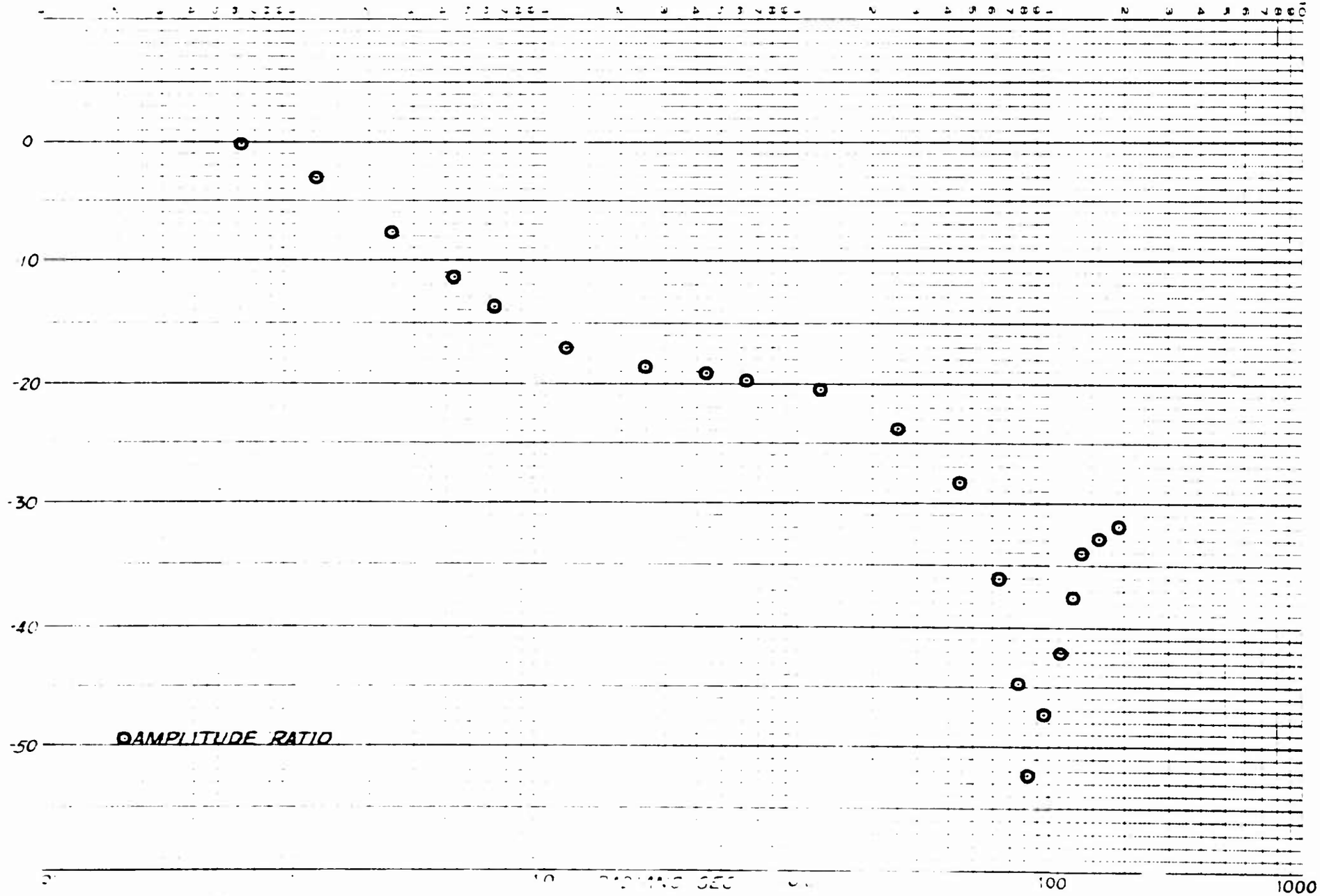

Figure 192 Stability Augmentation System Frequency Response Holding Mode with Notch Network (R = .1)

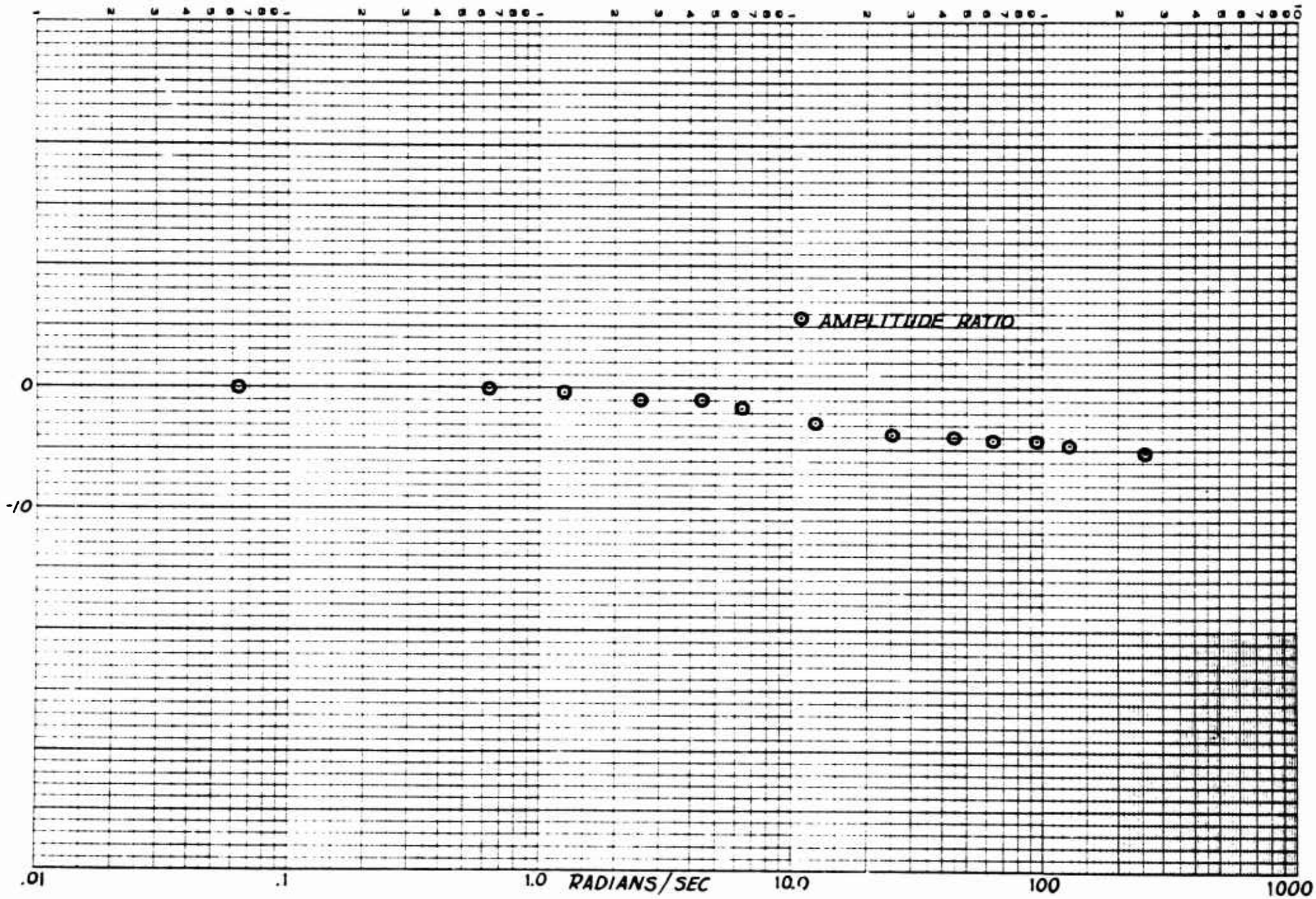

Figure 193 Stability Augmentation System Frequency Response Maneuvering Mode without Notch Network

Because the responses of both new servos are different from the response of the previous servos, the performance of the airframe/stability augmentation system is changed.

The following analysis was made to determine the effect of the servo change.

SERVO CHANGE ANALYSIS

From the definitions of vector and stagger deflections:

$$\beta_s = \beta_2 - \beta_1 \tag{1}$$

$$\beta_v = \frac{(\beta_2 + \beta_1)}{2} \tag{2}$$

The approximate transfer functions of the new servos are:

$$\frac{\beta_2}{\beta_{2_c}} = \frac{1}{\tau_2 S + 1} \tag{3}$$

$$\frac{\beta_1}{\beta_{1_c}} = \frac{1}{\tau_1 S + 1} \tag{4}$$

where: β_{2_c} is the commanded forward louver deflection

β_{1_c} is the commanded aft louver deflection

Substituting expressions 3 and 4 into expressions 1 and 2 we obtain:

$$\beta_s = \beta_{2_c}\left(\frac{1}{\tau_2 S + 1}\right) - \beta_{1_c}\left(\frac{1}{\tau_1 S + 1}\right) \tag{5}$$

$$\beta_v = \frac{\beta_{2_c}}{2}\left(\frac{1}{\tau_2 S + 1}\right) + \frac{\beta_{1_c}}{2}\left(\frac{1}{\tau_1 S + 1}\right) \tag{6}$$

If we define a $\beta_{v_{commanded}}$ and a $\beta_{s_{commanded}}$ as:

$$\beta_{v_c} = \beta_{1_c} = \beta_{2_c} \tag{7}$$

$$\beta_{s_c} = -2\beta_{1_c} = 2\beta_{2_c} \tag{8}$$

We then obtain from expressions 5 and 6:

$$\beta_s = +\frac{\beta_{s_c}}{2}\left(\frac{1}{\tau_2 S+1}\right) + \frac{\beta_{s_c}}{2}\left(\frac{1}{\tau_1 S+1}\right) \tag{9}$$

$$\beta_v = +\frac{\beta_{v_c}}{2}\left(\frac{1}{\tau_2 S+1}\right) + \frac{\beta_{v_c}}{2}\left(\frac{1}{\tau_1 S+1}\right) \tag{10}$$

$$\beta_s = \beta_{v_c}\left(\frac{1}{\tau_2 s+1}\right) - \beta_{v_c}\left(\frac{1}{\tau_1 s+1}\right) \tag{11}$$

$$\beta_v = \frac{\beta_{s_c}}{4}\left(\frac{1}{\tau_2 S+1}\right) - \frac{\beta_{s_c}}{4}\left(\frac{1}{\tau_1 S+1}\right) \tag{12}$$

Expressions 9 and 10 would both reduce to a single time constant if $\tau_1 = \tau_2$ and expressions 11 and 12 would go to zero in this case.

Simplifying expressions 9 thru 12 there obtains:

$$\frac{\beta_s}{\beta_{s_{comm}}} = \left(\frac{\tau_1+\tau_2}{2\tau_1\tau_2}\right)\left(\frac{S + 2/(\tau_1+\tau_2)}{(S + 1/\tau_1)(S + 1/\tau_2)}\right) \tag{13}$$

$$\frac{\beta_v}{\beta_{v_{comm}}} = \left(\frac{\tau_1+\tau_2}{2\tau_1\tau_2}\right)\left(\frac{S + 2/(\tau_1+\tau_2)}{(S + 1/\tau_1)(S + 1/\tau_2)}\right) \tag{14}$$

$$\frac{\beta_s}{\beta_{v_c}} = \left(\frac{\tau_2 - \tau_1}{\tau_1 \tau_2}\right)\left(\frac{S}{\left(S + 1/\tau_1\right)\left(S + 1/\tau_2\right)}\right) \tag{15}$$

$$\frac{\beta_v}{\beta_{s_c}} = \left(\frac{\tau_2 - \tau_1}{\tau_1 \tau_2}\right)\left(\frac{S}{\left(S + 1/\tau_1\right)\left(S + 1/\tau_2\right)}\right) \tag{16}$$

Expressions 13 and 14 give the new stagger and vector responses with the new servos in response to stagger and vector commands.

Expressions 15 and 16 give the stagger response to vector inputs and vector response to stagger inputs.

To check the compatibility of the new servo system with the aircraft in roll and yaw, root locus plots were drawn and gains for the instability point and the .5 critical damping point were determined.

Figures 194, 195 and 196 are the root locus plots of the system. The gains mentioned are given in Table 21.

Examination of the root locus and Table 21 shows that the new servo system does not substantially effect either roll or yaw systems and that the new servo system can be approximated by a single first order system with a time constant equal to the average of the time constants of the forward and aft servos.

CROSS COUPLING

Examination of expressions 15 and 16 shown above shows that a cross coupling effect from roll to yaw and yaw to roll arises when the time constants of the forward and aft louver servos differ.

This effect washes out with frequency, but to determine its importance it is examined.

A first block diagram of the systems showing this cross coupling effect is given in Figure 197.

A second block diagram showing the same system rearranged for analysis of the overall yaw response to yaw inputs is shown in Figure 198.

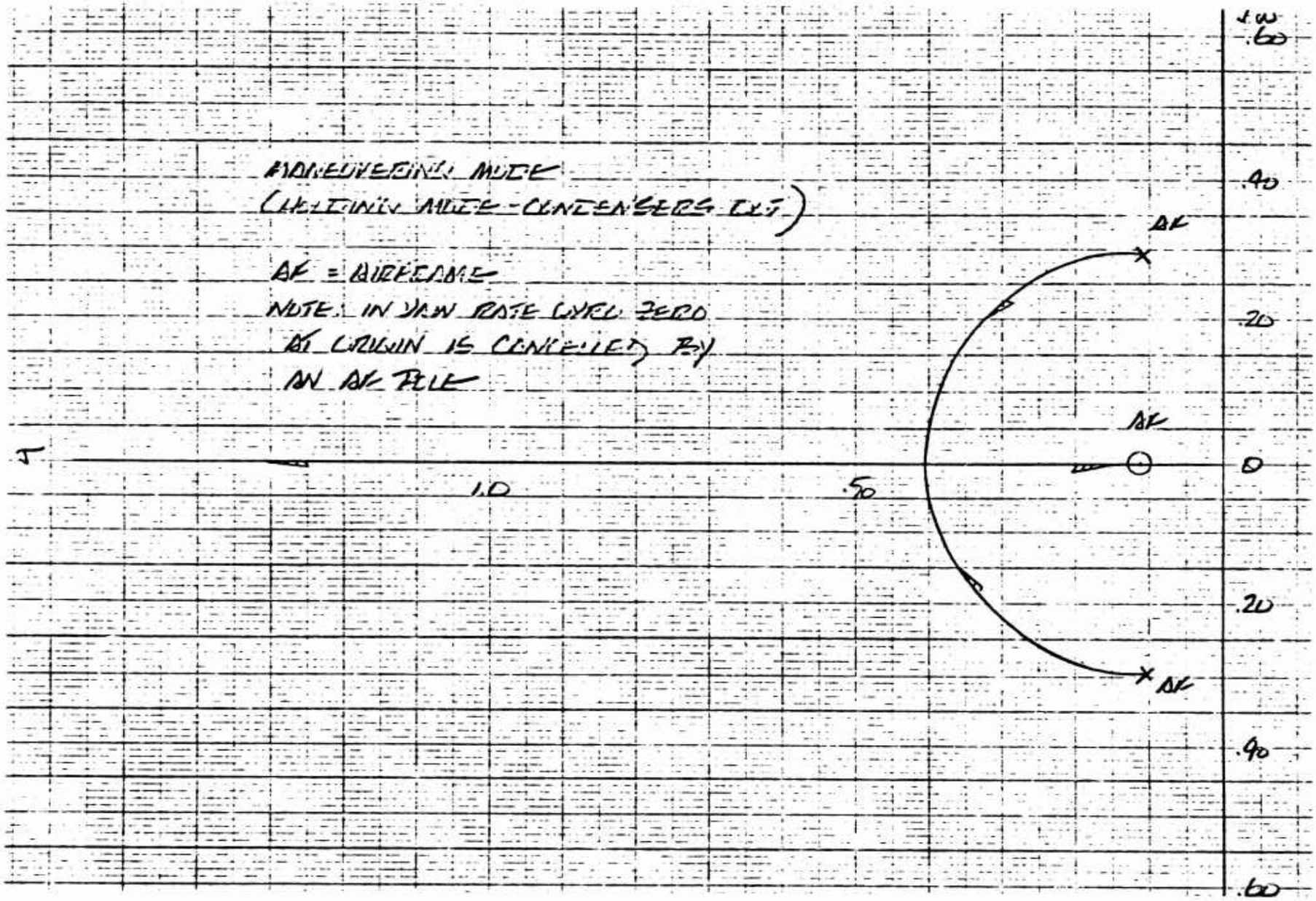

Figure 194 Final Yaw System Hover Root Locus

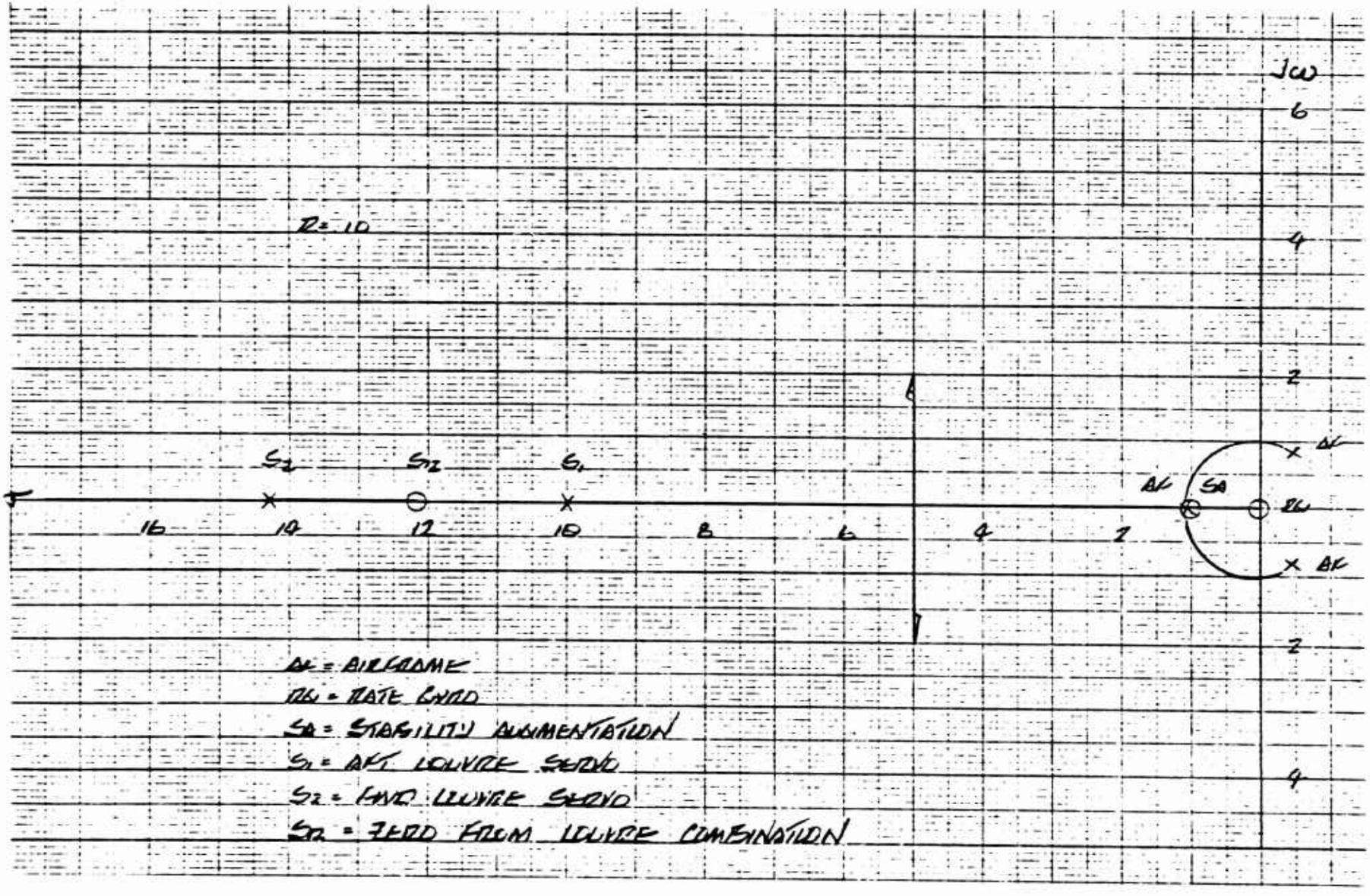

Figure 195 Roll System Hover Root Locus, R = .1 with Reworked Fore and Aft Louver Servo Time Constants

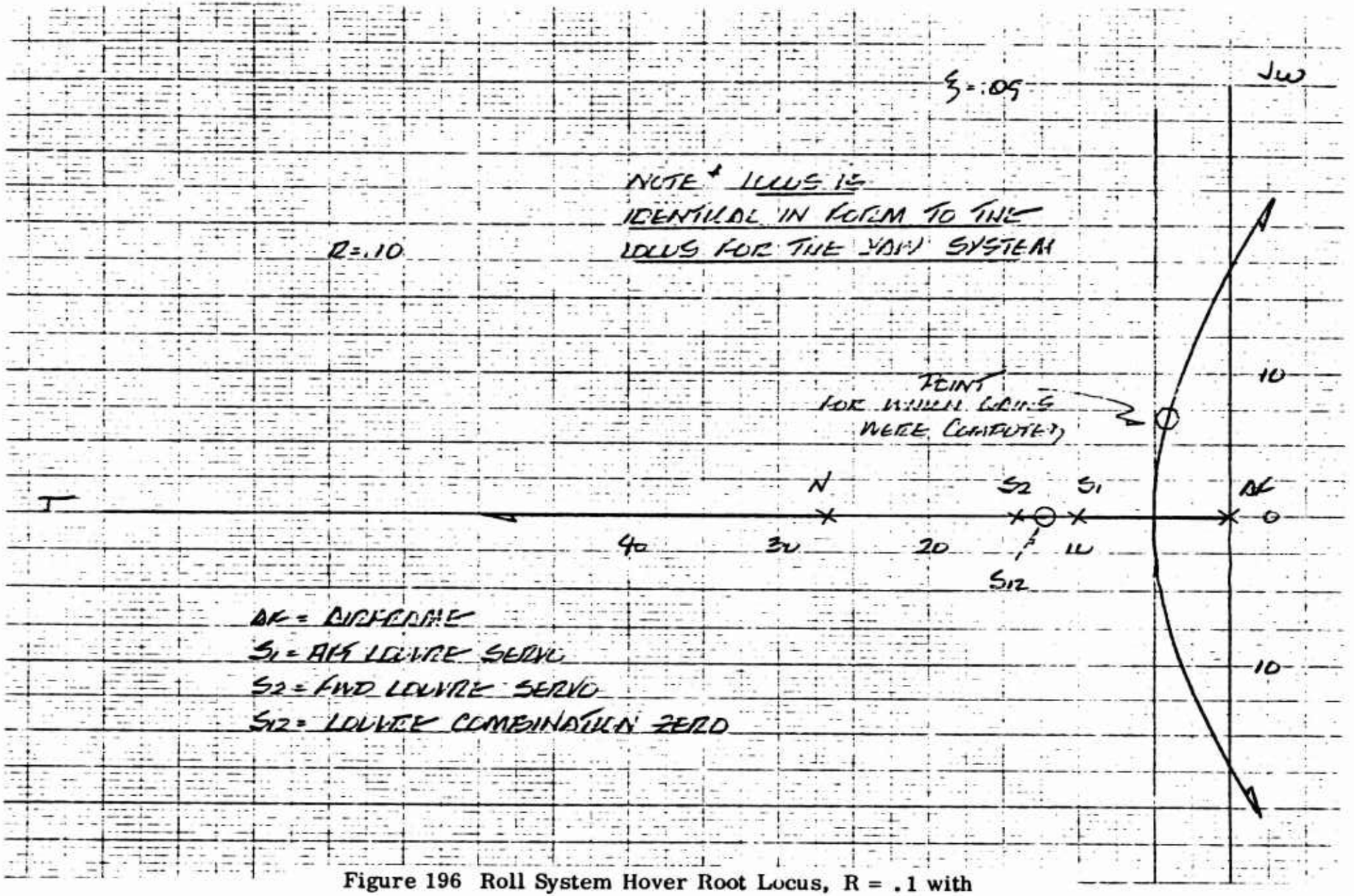

Figure 196 Roll System Hover Root Locus, R = .1 with Reworked Fore and Aft Louver Servo Time Constants

TABLE 21

YAW SYSTEM ***

		* GAIN FOR ξ=.5	GAIN FOR INSTABILITY
CAPACITOR OUT, HOVERING	RATIO SETTING		
	6	.398	2.15
	5	.794	4.31
	4	1.32**	7.15
	3	1.99	10.75
	MANEUVERING MODE	1.99	10.75

ROLL SYSTEM

		ξ=.5	INSTABILITY
CAPACITOR IN, HOVERING	RATIO SETTING		
	6	.131	.710
	5	.262	1.420
	4	.436	2.360
	3	.654	3.550
	MANEUVERING MODE	.695	3.78

* Refer to Figure 141 of Section 3.1 for corresponding pot settings.

** Maximum reachable gain is 1.00 (100% of present capability) Figures are given for possible future use.

*** Taken from Figure

ROLL TO YAW AND YAW TO ROLL CROSS COUPLING

The transfer function for roll angle due to yaw input can be seen from Figure 197 to be:

$$\frac{\varphi}{Y} = \frac{\left(\frac{\varphi}{\beta_s} \cdot \frac{\beta_s}{Y}\right)}{\left(1 + \left(\frac{\varphi}{\beta_s}\right)\left(\frac{\beta_s}{R}\right)(SA_\varphi)\right)} \tag{17}$$

The transfer function for roll angle due to roll input is:

$$\frac{\varphi}{R} = \frac{\left(\frac{\varphi}{\beta_s} \cdot \frac{\beta_s}{R}\right)}{\left(1 + \left(\frac{\varphi}{\beta_s}\right)\left(\frac{\beta_s}{R}\right)(SA_\varphi)\right)} \tag{18}$$

The relative strengths of these roll outputs can be compared by forming the ratio:

$$\frac{\left(\frac{\varphi}{Y}\right)}{\left(\frac{\varphi}{R}\right)} = \frac{\left(\frac{\beta_s}{Y}\right)}{\left(\frac{\beta_s}{R}\right)} \tag{19}$$

Substituting the transfer functions of the servo system as given in equations 15 and 16 and including the louver sensitivities to servo torque motor current inputs so that a comparison can be obtained in hover:

$$\frac{\left(\frac{\varphi}{y}\right)}{\left(\frac{\varphi}{R}\right)} = \frac{\left(\frac{3.4°}{8\ ma}\right)\left(\frac{\tau_2 - \tau_1}{\tau_1 \tau_2}\right) S}{\left(\frac{6.8°}{8\ ma}\right)\left(\frac{\tau_1 + \tau_2}{2\tau_1 \tau_2}\right)\left(S + \left(\frac{2}{\tau_1 + \tau_2}\right)\right)} \tag{20}$$

$$= \frac{(.425°/ma)}{(.850°/ma)} \frac{2(\tau_2 - \tau_1)}{(\tau_1 + \tau_2)} \left(\frac{S}{S + \frac{2}{\tau_1 + \tau_2}}\right) \tag{21}$$

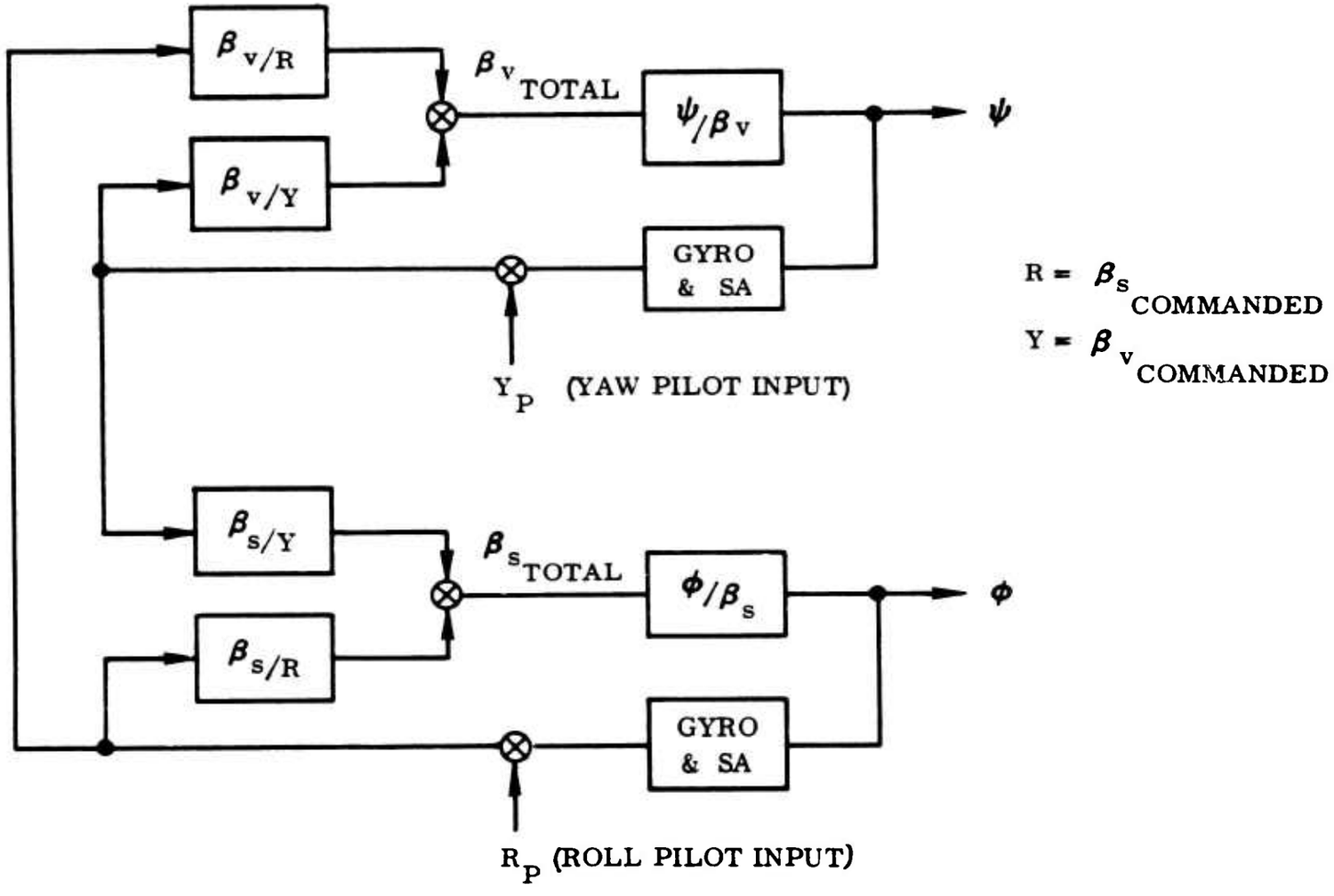

Figure 197 Basic Block Diagram Yaw-Roll Control System Showing Cross Coupling Effects

Substituting the given values for τ_1 and τ_2 and interpreting the results we find:

1. That at time 0, an instantaneous step yaw input will produce 1/8 the stagger deflection produced by an equivalent roll input.

2. That this deflection washes out to less than 1/3 of this value in .08 seconds.

These results would indicate that yaw to roll cross coupling due to the difference in forward and aft louver responses is negligible.

Further, since the transfer functions for roll to yaw cross coupling are identical to those shown above, the same conclusions can be drawn for roll to yaw cross coupling.

YAW TO ROLL TO YAW CROSS COUPLING

The change in yaw response of the aircraft due to yaw inputs that occurs because of yaw into roll into yaw cross coupling is examined below.

Referring to Figure 198 we can develop the following transfer function:

$$\frac{\Psi}{Y_R} = \frac{\left[\frac{\beta_v}{Y} + CL_2\left(\frac{\beta_s}{Y}\right)\left(\frac{\beta_v}{R}\right)\right]\frac{\Psi}{\beta_v}}{1 + SA_\Psi\left(\frac{\Psi}{\beta_v}\right)\left[\frac{\beta_v}{Y} + C_{L_2}\left(\frac{\beta_s}{Y}\right)\left(\frac{\beta_v}{R}\right)\right]} \tag{22}$$

$$\text{where } CL_2 = \frac{\left(\frac{\varphi}{\beta_s}\right)(SA_\varphi)}{\left(1 + \left(\frac{\varphi}{\beta_s}\right)\left(\frac{\beta_s}{R}\right) SA_\varphi\right)}$$

Expanding this transfer function we find the characteristic equation to be:

$$\left(1 + \frac{\varphi}{\beta_s} \cdot SA_\varphi \cdot \frac{\beta_s}{R}\right)\left(1 + \frac{\Psi}{\beta_v} \cdot SA_\Psi \cdot \frac{\beta_v}{Y}\right) + \left(\frac{\beta_s}{Y} \cdot \frac{\beta_v}{R} \cdot \frac{\varphi}{\beta_s} \cdot \frac{\Psi}{\beta_v} \cdot SA_\phi \cdot SA_\Psi\right) = 0 \tag{23}$$

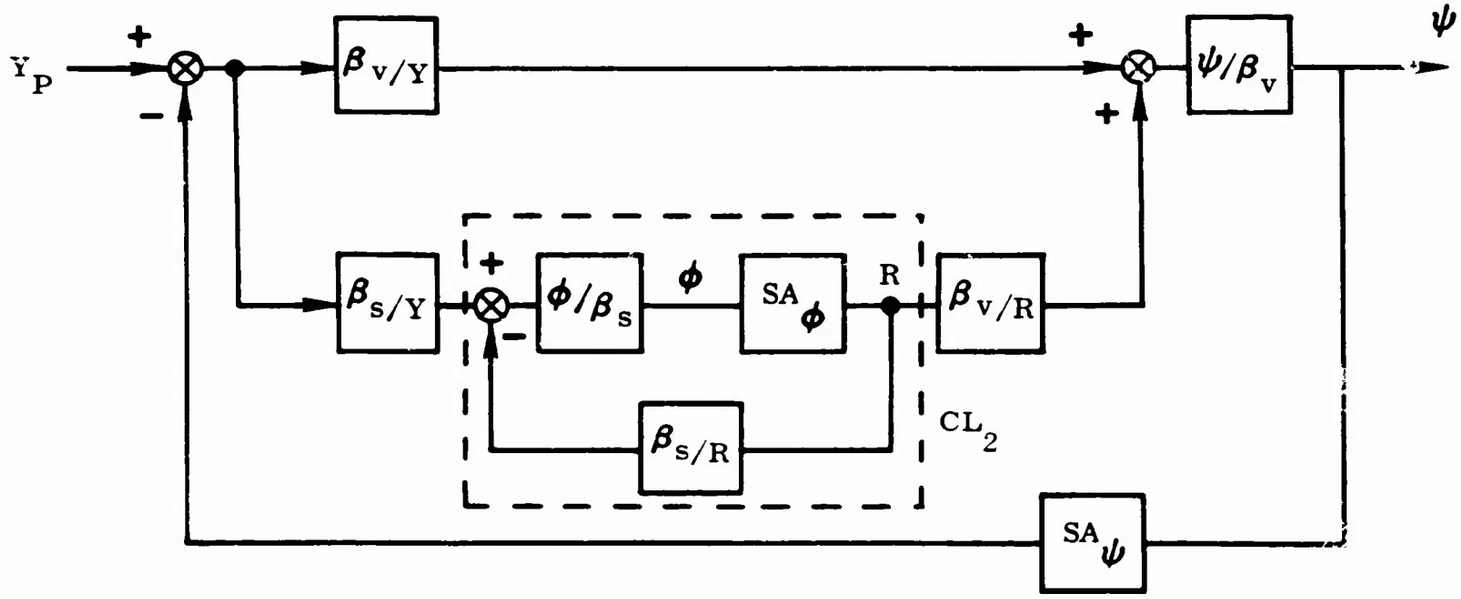

Figure 198 Block Diagram of Yaw Control System Showing Yaw to Roll to Yaw Cross Coupling

Examining this characteristic equation for the stability augmentation system settings and aircraft conditions in hover that were used in the first hover flight at Edwards AFB, we arrive at the following conclusions:

1. The characteristic equation is of the following form:

$$S^7 + (4.86 \times 10^1) S^6 + (9.20 \times 10^2) S^5 + (9.369 \times 10^3) S^4 \qquad (24)$$

$$+ (5.11 \times 10^4) S^3 + (1.44 \times 10^5) S^2 + (1.46 \times 10^5) S$$

$$+ 3.65 \times 10^4 = 0$$

2. Of these seven poles, three are located in the approximate positions that the yaw stability augmentation system poles are located with zero cross coupling ($\tau_1 = \tau_2$).

3. Of these seven poles, four are located close to the positions that would be occupied by the roll stability augmentation system poles with zero cross coupling.

Examining the transfer function from which this characteristic equation is derived, we see that the zeroes of this transfer function are the poles of the roll system without cross coupling.

Therefore, we conclude that the dominant modes in yaw without cross coupling are still the dominant modes with cross coupling. The effect of cross coupling is to add some slight residual roll modes at frequencies and dampings close to the zero cross coupling roll mode dynamics.

The strength of the change in the system can also be evaluated by comparing the polynomial of Equation 25 for zero cross coupling with Equation 24.

$$S^7 + (4.86 \times 10^1) S^6 + (9.20 \times 10^2) S^5 + (9.369 \times 10^3) S^4 \qquad (25)$$

$$+ (5.11 \times 10^4 - 3290\, k_\varphi k_\Psi) S^3 + (1.44 \times 10^5 - 3290\, k_\varphi k_\Psi) S^2$$

$$+ (1.46 \times 10^5) S + (3.65 \times 10^4) = 0$$

For $K_{\varphi} = K_{\Psi} = .10$, the SA settings used in the aircraft, the difference in equations 24 and 25 is negligible, as is yaw to roll to yaw cross coupling.

6.10 SETUP AND USE OF PADDED SERVO MULTIPLIER POTENTIOMETERS

A considerable use was made in this simulation of padded servo multiplier potentiometers for the generation of nonlinear functions incidental to the simulation.

Padded servo potentiometers have been widely used in analog simulation, but we mechanize the pot-padding in a way which is somewhat different.

In the usual analog facility, commercial pot-padding equipment is available which uses an adjustable small variable resistor connected to each of the 17 taps on each padded servo cup. This gear has two disadvantages. These are: (1) the size of the rack containing all of the padding resistors, and (2) each time a function is removed and another set up, the tap resistors must be reset.

The Ryan system is advantageous if two or more simulations must alternate on the same computer. This technique uses removable etched circuit boards which enable calculated values of tap resistors to be permanently soldered to the board. The boards plug into circuit board receptacles, so that once a function is set up it can be permanently retained, and may be used again with no further setup time, save the time it takes to plug it back in.

The boards use 1/2 watt or 1 watt 5% carbon resistors, and it is possible to set up functions within ±.2% of full scale.

The great advantage of pot padding is that a function may be generated and simultaneously multiplied by another function using only one servo cup, which effectively increases the size of the computer a significant amount.

Pot padding inherently has two disadvantages. These are: (1) the spacing of function break points is fixed, since the taps have equal spacing, and (2) the servo multiplier has limited bandwidth.

For these reasons it is necessary to use pot padding only where the independent variable has a sufficiently low bandwidth, and the restriction

of equal tap spacing does not compromise the accuracy of fit enough to make the fit unacceptable.

Referring to Figure 199, it is possible to write the modal equations determining the required values of tap resistor assuming the arm of the padded cup works into an infinite load.

These equations are:

$$\frac{E_n - E}{R_n} + \frac{E_n - E_{n-1}}{R} + \frac{E_n - E_{n+1}}{R} = 0 \qquad (1)$$

We can solve this equation for R_n:

$$R_n = \frac{(E - E_n)\,R}{2E_n - E_{n+1} - E_{n-1}} \qquad (2)$$

Where:

E = 100V, -100V, or Zero

E_n = the desired voltage on tap n

E_{n+1} = the desired voltage on tap n+1

E_{n-1} = the desired voltage on tap n-1

R = 1/16 of the pot resistance

If the loading effect of the finite resistance the pot arm feeds into is taken into account, the equations become too complex. However, equation (2) is approximate and sufficiently accurate if the load is held to 1 megohm. Further, when the circuit boards are set up and calibrated, the taps are properly loaded during the process, and errors are trimmed out. As a rule it is easy to keep the errors of the generated function to within the tolerance previously specified.

A digital computer is used to calculate the resistor values and pick the nearest standard 5% value. Unselected 5% resistors generally afford sufficient accuracy if just the two end resistors are trimmed.

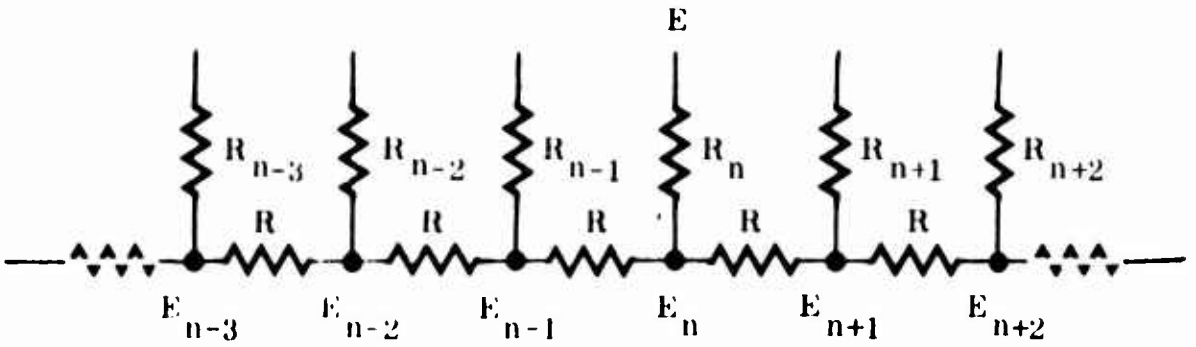

Figure 199 Schematic Diagram of a Typical Padded Servo Pot Showing Tap Resistors